2007

Design of an Electrospun Type II Collagen Scaffold for Articular Cartilage Tissue Engineering

Catherine Pemble Barnes
Virginia Commonwealth University

DESIGN OF AN ELECTROSPUN TYPE II COLLAGEN SCAFFOLD FOR

ARTICULAR CARTILAGE TISSUE ENGINEERING

A dissertation submitted in partial fulfillment of the requirements for the degree of
Doctor of Philosophy in Biomedical Engineering at Virginia Commonwealth University.

by

CATHERINE PEMBLE BARNES
M.S., Arizona State University, 1999
B.S.E., Mercer University, 1997

Director: GARY L. BOWLIN, PH.D.
ASSOCIATE PROFFESOR, BIOMEDICAL ENGINEERING

Virginia Commonwealth University
Richmond, Virginia
December 2007

Acknowledgements

I would like to thank Dr. Gary Bowlin, my mentor and advisor, for giving me the opportunity to work in his lab and on this research project. He has provided me with guidance in the lab and in life that I will surely use throughout my future endeavors. I am indebted to Dr. Simpson for the time he took to sit with me on multiple occasions to discuss at length any question I had – he is an outstanding teacher. To Dr. Haas I owe my interest in plastics – I will never forget "my PET polymer". Though I have not worked as closely with Dr. Diegelmann and Dr. Yang, I sincerely appreciate your support with my efforts to earn this degree, and I thank you both for participating on my committee. Thanks also go to the Tissue Engineering Lab members, including Josh Grant, Danielle Knapp, Michael McClure, Scott Sell, and Matt Smith. To Scott in particular, I have enjoyed and learned a great deal from our many brainstorming sessions.

Family is the key component to my success. I would like to thank my parents for their endless support and guidance through all of my schooling. Though my mother typically had no idea what I was describing, she would always listen and offer some advice about my research when I would hit a snag. To my brother Charles, thank you for the biochemistry lessons and for being my sounding board. Most importantly, I want to thank my husband Joe for his love and support – he is always "first on board" with my ideas and makes me feel like I can accomplish anything. Finally, to my son Carter, who

will be about 7 months old when I finish my degree – everything has taken on a new

meaning since you arrived; you are truly a special being and you make me special.

Table of Contents

List of Tables

List of Figures

Abstract

DESIGN OF AN ELECTROSPUN TYPE II COLLAGEN SCAFFOLD FOR

ARTICULAR CARTILAGE TISSUE ENGINEERING

By Catherine Pemble Barnes, M.S.

A dissertation submitted in partial fulfillment of the requirements for the degree of Doctor of Philosophy in Biomedical Engineering at Virginia Commonwealth University.

Virginia Commonwealth University, 2007

Major Director: Gary L. Bowlin, Ph.D.
Associate Professor, Biomedical Engineering

Traumatic defects in articular cartilage can lead to joint disease and disability including osteoarthritis. Because cartilage is unable to regenerate when injured, the field of tissue engineering holds promise in restoring functional tissue. In this research, type II collagen was electrospun, cross-linked, and tested as scaffolds for supporting chondrocyte growth. The mechanical, biochemical, and histological characteristics of the engineered tissue were assessed as a function of the electrospinning solution concentration (i.e. scaffold fiber diameter and pore properties) and as a function of the time in culture

(evaluated at 2, 4, and 6 weeks). Fiber diameter had a linear relationship with

concentration: mean diameter increased from 107 to 446 nm and from 289 to 618 nm,

measured with SEM and permeability meter, respectively, with increasing concentration,

from 60 mg/mL to 120 mg/mL. Pore size revealed no relationship with concentration but

mean values ranged in size from 1.76 to 3.17 μm^2 or from 0.00055 to 0.0028 μm^2,

depending on the measurement technique. Average porosity ranged from 84.1 to 89.1%,

and average permeability was between 6.82×10^{-4} and 35.0×10^{-4} D. Histological analysis

revealed a relatively high number of spherical cells, possibly indicating the expression of

the chondrocyte phenotype. However, there were very little glycosaminoglycans and type

II collagen synthesized by the cells despite an increase in the cell density over time for the

60, 80, and 100 mg/mL concentrations. The mean values for peak stress (between 0.17

and 0.35 MPa) and tangential modulus (between 0.32 and 0.64 MPa) for the mats are at

least an order of magnitude less than that for native cartilage, while the mean values for

strain at break (between 93 and 150%) for the mats are at least an order of magnitude

greater than that for native cartilage. The equilibrium stiffness for all concentrations

decreased from week 2 to week 6 of tissue culture (which may correlate with increasing

cell density); the 100 mg/mL concentration had the highest mean value (0.084 MPa at

week 2) and the lowest mean value (0.010 MPa at week 6). This research did not indicate

any significant findings regarding the influence of concentration or culture time on

chondrogenesis. Because the cells appeared to grow on the surface of the scaffold but

there was a lack of cell migration into the scaffold, the scaffold material may be sufficient

to support chondrocyte growth but the scaffold physical design must be reconsidered.

Introduction

Articular cartilage is a thin layer of connective tissue covering synovial joint surfaces that functions to absorb energy, distribute loads uniformly between bones, and provide low-friction articulation. Traumatic defects in articular cartilage can lead to joint disease and disability, which manifest as joint pain, stiffness, and a decrease in or loss of mobility. Progressive degeneration (i.e. loss of normal structure and function) of articular cartilage can lead to osteoarthritis (OA), also known as osteoarthrosis or degenerative joint disease, in which the breakdown of the cartilage can lead to bones rubbing against each other [1, 2]. This disease affects an estimated 21 million people in the United States [2]. OA is more prevalent in women, and its incidence increases with age. In fact, about 10% of adults over the age of 50 years are afflicted with OA, and it is one of the leading causes of disability in the elderly [3]. It can occur in any synovial joint, but occurs most frequently in the knees, hips, hand joints, neck, and lower back [1, 2]. In the United States the cost of arthritis and related conditions including OA is almost $86.2 billion per year in medical care and indirect expenses, including lost wages and productivity [2]. Put another way, the total cost of arthritis (including OA) in the United States has been estimated to be over 2% of the gross domestic product [3].

Though the etiology of OA is not fully understood, the disease is characterized by a decline in the biomechanical properties of articular cartilage and a deterioration in the

balance between the chondrocyte anabolic (synthesis) and catabolic (resorption) processes which are essential for homeostasis [4]. Surgical attempts at repair can result in chondrocyte and tissue loss because disruption of healthy tissue may cause cell apoptosis and/or necrosis [5]. Currently, the main treatment is the replacement of the joint with metal prostheses that do not perform to the physical demand, wear out, loosen, or even break *in situ* [4]. To avoid joint replacement, clinicians and scientists have turned to tissue engineering for the repair of the cartilage prior to complete degeneration. There are an abundant number of investigations into the tissue engineering of articular cartilage; however, thus far there have been no successes in the development of a tissue that exactly duplicates the material properties or durability of articular cartilage and thereby restores a normal joint surface. Understanding the structure and function of healthy articular cartilage as well as the structural and biochemical alterations (i.e. matrix and cellular changes) that develop in OA are crucial in developing methods of repairing, restoring, or regenerating new tissue with the same function as the native tissue.

Tissue engineering, or regenerative medicine, is an interdisciplinary field that merges principles and innovations from engineering and life sciences for the purpose of addressing the improvement, repair, or replacement of tissue/organ function [6, 7]. Since its inception, the field has delved into three main areas: the injection of cells only, the development of encapsulated systems of cells, and the *in vitro* growth of cells in a scaffold (i.e. an artificial extracellular matrix) [8]. The latter is logical since every tissue or organ in our body is composed of parenchymal cells (functional cells) and mesenchymal cells (support cells) contained within an extracellular matrix (ECM) to form a dynamic

microenvironment. Composition (i.e. biomaterials of synthetic or natural origin) and architecture of a tissue-engineered scaffold result in cell-environment interactions that determine the structure's fate. The tissue engineering of articular cartilage has developed out of the need to treat the chondral defects (on the surface of or within the cartilage). Since mature articular cartilage is aneural, avascular, and alymphatic, the tissue has a limited capacity for repair and regeneration [4, 9].

The design and development of a scaffold for articular cartilage tissue engineering is of interest in this research. In general, the functions of the scaffold include the following: provide a defined space (with structural integrity) on/in which cells can migrate and proliferate, serve as a guide for tissue restructuring (i.e. new growth *in vitro* and/or incorporation *in vivo*), allow the diffusion of nutrients and wastes, and act as a cellular transducer of mechanical forces [8]. Biochemical and biomechanical considerations will be given to the tissue-engineered constructs, developed in this research study, designed to treat chondral defects.

Background

Structure of Native Articular Cartilage Tissue

Articular cartilage is a thin layer of connective tissue covering synovial joint surfaces; it is the almost frictionless bearing surface for diarthrodial joints. For humans the thickness of the cartilage layer may vary from 1 mm in finger joints to 6 mm on the articulating surface of the patella [10]. In normal physiologic conditions, articular cartilage is porous and highly hydrated. With the application of a load, fluid flows in and out of the tissue, thereby resulting in changes in the mechanical, chemical, and electrical properties of the cartilage [11]. Articular cartilage functions to absorb energy, distribute loads uniformly between bones, and provide low-friction articulation. Thus, to handle the forces imposed upon it, articular cartilage possesses a variable compressive stiffness and permeability (that depend on both current and previous loading conditions) as well as a low wear rate and a low coefficient of friction (ranging from 0.005 to 0.05) [10, 12]. Its function under a wide range of loading conditions ultimately depends on the structural arrangement of its major components (which differs within the tissue), the integrity of the extracellular matrix (ECM), and how these components respond to one another under loading.

Cartilage can be considered a fiber-reinforced composite material, that is both inhomogeneous and anisotropic, consisting of three major structural macromolecules

(collagen, proteoglycans, and glycoproteins) and cells known as chondrocytes (all of which

are collectively considered the solid phase), water (considered the fluid phase), and solutes

including ions and nutrients (sometimes considered a third phase, the ion phase). In

human articular cartilage, water accounts for more than 60% by wet weight, collagen

comprises 60 to 80% of the dry weight or approximately 20% of the wet weight, and

proteoglycans contribute 20 to 40% of the dry weight or about 7% of the wet weight [10,

13]. Collagen and proteoglycan macromolecules are intertwined to form a solid structure

that is anchored to the subchondral bone and through which water and solutes move freely

to provide nourishment to chondrocytes as well as lubrication to the joint. The

cartilaginous ECM is depicted in Figure 1. Molecular interactions among the structural

macromolecules include collagen-collagen covalent (crosslinks) and noncovalent

interactions, proteoglycan-proteoglycan noncovalent interactions, and collagen-

proteoglycan noncovalent interactions. These molecular interactions achieve an

immobilized network of collagen and proteoglycans (depending on shape and size) with

pore sizes ranging from 25 to 75 Å that prevent the transport of large molecules through

the tissue [14].
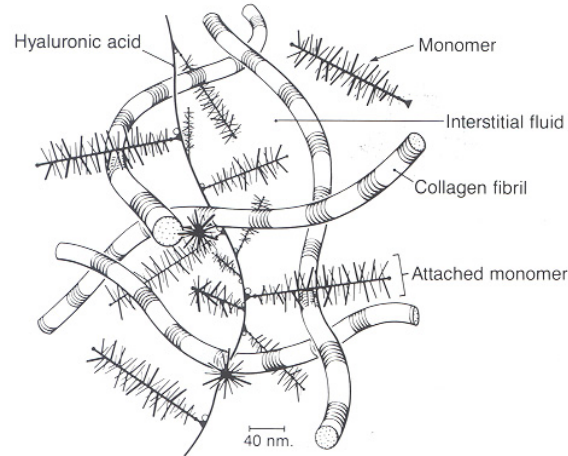
Figure 1. Illustration of collagen fibrils and proteoglycans in articular cartilage ECM [10].

Type II collagen is the main collagen type found in articular cartilage, though types VI, IX, X, and XI can also be found in small amounts [13, 15]. A collagen fibril (Figure 2) consists of the basic tropocollagen structural unit composed of three procollagen polypeptide chains, or α chains (each designated $\alpha1(II)$ for type II collagen), which contain the repeating amino acid sequence of glycine-X-Y (in which X is frequently proline and Y hydroxyproline) and contain 990 to 1020 amino acids per polypeptide chain [16]. Each α chain is a left-handed helix, and the three chains are coiled about each other in a right-handed triple helix. The tropocollagen molecules (rod-like in shape) are approximately 1.4 nm in diameter and 300 nm in length [14]. These molecules self-assemble/polymerize outside of the cell into larger collagen fibrils. Type II collagen fibrils exhibit an axial, periodic banding pattern of 64 nm separations (known as the D-periodic banding) [17]. Type I collagen fibrils form large fiber bundles that range in diameter from 2 to 10 μm. However, type II collagen fibrils do not form fiber bundles and range in

diameter from 20 to 200 nm [14, 18]. Intramolecular and intermolecular covalent

crosslinks form between the α chains and between collagen molecules [14, 19]. Tensile

stiffness and strength are the two most important contributions of collagen fibrils to the

mechanical properties of the tissue as a whole [10].
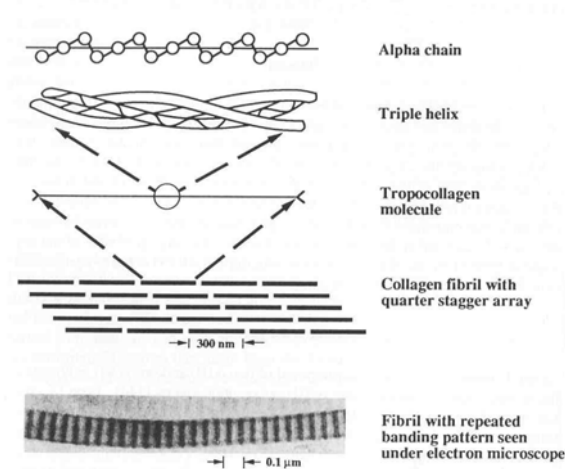
Figure 2. Structure of collagen fibrils [14].

Proteoglycans are aggregates composed of 100 to 200 monomers, known as

glycosaminoglycans (GAGs), attached to a single backbone of hyaluronic acid, as shown

in Figure 3. Proteoglycans are entrapped within the collagen meshwork because of their

size and electrostatic and frictional interactions with the collagen fibers (Figure 1). Link

proteins associate the monomers with the hyaluronic acid. The two most abundant GAGs

in articular cartilage that form proteoglycans (and in particular aggrecan) are chondroitin

sulfate and keratan sulfate, with the former in more abundance typically than the latter

depending on the zone [9]. Amounts, distribution, and composition vary among

individuals, and age- and disease-related changes in structure such as GAG monomer chain

shortening and decreased aggregate size do occur [9, 14].
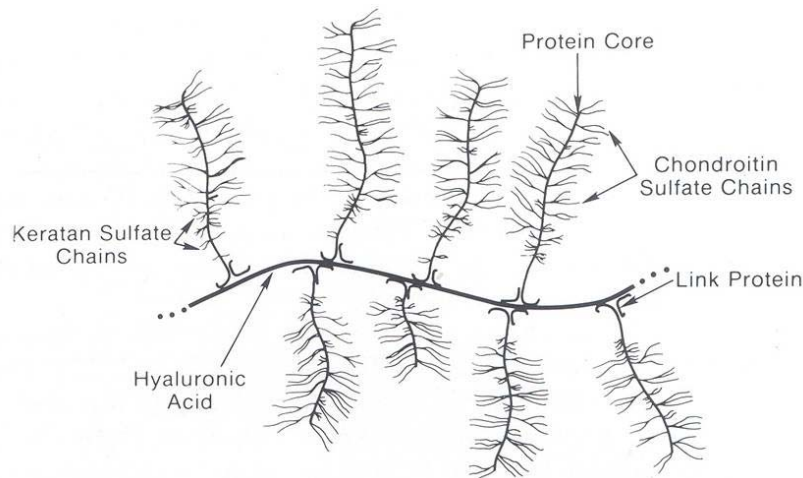
Figure 3. Structure of proteoglycan aggregate [9].

GAGs are hydrophilic molecules with many negatively charged side chains that

repel each other due to like charge, and thus fan out from the proteoglycan backbone

giving the tissue a compressive resistance [9, 10]. As the proteoglycan is compressed and

the side chains are brought into closer proximity, the effective repulsive force and charge

density increases. The negative charges attract the positive ions in the aqueous interstitial

fluid, thereby leading to swelling of the tissue. This swelling stresses the collagen fibers

that restrain the proteoglycans such that the tissue can withstand the compressive stresses

caused by matrix deformation during joint loading. Thus, when a load is applied, the

proteoglycans are compressed and the interstitial pressure increases; fluid flow then occurs

through the matrix down the pressure gradient until equilibrium is reached and flow stops.

Upon release of the load, the proteoglycans expand and fluid flows in the reverse direction

back into the matrix until the original shape (non-stressed) of the ECM is reestablished [9]. As the interstitial fluid flows through the pores of the ECM, viscous frictional forces (drag forces) develop on the walls of these pores. Cartilage deformation (compression and expansion) is determined by a balance of forces between the pressure exerted by proteoglycans and the tension generated within the collagen meshwork.

Articular cartilage consists of cells known as chondrocytes thinly dispersed within the ECM; the cells are more widely scattered within the ECM with increasing distance from the articular surface as depicted in Figure 4. Chondrocytes, which arise from pluripotential mesenchymal stem cells, are metabolically active cells that produce, organize, maintain, and degrade cartilage matrix components [20]. The cells are, themselves, influenced by the ECM which responds to the loading conditions and the electrochemical signals imposed on the tissue (see Figure 5) [9, 10, 21]. During the development of cartilage, the cells proliferate rapidly and synthesize great amounts of matrix until maturation when the cells slow and cell density decreases. In mature human articular cartilage, chondrocytes represent about 1% of the total volume, no longer divide, and decrease in density with age [10, 13, 15]. These cells do not form cell-to-cell contacts but surround themselves with ECM [9]. The structural matrix molecules maintain and direct tissue fluid flow through the tissue; thus, via diffusion and/or convection, nutrients are delivered to the chondrocytes by the synovial fluid carrying the nutrients from the interior lining of the synovial joint. This solute transport is critical for chondrocyte nutrition as well as for the mechanical behavior of cartilage and joint lubrication [10]. Chondrocytes vary in shape, and thus function, depending on the location within the

cartilage thickness, and the diameter can measure 10 μm or more at a circular cross-section [22]. In adult human articular cartilage, the flattened, discoidal cells (found more superficially) have been shown to have a reduced rate of protein synthesis; the spheroid-shaped cells (found deeper within the cartilage thickness) are more actively involved in protein synthesis, particularly that to be processed into sulphated proteoglycans [22].
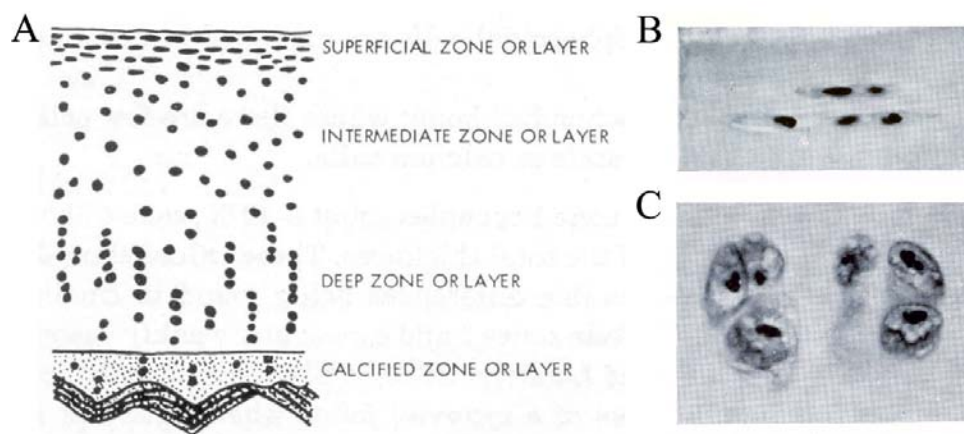
Figure 4. A) Illustration of cell distribution within the ECM (white area is uncalcified matrix, black dots are cells) [23]; B) flattened, discoidal cells of the superficial zone and C) spheroidal cells from the deep zone [22].
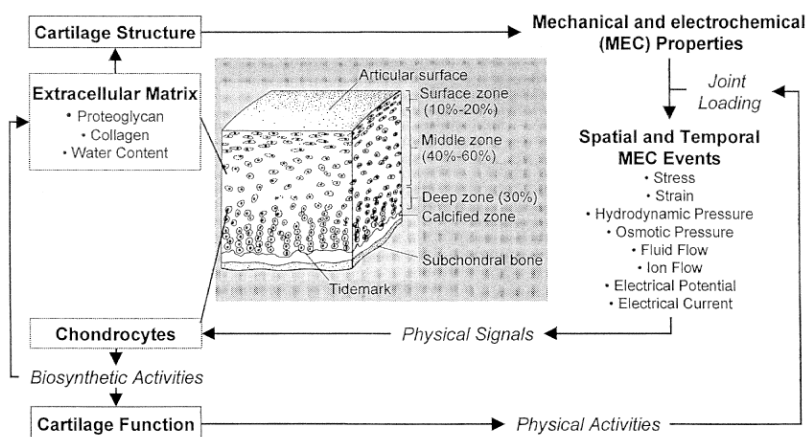
Figure 5. Diagram of the structure-function relationship of articular cartilage including chondrocyte and ECM interdependence [24].

Articular cartilage is divided into zones, or layers, based upon the inhomogeneous structural organization of the major tissue components throughout the depth of the tissue. Figure 6 gives a representation of the collagen organization within the zones. Collagen varies with depth; it is found in greater concentrations nearer the surface, and collagen fibril diameter increases with depth [9, 10, 14]. Collagen fibrils are densely packed and run tangentially to the articulating surface in the superficial zone. Fibrils are more randomly arranged in the middle zone but are oriented perpendicular to the surface in the deep zone where the fibrils are anchored in the tidemark region to the subchondral bone. The concentration of proteoglycans is maximal in the middle zone; GAG distribution is lowest at the surface, increases to a maximum in the middle zone, and decreases in the deep zone [14, 15]. Chondrocytes vary in morphology depending on the zone in which they are located (Figure 4 and Figure 7); in the superficial zone chondrocytes are flattened and elongated (discoidal), in the middle zone the cells are more spherical, and in the deep zone the cells are elliptical in shape and more vertically oriented [15, 22].
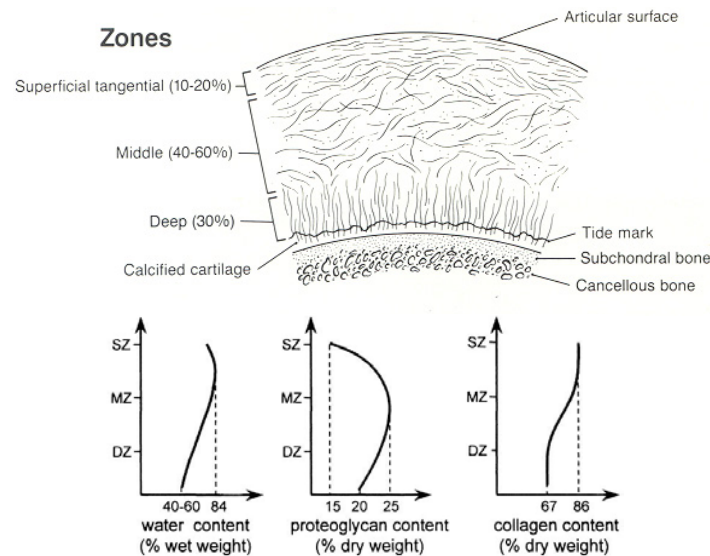
Figure 6. Schematic of articular cartilage zones with collagen fibril organization [10] and graphical representations of the inhomogeneous distributions of water, proteoglycans, and collagen within those zones (superficial zone – SZ, middle zone – MZ, deep zone – DZ) [24].

Within the cartilaginous zones, there are distinct regions of matrix around the chondrocytes in which the cells can establish and maintain an environment conducive to their needs (mechanically and metabolically) [9]. Figure 7 illustrates these matrix regions. The pericellular matrix is a thin layer of matrix that surrounds the cell and contains little or no fibrillar collagen. Surrounding the pericellular matrix is the territorial matrix which can encase one chondrocyte or clusters of chondrocytes and their pericellular matrices; it consists of a dense network of fine collagen. The interterritorial matrix establishes the mechanical properties of the cartilage; it surrounds the territorial matrix and forms the largest matrix region consisting of large collagen fibrils.
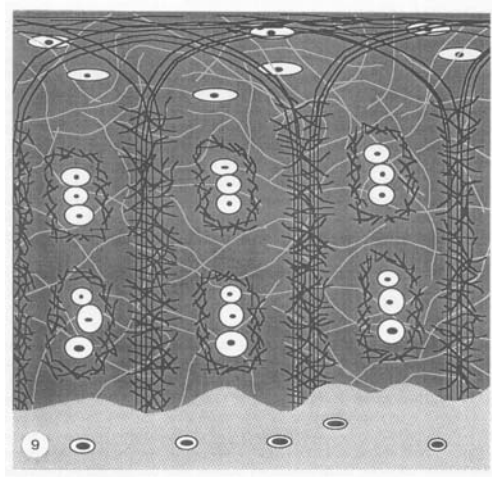
Figure 7. Schematic of articular cartilage matrix regions (pericellular, territorial, and interterritorial) with chondrocyte and collagen fibril organization [25].

Biomechanical Properties of Articular Cartilage

In articular cartilage, collagen is responsible for the tensile and shear stiffness and strength, and proteoglycans are responsible for the equilibrium compressive stiffness of the tissue. Since these proteins vary with depth and site within the tissue, it follows that the mechanical properties of the tissue are also depth- and site-dependent [26].

In uniaxial tensile measurements performed at a constant strain rate, the stress-strain behavior is nonlinear, the curve of which consists of three areas of interest (shown in Figure 8). The initial non-linear toe region is a result of the straightening of the coiled collagen fibrils at small extensions. As tension increases, more fibrils are straightened and stretched; this is known as fiber recruitment. The linear region involves the actual stretching of those fibrils into a parallel array, and the slope of this region gives an indication of the stiffness of the collagen fibrils as the tensile modulus (tangential

modulus) of the tissue. After the linear region, the collagen fibrils fracture at the ultimate stress, which gives a measure of the strength of the collagen fibrils. The mechanical properties of cartilage are dependent on depth, location (anterior, central, posterior), orientation relative to the predominant collagen fibril direction, and degree of degeneration. Table 1 gives tensile properties of articular cartilage and collagen. Tensile stresses develop in articular cartilage under compressive loading in the following manners: parallel to the surface in the superficial zone, various angles in the middle zone, and at 45º relative to the tidemark near the calcified region [10].
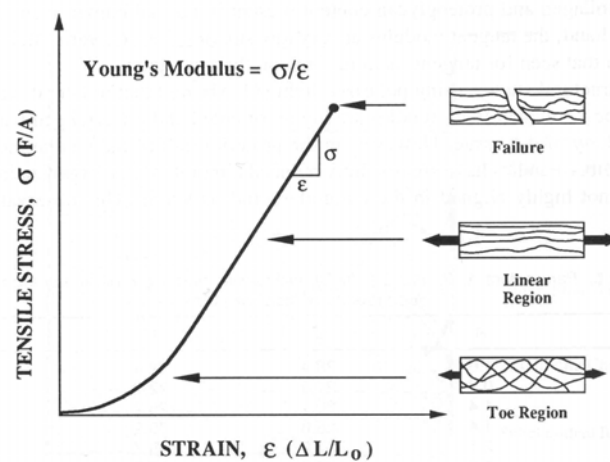
Figure 8. Typical stress-strain curve for articular cartilage tested in uniaxial tension [14].

Table 1. Tensile properties of healthy hyaline cartilage and collagen fibers.

	Tangential Modulus (MPa)	Peak Stress (MPa)	Strain at Break (%)
Hyaline Cartilage [27-29]	5-25	1.3-4.4	9.2-25.9
Collagen [30]*	100-2900	5-500	5-50

*This is not type II collagen; these values are given for a general comparison.

Articular cartilage displays both an elastic response and a time-dependent response to a perturbation; thus, the tissue is viscoelastic. The viscoelastic properties of articular cartilage are primarily due to the frictional drag of the interstitial fluid flow through the permeable, porous, solid collagen-proteoglycan ECM [12, 14]. The compressive creep and stress relaxation behaviors are studied by applying theories describing the multiphasic nature of the tissue, including the solid phase consisting of the matrix of collagen fibrils, proteoglycans, and cells, the fluid phase consisting of interstitial water, and the ion phase [24, 31]. The model treats the tissue as a combination of a viscous fluid and an elastic solid. Indentation experiments are typically used to test the viscoelastic properties of cartilage for several reasons: no special specimen preparations are needed, material properties can be determined *in situ* for native tissue, the whole joint surface can be tested easily, and neither the composition nor ultrastructure of the tissue is affected. This simple setup involves compressing a specimen with a rigid, smooth cylinder, known as the indenter.

The creep response of articular cartilage to a constant compressive load is due to the flow of interstitial fluid (exudate) out of the matrix (Figure 9). Upon initial application of the load, fluid leaves the matrix rapidly. The straining of the fluid through the solid mesh creates a frictional drag. With the loss of fluid pressure the collagen-proteoglycan matrix crushes and a compressive stress is developed within. As time passes, flow gradually decreases and, at the point of equilibrium, when fluid flow ceases, there is a balance between the stress generated within the matrix and the applied load.
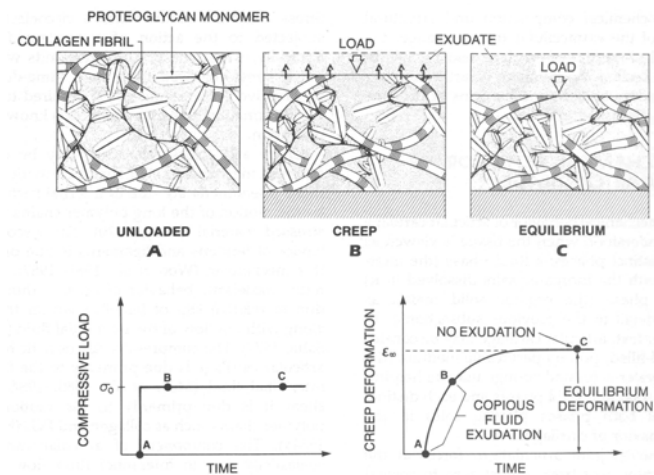
Figure 9. General illustration and typical curve showing the deformation of articular cartilage for the creep response following an applied step load [32].

Stress relaxation of articular cartilage occurs due to the redistribution of interstitial fluid within the matrix (Figure 10). Following the application of a compressive deformation at a constant rate, high stress is initially created within the solid matrix near the point of application as the fluid is forced out. As the deformation is held constant, fluid flows from and is redistributed within the matrix until an equilibrium compressive stress is established at which fluid flow ceases.
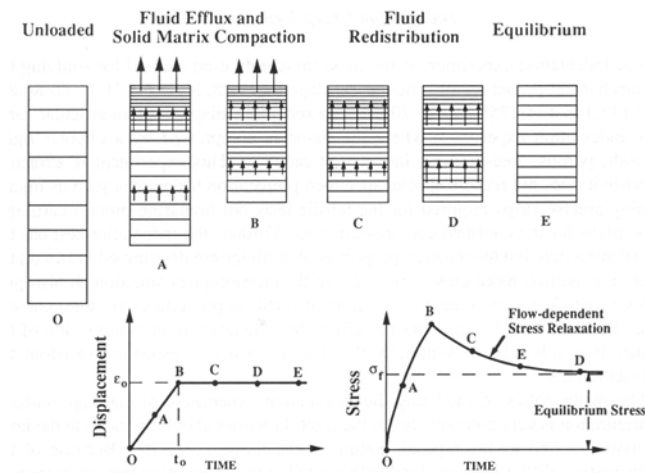
Figure 10. General illustration and typical curve showing the stress response of articular cartilage for stress relaxation following an applied ramp displacement [14].

Articular cartilage is considered a highly porous tissue with interconnected pores ranging in size from 25 to 75 Å [14, 32]. Permeability is a measure of resistive force at a given speed at which fluid flows through the pores, and it is inversely proportional to frictional drag exerted by the fluid. Articular cartilage has a very low permeability, which means high frictional forces are generated within the pores. The permeability of normal cartilage ranges from 10^{-16} to 10^{-15} m^4/N·sec and that for degenerated cartilage is on the order of 10^{-14} m^4/N·sec [12, 14, 32]. Permeability is strain dependent and decreases with increasing compressive strain; thus, excess fluid exudation is limited when compressive strain is prolonged.

Articular Cartilage Damage and Potential for Native Repair

Diarthrodial joints withstand large ranges of loading conditions (very high loads and stresses typically at low operating speeds for an individual's lifetime), but cartilage

sustains little wear and tear under normal conditions. Mature articular cartilage is aneural,

avascular, and alymphatic [9]. Based upon this structure, articular cartilage has a limited

capacity for repair and regeneration of tissues in chondral defects (on the surface of or

within the cartilage) [3]. In osteochondral defects, on the other hand, the void may be

filled in with fibrocollagenous (composed mainly of fibrous collagen) and

fibrocartilagenous (composed of parallel bundles of thick collagen fibers between

chondrocytes, a low content of glycosaminoglycans, and small amounts of cartilage matrix

only around chondrocytes) tissues, but hyaline cartilage repair tissues are rarely seen [33].

Though healthy chondrocytes may proliferate and synthesize proteoglycans (in acute

cartilage injuries), the cells do not migrate into and do not fill in the defects caused by

injuries with newly synthesized matrix [9]. Damage to articular cartilage does not elicit an

inflammatory response. It is proposed that the lack of pluripotent marrow cells (i.e.

parenchymal cells that are present in the bone) in the cartilage and the absence of a fibrin

clot (i.e. the natural provisional scaffold) for the cells to migrate into are the reasons tissue

regeneration does not occur in chondral defects [33]. In situations of trauma or overuse or

misuse, degenerative changes may occur that can eventually lead to the development of

OA [1]. Early changes seen in OA include loss of proteoglycans from the ECM, a

disruption in the collagen fiber network due to excessive mechanical stresses (such as

loosening) in the superficial zone extending into the transitional zone (considered fraying

or fibrillation of the cartilage), changes in proteoglycan properties (molecular structure,

disaggregation, etc.), abnormal proteoglycan expansion leading to excessive tissue

swelling (and increased water content), changes in the collagen-proteoglycan interactions,

and remodeling of subchondral bone [1, 5, 10]. Macroscopically, softening, fibrillation,

and erosions can be seen while clefts, loss of cartilage layers, cellular necrosis, cell

cloning, and tidemark duplication are seen histologically; additionally, the superficial zone

seems to be affected first in early OA [3]. Figure 11 presents two scanning electron

micrographs (SEMs) showing the surfaces of healthy human articular cartilage (densely-

packed, randomly-arranged collagen fibrils and fine pores) and osteoarthritic human

articular cartilage (degenerative characteristics including tears). The presence of any

surface irregularities on articular cartilage can have tremendous consequences, such as

effects on friction (i.e. lubrication) and on the rate of further degradation. Figure 12

presents histological sections of healthy and osteoarthritic human articular cartilage.
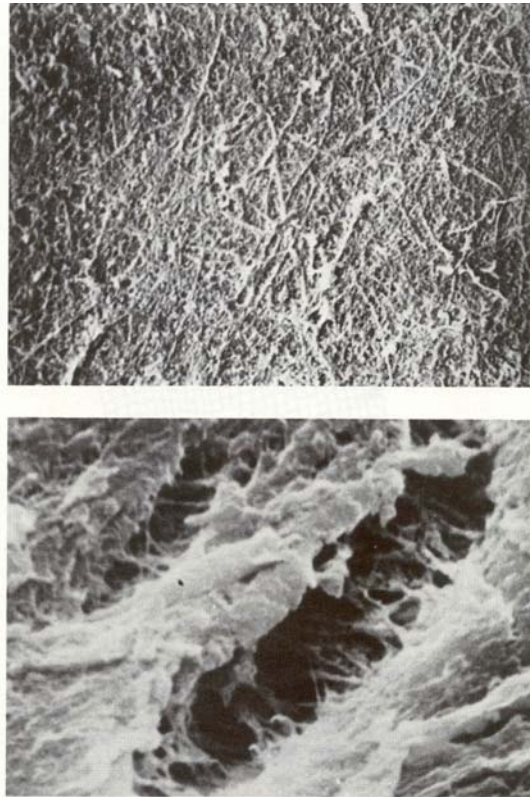
Figure 11. Scanning electron micrographs of the surfaces of human articular cartilage from a healthy specimen (top) and an osteoarthritic specimen (bottom); X3,000 magnification [34].
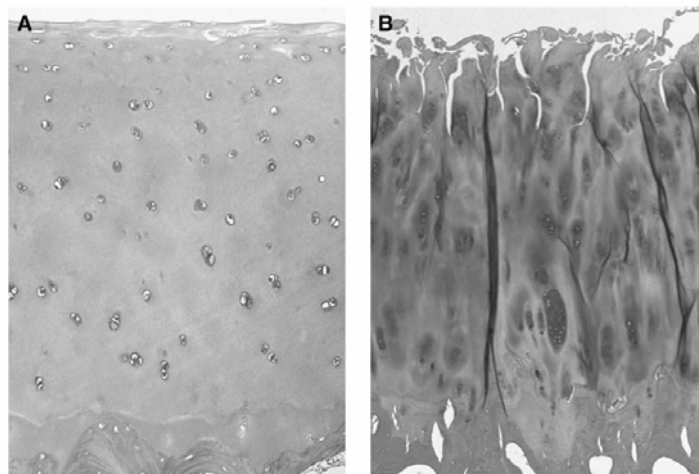
Figure 12. Histological sections of adult (A) healthy articular cartilage and (B) articular cartilage in early OA (showing clefts, cellular cloning, and cell necrosis) [3].

Matrix metalloproteases (MMPs) are the family of proteolytic enzymes responsible for the digestion of the cartilage ECM in OA [3]. It is believed that type II collagen is digested by collagenase-1 (MMP-1) and collagenase-3 (MMP-13), and stromelysin-1 (MMP-3) and aggrecanase-1 (ADAMTS-4) are the primary MMPs involved in proteoglycan degradation. Homeostasis of the MMPs in joints is normally maintained by such physiologic activators as cathepsin B and plasminogen activator/plasmin and by their inhibitors known as tissue inhibitors of MMPs, or TIMPs. Researchers have found an imbalance between the amounts of MMPs and TIMPs in OA tissues [3].

The most obvious deleterious effect of any sort of damage to articular cartilage is the loss of matrix proteoglycans, though the other components may suffer effects as well [5, 9]. There is a threshold of damage at which chondrocytes can replace the proteoglycans lost (as long as the collagen matrix remains intact and the chondrocytes are healthy), but beyond which the cartilaginous damage is irreversible [9]. The quality of the minimal amount of repair depends on the extent (volume or surface area of tissue injured) and severity of the damage as well as the location of injury. Evidence has shown that smaller defects heal better than larger defects [9]. Causes of damage can include a variety of means: trauma (surgical or otherwise) to the synovial membrane, infection or inflammatory diseases, prolonged joint immobilization, mechanical disturbances (penetrating injuries even into subchondral bone, blunt trauma, frictional abrasion, concentrated loads), some anti-inflammatory agents, and anything that kills chondrocytes and disturbs the matrix.

Repair is defined as the "replacement of damaged or lost tissue with new tissue" [9]. The two main symptoms propagating the search for ways to repair cartilage are the pain and disability. Success of repaired tissue is described as that which restores normal pain-free motion of the joint and prevents deterioration of the joint. Doctors, scientists, and engineers operate under the assumption that the repaired/regenerated tissue must have the same structure and function (including composition, material properties, and durability) as native tissue [9, 35].

There are numerous autologous and allogeneic therapies and tissue grafts/transplantations that have been investigated for the therapeutic treatment of articular cartilage defects, all of which have had varying results [1, 4, 5, 13, 20, 36-41]. Autologous implants have involved the use of filling cartilage defects with grafts of the lining tissues perichondrium and periosteum; these grafts have resulted in complications including incomplete filling with a tissue that has only some cartilaginous characteristics, detachment of the graft, and graft ossification. In mosaicplasty, osteochondral plugs from low weight-bearing areas on the femoral condyles are removed and press-fitted into the cored out damaged areas of the cartilage; though these autografts may result in temporary pain relief and restoration of function, they have not been shown to possess longevity, they may be damaged by the insertion method, and a loss of chondrocytes can result at the donor site. Cadaver allografts have been utilized to restore function with minimal pain; though they offer the benefit of not creating new pathological sites, they do not become integrated with the surrounding tissue and there are always the concerns of immunological responses and disease transmission. The delivery of cells-only to the defect site, known as

autologous chondrocyte implantation (ACI) or autologous chondrocyte transplantation

(ACT), is clinically available in the United States; such an approach involves filling a

defect with autologous chondrocytes or mesenchymal stem cells and suturing a flap of

periosteum over the defect to hold the cells in place. Drilling and debriding can provide

immediate relief of symptoms, but fibrocartilagenous tissue forms with a poor outcome

long-term [42]. Surgical penetration of the subchondral bone, which disrupts the blood

vessels, leads to the formation of a fibrin clot, and enables the migration and proliferation

of mesenchymal cells (which can differentiate into cells with chondrocytic morphology) as

well as the potential release of growth factors, has been shown to result in the stimulation

of new surface tissue, though this is again fibrocartilagenous tissue [1]. Since

transplantation involves complications (such as insufficient donor tissue supply, donor site

morbidity, and difficulty obtaining correct three-dimensional shapes) and artificial

prostheses can lead to the undesirable results of infection, protein deposition, and immune

responses [42], other approaches for repair are under investigation.

Tissue Engineering of Articular Cartilage

Due to the avascular nature and relatively low cellular content of articular cartilage

and, hence, the inability of cartilage to regenerate when injured, tissue engineering holds

much promise in the repair of larger cartilage defects. Most often the tissue engineering of

articular cartilage involves the use of a scaffold onto which articular chondrocytes or their

precursor cells are seeded in order to grow a three-dimensional tissue that can be implanted

into the joint defect. Additionally, growth factors may be incorporated into scaffolds (with

or without cells) to encourage tissue growth. The goal is to have *in vitro* chondrogenesis within the cell-scaffold complex that matches native *in vivo* chondrogenesis. This *in vitro* chondrogenesis is dependent upon cell type, initial cell density, scaffold characteristics, and culture conditions. Tissue engineers of articular cartilage have agreed that the way to achieve this *in vitro* chondrogenesis is by mimicking the native tissue's mechanical and biochemical properties [35].

Cell proliferative capacity, phenotype stability, and immunogenicity must be considered when selecting the cell type to use in cartilage tissue engineering. Chondrocytes are used as in ACI/ACT, but these cells exhibit replicative senescence and, thus, their *in vitro* expansion may be limited. When chondrocytes are expanded in monolayer, the cells lose their differentiated phenotype and transform into a fibroblastic morphology characterized by a decrease in the expression of type II collagen and proteoglycans and an increase in the expression of type I collagen [43, 44]. Mesenchymal stem cells (MSCs), multipotent progenitor cells prevalent in adult bone marrow with the capacity to differentiate into chondrocytes among other cell types, are of extreme interest because isolation, expansion, and differentiation into chondrogenic cells would eliminate the need to harvest chondrocytes/cartilage from the patient. MSCs have been induced into the chondrogenic pathway with transforming growth factor-beta (TGF-β).

An ideal characteristic of a scaffold is the support of cells at the early stage of tissue growth and then the slow degradation of the scaffold (into nontoxic products) as new ECM becomes functional. A wide variety of natural and synthetic materials have been investigated to accomplish this goal. Natural materials are of interest in scaffold materials

for cartilage tissue engineering [4, 5, 36, 38, 42, 45] because these materials may contain or present the biochemical and ultrastructural characteristics required by cells for proper cell-ECM communication. Fibrin, the major component of wound site clots, has been investigated in a polymerized form and as a glue. Agarose and alginate, linear polysaccharide polymers extracted from seaweed, form hydrogels that have performed well in filling the defects. Since collagen is the main component of the native ECM and it can be degraded by the cells, it is very popular as a scaffold; collagen gels, sponges, and fibrous meshes have been investigated. Cross-linking can be used to increase degradation rates and tailor mechanical strength. Collagen gels have been shown to maintain chondrocyte phenotype, and collagen sponges can stimulate collagen synthesis. Chitosan hydrogels and molded porous structures are also under investigation as defect-filler materials. Hyaluronan, which makes up 1 to 10% of cartilage glycosaminoglycans and plays an important role in cell attachment, hydration, and matrix synthesis, has been used to prepare scaffolds to mimic embryonic cartilage tissue formation. Natural polymers may interact with cells in a more native manner, but typical problems with natural materials include batch-to-batch quality variability and weak structural properties [42].

Of the synthetic materials utilized as scaffolds for articular cartilage tissue engineering, the most widely used are the polyesters poly(lactic acid) (PLA), poly(glycolic acid) (PGA), and their copolymers [4, 5, 36, 38, 41, 45, 46]. In particular, PGA scaffolds have been shown to improve proteoglycan synthesis by chondrocytes [42, 47]. Advantages to using synthetic materials include the ability to customize the polymer chemistry and, hence, the mechanical properties which, in turn, can result in improved

retention at the implantation site; controlled polymer degradation; more consistent quality; and tailored surface morphology. Frequently, different materials (synthetic and natural) are combined to create scaffolds with tailored biochemical and mechanical characteristics. These scaffolds can be produced in the forms of foams, hydrogels, woven and nonwoven fiber meshes, or multi-phase structures (e.g. fibrous PLA combined with an alginate gel) [36, 48]. Polyester scaffolds have, unfortunately, demonstrated poor cell attachment, difficulty in manufacturing, and some inflammatory reactions *in vivo*.

Numerous studies have compared the responses of cells, particularly chondrocytes, to various scaffold materials in different culture environments, and thus have attempted to demonstrate the effects on cellular metabolism. Grande et al. cultured chondrocytes on non-woven PGA (fibers 14 μm in diameter and 200 μm pores), woven PLA-PGA copolymer (Vicryl™, 210 μm pores), knitted nylon (90 μm pores), and non-woven fibrillar type I collagen (100 to 300 μm pores) in static culture and in a closed-loop recirculating system. The greatest number of cells attached to the collagen scaffold, while the least number attached to the nylon scaffold; all of the synthetic materials displayed cells of both fibroblastic and chondrocytic morphologies after 5 weeks of culture. Additionally, the synthetic materials resulted in the increased rate of production of proteoglycans compared to the collagen scaffold, but collagen scaffolds stimulated the synthesis of collagen compared to the others [47]. Buschmann et al. prepared agarose gel scaffolds for chondrocyte seeding, and they reported that cell density, GAG concentration, and stiffness of the engineered tissue (following 5 week culture) was about 25% that of calf articular cartilage [49].

Though scaffolds in the form of gels and glues are conducive to cell growth [41], most are mechanically weak and cannot withstand handling. There are a number of fabrication techniques routinely employed to create three dimensional scaffolds with desired features including high porosity, pore interconnectivity, large surface area, and mechanical integrity [50]. In fiber bonding a non-woven mesh of polymer fibers is chemically treated and then melted to bond the fibers at their cross-points. Similarly, in spray casting external fibers of a non-woven mesh are bonded at their cross-points by a coating of polymer when they are sprayed with a polymer/solvent solution and the solvent is removed (the solvent does not dissolve the fibers of the mesh). Solvent casting and particulate leaching involve the use of particulates that are dispersed within a polymer solution that is cast on a surface; the solvent is removed and the particulates are leached from the remaining polymer solid. For membrane lamination, multiple scaffolds (membranes) are created using solvent casting and particulate leaching and then bonded together (on top of one another) to form a more complex three dimensional structure. Melt molding involves heating a polymer solution (placed in a mold) containing particulates above its glass transition temperature followed by leaching of the particulates in a water bath. As another fabrication technique, polymers can be extruded into tubular shapes or fibers via heating and applying pressure to push the heated polymer through an opening; non-woven, fibrous meshes can be created or solvent casting and particulate leaching can be combined with extrusion to create porous solid structures. One form of gas foaming involves the saturation of polymer discs with carbon dioxide in a high pressure chamber followed by a rapid drop in pressure to ambient level. Freeze drying is typically performed

on a frozen emulsion of two immiscible, but homogenized solutions in a lyophilizer via the process of sublimation. Phase separation can be performed on liquid-liquid or liquid-solid preparations via such techniques as vacuum drying or freeze drying. Finally, in electrospinning a charged polymer solution is passed through an electric field; as the solvent evaporates, a dry polymer fiber is collected to form a non-woven, fibrous mesh. Many of these techniques involve the use of toxic solvents, require significant amounts of time, cannot be performed with bioactive molecules, may result in closed pore morphology, or are unable to form complex three dimensional shapes; thus, many of these techniques do not lend themselves easily or economically to mass production.

Though the choice of scaffold material and fabrication technique have not been agreed upon, there is consensus that mechanical stimuli are necessary in the tissue engineering of articular cartilage though these details are still to be determined [4, 15, 35, 51, 52]. Chondrocytes in native articular cartilage experience mechanical stimulation including compressive and shear forces and hydrostatic pressure. Investigations *in vitro* of mechanical stimulus/response mechanisms include the effect of hydrostatic pressure on the protein production of cells grown in monolayer, the effect of direct compression of cell-seeded scaffolds on proteoglycan and collagen production, and the effects of low-shear on protein production as a result of more effective diffusion of oxygen and nutrients into the scaffolds within the culture environments. For example, dynamic, direct compression has been found to increase ECM synthesis and produce greater equilibrium moduli [35]. Buschmann et al. exposed agarose gel scaffolds with chondrocytes to static (maintained at a specific thickness) and dynamic (a sinusoidal displacement with a specific amplitude)

compression up to 47 days to study the effects on protein synthesis rates; dynamic compression showed enhanced synthesis of GAGs and collagen [53]. Carver and Heath designed a perfusion system that intermittently compressed the chondrocyte-seeded PGA scaffolds; in general, the compression reduced cell proliferation and increased GAG and collagen synthesis within the scaffolds [54].

Bioreactors (in which cell-seeded scaffolds are cultured) have become quite popular in the tissue engineering of articular cartilage since the systems allow the control of *in vitro* culture conditions (including temperature, pH, oxygen concentration, pressure, and biochemical factors in the growth medium) and provide low-shear mechanical stimuli to cells [4, 13, 41, 52, 55-58]. For example, it has been shown that dynamic deformational loading or shear of chondrocytes within a three-dimensional structure results in GAG synthesis, and strain of mesenchymal progenitor cells within a collagen gel results in cell alignment and oriented collagen fibers [57]. Theoretically, a bioreactor can provide an initial uniform distribution of cells to be seeded onto the scaffolds placed within the bioreactor chamber. Additionally, mass transport can be controlled to more directly influence cell function. Vunjak-Novakovic et al. have performed extensive bioreactor studies of tissue engineered articular cartilage to reveal that the biochemical and mechanical properties of the tissue can be controlled by the duration and conditions of the bioreactor culture [55, 56, 59, 60]. In most of the studies, the scaffolds consisted of extruded, biodegradable PGA in a non-woven mesh structure (13 μm fiber diameters), measuring 5-10 mm diameter x 2-5 mm thick, with a typical void volume of 96%. An initial seeding density of 5-7x10^6 freshly isolated chondrocytes per scaffold was typical,

and seeding was performed over 3 days in well-mixed spinner flasks. Cell-polymer structures as well as harvested cartilage explants were placed into static flasks (no movement of scaffolds or medium), mixed flasks (no movement of scaffolds, but turbulent flow of medium), or rotating bioreactors (scaffolds suspended in laminar flow of medium) for culture for 6 weeks (standard culture conditions, with 5-10% CO_2, were maintained within the incubators and 50% of the culture medium was replaced every 2-3 days). An increase in GAG content and total collagen amount was seen over the 6 weeks for the cell-scaffold structures in all three culture conditions, but the hydrodynamic environment of the rotating bioreactor demonstrated the largest increase compared to the other two culture conditions due to the mechanical stimulation provided to the cells. The primary determinant of GAG and collagen content in these bioreactor studies was the presence of mixing within the culture vessels as opposed to the intensity of the mixing [61]. Novel bioreactors have been designed and developed by other groups with the goals of lowering the shear stress, allowing more controlled gas and nutrient exchange, and creating a large growth area to give room for more or larger scaffolds [57].

There are a number of proteins that have an influence on the differentiation and phenotypic expression of chondrocytes, including the TGF-β family, insulin-like growth factor (IGF-1), bone morphogenic proteins (BMPs), fibroblast growth factors (FGFs), and epidermal growth factor (EGF) [35, 42]. This diverse group of growth factors influences chondrogenesis of mesenchymal cells during embryonic development [4]. These molecules can have the following effects: proliferation induction, increased ECM synthesis and deposition, and chondrogenesis induction by MSCs. Both TGF-β1 and IGF-1 can

stimulate both GAG synthesis and type II collagen synthesis. Incorporation of such growth factors or other biological signaling moiety (such as the cell adhesion peptide RGD, or arginine-glycine-aspartic acid) gives the scaffold the biological activity to elicit desired cellular responses.

Electrospinning in the Tissue Engineering of Articular Cartilage

Many of the scaffolds tested thus far have not resulted in regenerated tissue with the biochemical or morphological properties of native normal articular cartilage [36]. Due to limited availability of suitable donor tissue and the desire to match the mechanical properties of the implant with the mechanical requirements *in vivo*, investigators have recently become interested in designing electrospun scaffolds for the tissue engineering of articular cartilage.

Electrospinning is a process that was first conceived in the late 19th century by Lord Rayleigh, with the first US patent being issued in 1934 to Formhals [62, 63]. In electrospinning (Figure 13), a polymer solution within a reservoir is charged via application of an electric potential (kilovolt range) to an electrode (nozzle) attached to the reservoir. A ground target is placed some distance away from the nozzle such that an electric field is created. As the intensity of the electric field is increased, the force of electrostatic repulsions in the solution exceed the force of its surface tension and a liquid jet is formed at the nozzle tip; the conical shape of solution seen at the nozzle tip is known as the Taylor cone. The liquid jet is ejected from the nozzle and attracted to the grounded target; the trajectory of the jet is dictated by the electric field and the charges within the

polymer. If there are significant chain entanglements within the polymer solution and the solvent is relatively volatile, evaporation of the solvent yields the formation of a fiber. The fiber collects on the target to form a fibrous, non-woven fabric/structure. If the process is at steady state, then electrospinning is producing a single, continuous fiber that is collected. The adjustment of several electrospinning parameters allows for further control and refinement of scaffold characteristics [64, 65]. Altering the concentration or molecular weight (and, hence, viscosity and polymer chain entanglements) of the polymer solution affects fiber diameter: the higher the concentration the larger the diameter of the fibers. Varying the geometry of the grounded target will change the size and shape of the electrospun scaffold. Scaffold thickness is dependent on the volume of polymer solution electrospun: greater volumes equate to thicker specimens. Fiber alignment is controlled by rotation of the grounded target: a high rotational speed will draw the fibers into a highly aligned formation parallel to the direction of rotation, while low rotational speeds allow the fibers to collect randomly on the grounded target. Structures composed of multiple polymeric components can be created by electrospinning the components simultaneously from the same nozzle or from different nozzles (resulting in one layer) or one at a time on top of one another to create multiple layers [66].
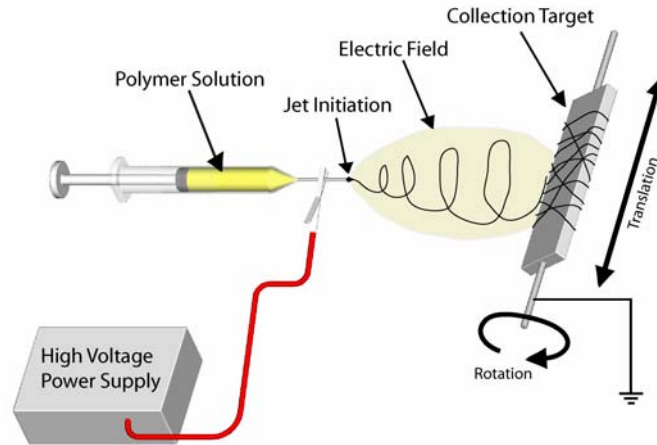
Figure 13. Schematic of the electrospinning apparatus showing the basic components.

Type II collagen was first electrospun for potential use in cartilage tissue engineering by Matthews et al. since type II collagen accounts for 50-80% of the dry weight of articular cartilage. Type II collagen from chicken sternal cartilage dissolved in 1,1,1,3,3,3-hexafluoro-2-propanol (HFP) was electrospun at 40 mg/mL and 100 mg/mL, which resulted in fiber diameters of 110 ± 90 nm and 1750 ± 900 nm, respectively. The collagen scaffold was fixed in glutaraldehyde vapors prior to seeding with normal human articular chondrocytes. Histological analysis showed that the cells were evenly distributed across the scaffold thickness. After two weeks in culture in a rotary cell culture system, there was a nearly confluent layer of cells on the external seeded surface, and there was some degree of remodeling of the matrix [67]. Shields et al. electrospun type II collagen in HFP, cross-linked the scaffolds with glutaraldehyde vapor, performed mechanical testing of dry uncross-linked samples, and seeded the cross-linked samples with adult human articular chondrocytes (scaffolds were statically cultured for 7 days). Average fiber

diameter was 496 nm for the uncross-linked scaffolds and 1.6 μm for the cross-linked

scaffolds. Tensile mechanical properties of the uncross-linked samples were as follows: a

tangential modulus of 172.5 ± 36.1 MPa, an ultimate tensile strength of 3.3 ± 0.3 MPa, and

an ultimate strain of 0.03 ± 0.005 mm/mm. Chondrocytes were shown to adhere and

infiltrate the thickness of the scaffolds [68].

Other materials have also been electrospun for the tissue engineering of cartilage.

Bhattatai et al. electrospun alginate-poly(ethylene oxide) (PEO) in water solutions to create

scaffolds with mechanical properties within the range of articular cartilage following cross-

linking with calcium chloride [69]. Cellular compatibility was investigated (3 days) with

chondrocytes and resulted in the cells attaching well, forming clusters, and maintaining

their round morphology [69]. Li et al. electrospun poly(ε-caprolactone) (PCL), at 0.14

g/mL in tetrahydrofuran (THF) and dimethylformamide (DMF) (700 nm diameter fibers),

to investigate the responses of fetal bovine chondrocytes *in vitro* [70]. The chondrocytes

on the PCL scaffold appeared round and adhered to and extended along the fibers; the cells

expressed cartilage-associated ECM genes. PCL was found to provide better mechanical

and structural properties with a better degradation profile for culturing these cells. Results

showed that cellular proliferation and differentiation were controlled by the morphology of

the scaffold and the composition of the medium which support the differentiation state of

the cells. This is as opposed to cultures in monolayers which do not maintain the

chondrocytic phenotype [70]. In another study, Li et al. electrospun PCL again at 0.14

g/mL in THF and DMF, but the scaffolds were seeded with human bone marrow derived

mesenchymal stem cells (MSCs) and maintained in medium supplemented with

recombinant human transforming growth factor-β1 (TGF-β1) prepared to promote

chondrogenesis [71]. In the presence of TGF-β1, the three-dimensional PCL scaffold

induced greater expression of sulfated glycosaminoglycan synthesis and collagen types II

and IX were up-regulated; the cell count remained constant after 21 days. Chondrogenesis

was induced and the electrospun scaffold (cell-matrix interactions) proved more effective

at supporting chondrogenesis than the more commonly used method of MSC

chondrogenesis in a high density cell pellet culture (cell-cell interactions) [71]. Recently,

Li et al. electrospun six different poly(α-hydroxy ester) polymers, including PGA, poly(L-

lactic acid) (PLLA), poly(D,L-lactic acid) (PDLLA), the copolymer poly(D,L-lactic-*co*-

glycolic acid) at two ratios (50:50 and 85:15) (PLGA5050 and PLGA8515), and PCL.

These polymers were electrospun from HFP for PGA (4 g/40 mL), a 50:50 mix of THF

and DMF for PDLLA (4 g/11.4 mL), PLGA5050 (4 g/11.4 mL), PLGA8515 (4 g/13.4

mL), and PCL (4 g/28 mL), and a 10:1 ratio of chloroform to DMF for PLLA (4 g/27.5

mL). Tensile testing was performed on dry samples with the following results.

PLGA5050 and PGA scaffolds had the highest Young's modulus and PLLA and PCL were

the least stiff scaffolds. PLGA5050 and PGA also had the highest values of yield stress,

while PCL had the highest value of yield strain. The different materials had varying

degradation rates, with PCL and PLLA scaffolds maintaining their structure for the full 42

days of incubation in PBS at 37ºC. PDLLA, PLGA5050, and PLGA8515 all shrank after 3

days, with PLGA5050 showing the most severe shrinkage. For the PLLA and PCL

scaffolds, in which degradation occurred the slowest, the seeded chondrocytes adhered to

the fibers and began migrating through pores during the 7 days of incubation. Results

showed that the properties of the electrospun fibers are dependant upon the polymer used [72]. Shin et al. electrospun 25 wt% solutions of 75:25 PLGA in a 1:1 mixture of DMF and THF resulting in a mean fiber diameter of 550 ± 150 nm and a porosity of 80.68%. Tensile testing of dry samples revealed the following mechanical properties: a mean tensile modulus of 95.53 ± 6.60 MPa, a mean ultimate tensile stress of 3.10 ± 0.49 MPa, and a mean ultimate tensile strain of 78.95 ± 12.63 %. There was little degradation of this scaffold even after 7 weeks of incubation. Their conclusion is that these mechanical properties, though not quite equivalent to those of cartilage, would be able to be implanted and can support tissue regeneration [73]. 1% (w/v) chitosan was mixed with a small amount of PEO in an undisclosed solvent and electrospun by Subramanian et al. Tensile testing of wet samples gave results of 2.25 ± 0.67 MPa for the modulus and 0.63 ± 0.16 MPa for the ultimate tensile strength. Following cell seeding, canine chondrocytes attached to the fibers of the electrospun scaffold, and it was concluded that cell growth was not inhibited by the electrospinning reagents or process [74].

These investigations were aimed at evaluating the usefulness of different electrospun materials for the application of articular cartilage tissue engineering. A variety of materials, natural and synthetic polymers, can be electrospun and the properties of the resulting scaffolds can be modulated via polymer selection, concentration, and blending. Thus far, a number of investigators have shown positive and promising results with chondrocyte-scaffold interactions and scaffold mechanical properties.

Scaffold Design

The native ECM network creates a dynamic, three-dimensional microenvironment in which cells are maintained. The ECM functions as both the structural matrix for tissue as well as the regulator of cellular activity via cell-ECM communications. Signals are transmitted between the cell nucleus and the ECM enabling communication between both for cell adhesion, migration, growth, differentiation, programmed cell death, modulation of cytokine and growth factor activity, and activation of intracellular signaling [75]. The influence of the ECM on cellular activities occurs via binding of specific factors to specific ECM molecules and binding of ECM molecules to cell surface receptors known as integrins, which then influence local release of growth factors or separation of molecules (for cell attachment, spreading, and growth) [76, 77]. Beginning as soluble components processed within the cells, the ECM is secreted from the cells and is highly regulated by and specific to each tissue type and developmental stage [78]. With the goal of imitating nature [6], the engineered scaffold must be able to interact with cells in three dimensions and facilitate this cell-matrix communication. In the native tissues, the structural ECM proteins (20-500 nm in diameter) are 1 to 2 orders of magnitude smaller than the cell itself, which allows the cell to be in direct contact with many ECM fibers, thereby defining its three dimensional orientation. The environmental conditions must be appropriate such that signals can be exchanged between cells and between cells and the environment with the goal of restoring tissue function. Thus, the scaffold material, the scaffold fabrication technique, and the tissue development methodology must be selected such that *in vivo* chondrocyte-matrix interactions are simulated *in vitro*.

The three dimensional scaffold provides a structure to which cells can attach, migrate, and grow giving the regenerating tissue an initial predefined shape and size. These engineered ECMs, or scaffolds, should be designed to conform to a specific set of requirements [36, 79-83]. The first requirement is that the material must be biocompatible and function without interrupting other physiological processes. This functionality includes an ability to promote normal cell growth and differentiation while maintaining a three dimensional orientation/space for the cells. Secondly, the scaffold should not promote or initiate any adverse tissue reaction; this includes any degradation products. Once implemented *in vitro* or *in vivo*, the material should either be removed via degradation and absorption or incorporated via innate remodeling mechanisms, leaving only native tissue. Degradation should be at an appropriate rate such that the newly regenerating tissue can support itself and allow effective diffusion of nutrients and wastes. The scaffold must possess the mechanical properties necessary to withstand not only the forces experienced *in situ* at the joint (i.e. site of implantation) but also the handling/manipulation forces experienced during the implantation procedure. Additionally, the scaffold must possess the ability to be retained at the implantation site. If the scaffold has been designed for drug, protein, or cell release, it has to have the proper release profile. In addition, for clinical and commercial success, scaffold production should be simple yet versatile enough to produce a wide array of configurations to accommodate the size, shape, strength, and other intricacies of the target tissue/organ. Finally, surgeons prefer uncomplicated preparation and handling procedures for any scaffold.

The native ECM fiber components are one to two orders of magnitude smaller than the cell itself, thereby allowing the cell to be in direct contact with many of the fibers defining its three-dimensional orientation. Thus, the determination of suitable pore size, total porosity, and ECM fiber size may be crucial in determining the success or failure of a tissue-specific tissue-engineering scaffold. Highly porous scaffolds, such as those with porosities greater than 90%, provide sufficient space for cellular infiltration where the cells perform actively and exchange nutrients and wastes with the environment [84].

Material Selection: Type II Collagen

As described above, there are a number of natural and synthetic materials that have been investigated for use in scaffolds for cartilage tissue engineering. Frenkel and Di Cesare have composed a table presenting a summary of *in vivo* findings of the performance of various materials (autologous, natural, and synthetic) (see Appendix A) [36]. Of particular interest for this research is type II collagen. In general it is known that cell-collagen interactions influence cell growth and differentiation depending on how well the cells are able to penetrate the fibrillar collagen ECM [85].

Collagenous scaffolds (of various types of collagen) are of particular interest in tissue engineering because these scaffolds mimic the biochemical and ultrastructural properties of the native extracellular matrix (ECM) of tissues, which is known to influence cell behavior [75, 85]. Since type II collagen is the predominant collagenous component of articular cartilage, it is of interest for use in scaffolds for tissue engineering articular

cartilage [5, 13, 33]. Nehrer et al. fabricated type I collagen-GAG copolymer sponge scaffolds (via freeze drying and dehydrothermal cross-linking) and type II collagen-GAG copolymer sponge scaffolds (via reconstituted porcine cartilage and UV irradiation cross-linking), with an average pore diameter of 85 μm and porosity of 85%; the sponges were seeded with autologous chondrocytes, cultured for no longer than 12 hours, and implanted into adult canine models for a 15 week study. The type I and type II collagen structures resulted in increased amounts of reparative tissue, both types resulting in comparable amounts, but the type II collagen scaffold induced a greater percentage of and more uniformly spaced cartilage-like material though it was mostly fibrocartilagenous [33]. Conclusions were drawn that more time is required to reveal if the transitional tissue will eventually convert to hyaline cartilage; also, cell densities and scaffold modifications may influence the reparative qualities of the chondral defects. Previous *in vitro* studies by Nehrer et al. have shown that type II collagen scaffolds have better maintained chondrocyte morphology (spherical instead of elongated and flattened) and resulted in greater GAG production than have type I collagen scaffolds [86, 87]. Lee et al. used similar type II collagen sponges as Nehrer et al. (but with cross-linking in an aqueous solution of 1-ethyl-3-(3-dimethylaminopropyl)carbodiimide hydrochloride and *N*-hydroxysuccinimide) and investigated the implantation (into chondral defects in a canine model) of the chondrocyte-seeded sponges following 4 weeks of *in vitro* static culture. Results showed the large production of hyaline-like tissue (51%) in the defects, a fill volume of 88%, and little histological evidence of the collagen scaffolds after the 15 week implantation period [88]. In a more recent study by Dorotka et al., a collagen membrane

(composed of types I and III collagen on the inner, rough surface and type II collagen on the outer, porous, cell-seeded surface) was prepared and inserted into osteochondral defects already treated with microfracture. More hyaline tissue (as well as fibrocartilage tissue) was observed to grow in these defects over the 4 month study compared to the defects treated with microfracture only or microfracture and non-seeded collagen scaffolds; from 4 to 12 months, however, the amount of hyaline tissue decreased and the repair tissue generally deteriorated [89]. Isolated and purified types I and II collagen have been lyophilized and cross-linked by Pieper et al. to prepare scaffolds (pore sizes ranging from 50 to 100 μm) onto which chondrocytes were seeded and cultured for up to 14 days; results showed cells and some clusters of cells with preserved chondrocytic phenotype throughout the thickness of the type II collagen scaffolds, a cartilaginous-like layer on the surface of the scaffolds (after 14 days of culture), and the presence of newly synthesized GAGs [90]. Shi et al. created sponge-like scaffolds (with open, interconnected pores between 100 and 250 μm, and a porosity of 87%) composed of chitosan and type II collagen via a freeze drying method followed by cross-linking that were cultured *in vitro* for 15 days; the scaffolds sustained the chondrocytic phenotype and the cells formed some clusters and synthesized type II collagen, but the majority of the cells remained on the periphery of the scaffolds [91]. Yang et al. compared the redifferentiation of human chondrocytes cultured in a pellet and on type II collagen-coated filters. The cell on the collagen-coated filters appeared to have improved type II collagen synthesis compared to those in the pellet culture. Additionally, cells on the filters appeared to be more like native chondrocytes

ultrastructurally, and, though cell content decreased in both redifferentiation models, the decrease was less on the filters [92].

The scaffold under investigation in this research is composed only of type II collagen. Only one scaffold material was chosen in order to minimize the variables associated with scaffold design. The other interest in using collagen alone is the finding that the presence of proteoglycans in the ECM can prevent cell adhesion [13].

As with the other collagenous scaffolds, which have been fabricated in numerous ways, particularly as gels and sponges [93-96], freeze-dried solutions of collagen [97, 98], and more recently as electrospun fibrous mats [66-68, 99-103], the type II collagen scaffolds lack substantial strength upon hydration. Thus, the structures must be treated or fixed in some capacity to render sufficient mechanical integrity to the scaffolds [104].

Fabrication Technique: Electrospinning

Conventional polymer processing techniques cannot produce fibers much less than 10 μm in diameter, which is several orders of magnitude greater than the diameter of native ECM fibers, particularly that of collagen. Thus, scientists in tissue engineering have turned to nanotechnology and, specifically, the development of nanofibers, to find solutions to the development of tissue engineering scaffolds. Nanofibers with diameters on the order of 20 to 200 nm mimic the geometry of the sub-micron diameter fibers of the native articular cartilage ECM, specifically the diameters of native type II collagen fibrils [14, 18]. At present, there are only a few processing techniques at the forefront that

successfully produce fibers, and subsequent scaffolds, on the nano-scale; Jayaraman et al. and Smith and Ma have recently reviewed these techniques [105, 106]. Self-assembly involves the spontaneous organization of individual components into an ordered and stable structure with non-covalent bonds [107, 108]. Peptide self-assembling systems that form nanofibers, with diameters ranging from 30 to 50 nm, for applications as tissue engineering scaffolds, have been used by several groups [106-109]. The complexity of the procedure and the low productivity of the method limit self-assembly as a large-scale tissue engineering option [110]. Ma and Zhang have developed a phase separation technique (a thermodynamic separation of a polymer solution into a polymer-rich component and a polymer-poor/solvent-rich component) that produces nano-fibrous three-dimensional scaffolds. An advantage to this technique is the control over macroporous networks within the fibrous matrices [111, 112]. Additionally, fibers with diameters in the range of 50 to 500 nm and porosities exceeding 98% are possible [112]. However, this method is limited to being effective with only a select number of polymers and is strictly a laboratory scale technique [105]. Electrospinning, described previously, is the third technique capable of creating polymeric nanofibers, which can be collected in various orientations to create unique structures in terms of composition and mechanical properties [50, 62, 64]. Electrospinning offers further advantages including being cost effective and capable of mass production [105].

Electrospinning has been chosen as the fabrication technique to create the scaffolds for cartilage tissue engineering in this research. This technique allows control over fiber diameter as a function of polymer concentration (linear relationship); thus, diameters

approaching those of native ECM fibers can be achieved. Pores are created in the electrospun mats by overlapping fibers. The scaffolds must possess appropriate porosity to allow cell penetration and to provide a place for the cells to be housed [84]. The non-woven structure of electrospun meshes have porosities greater than 80% [50]. Historically, in biomaterials and tissue engineering scaffold design, the most commonly held paradigm requires pores larger than 10 microns, and in some cases larger than 100 microns, to allow cellular in-growth and vessel formation [113]. Though pore size should be large enough for the particular cells to be grown within the scaffold, hypotheses have been made that the non-woven structure of the electrospun mats allow migrating cells to maneuver amongst the fibers by actually moving the fibers [84, 101] or that fiber degradation occurs during cell migration [101], both of which suggest pore size may not be absolutely critical for electrospun nanofibrous scaffolds.

Cross-linking: Carbodiimide in Ethanol

Cross-linking can be utilized to tailor degradation rate and biomechanical characteristics (typically to match those characteristics of the tissue designated for regeneration), but it may compromise biocompatibility. The requirement for tissue engineering scaffolds to not elicit any prolonged immune responses has led to research and development of fixation techniques that may prove more biocompatible than popular chemical cross-linking agents including glutaraldehyde, formaldehyde, and epoxy compounds, which have been shown to be cytotoxic because of the reactive moieties that

are covalently coupled between neighboring collagen fibrils [104, 114-116]. Glutaraldehyde, in particular, does offer the advantages of being less expensive, reacting relatively quickly, cross-linking over varying distances, and reacting with a larger number of amino groups present in a protein molecule [114]. It is the most commonly used and accepted agent for the cross-linking of biological tissues, but it has also been implicated in the development of calcification [114, 117, 118].

Our laboratory has previously shown that the electrospinning process can facilitate the assembly of type I collagen molecules into fibrils that demonstrate the characteristic D-period banding pattern [99]. Unfortunately, the native intramolecular and intermolecular crosslinks (via lysyl oxidase [119]) do not form to a significant degree, if at all, among the electrospun fibers. Herein lies several critical issues involved in the cross-linking of electrospun collagen. Upon hydration in any aqueous solution, the electrospun collagenous mats immediately shrink and disintegrate such that the scaffold breaks itself apart but does not dissolve. Thus, cross-linking is a necessity in order to maintain the structural integrity of the scaffold. However, typical protocols for cross-linking electrospun collagen have utilized glutaraldehyde, but even then the scaffolds tend to gel (unless more severe cross-linking protocols are followed) and lose their nanofibrous morphology, which is one of the most important features of the scaffold to begin with. To avoid this, our laboratory has previously electrospun blends of collagen with synthetic polymers [120], which has proven successful in initial cell studies, but it is desirable to be able to work with collagen-only electrospun scaffolds for cartilage tissue engineering.

Thus, a complementary/exogenous cross-linking agent is required if pure collagen electrospun scaffolds are to be utilized as tissue engineering scaffolds.

Choice of cross-linking agent requires knowledge of the reactive group(s) present, typically an amino acid side chain, and appropriate ambient conditions (such as pH, temperature, solvent, etc.) that do not negatively affect the protein [104]. In choosing a cross-linking agent for collagen, heterobifunctional agents, which contain two different reactive groups that are able to directly link two different amino acid side chains [121], are of interest in maximizing the extent of cross-linking. The great interest in heterobifunctional carbodiimides, in particular 1-ethyl-3-(3-dimethylaminopropyl)carbodiimide hydrochloride (EDC), is that these are zero-length cross-linking agents, i.e. the agent itself is not incorporated into the macromolecule. The protonated carbodiimide reacts with the carboxylic functional groups of aspartic and glutamic amino acids and forms the intermediate *O*-isoacylurea, which then undergoes nucleophilic attack by the amine functional groups of lysine and hydroxylysine amino acids on adjacent collagen fibrils. The crosslink, an iso-peptide bond (that mimics the natural peptide bonds in proteins), is formed thereby bridging neighboring polypeptide chains, and a urea derivative is released that can be removed via rinsing [116, 122]. By modifying the ratio of EDC to collagen, the extent of cross-linking can be controlled [104]. EDC has been used to cross-link reconstituted collagen fibrils, i.e. collagen molecules removed from tissues via acid or enzyme extraction that spontaneously form fibrils [90, 123, 124], insoluble collagen, and collagen fibers from intact tissues [104, 122, 125-127]. EDC is suited for use with type II collagen from bovine cartilage because each of the three

α1(II) chains that constitute the triple helical structure consists of 15 lysine, 23

hydroxylysine, 43 aspartic acid, and 87 glutamic acid residues per thousand residues per

chain [128].

A method of cross-linking electrospun type II collagen (highly purified) scaffolds

utilizing carbodiimide in an ethanol solution has been developed to effectively cross-link

the collagen by creating iso-peptide interfibrillar bonds while minimizing the shrinkage of

the collagenous mats [129]. The use of EDC in a non-aqueous solution will cross-link

electrospun type II collagen fibrous matrices in a comparable manner to typical

glutaraldehyde fixation protocols. Ethanol has been used previously with collagenous

materials without report of deleterious effects such as denaturation. Additionally, ethanol

has been used with glutaraldehyde in the treatment of aortic cusps to minimize the effects

of calcification [130]. Pieper et al. have investigated the cross-linking of lyophilized

collagen matrices (extracted from bovine achilles tendon) in the presence of 40% v/v

ethanol to preserve the porosity of the collagen matrix; these matrices resulted in

comparable tensile strengths to matrices cross-linked in aqueous EDC alone [90, 123].

Buttafoco et al. utilized EDC and N-hydroxysuccinimide (NHS) in a 2-morpho-linoethane

sulfonic acid (MES) buffer in 70% v/v ethanol/water for cross-linking electrospun type I

collagen (electrospun from hydrochloric acid with poly(ethylene oxide) and sodium

chloride added).

Tissue Development Methodology

Most often the tissue engineering of articular cartilage involves the use of a scaffold onto which articular chondrocytes or their precursor cells are seeded in order to grow a three-dimensional tissue *in vitro* that can later be implanted into the joint defect [35, 55]. The goal is to achieve *in vitro* chondrogenesis that matches native *in vivo* chondrogenesis and mimics the mechanical and biochemical properties of the native tissue. This *in vitro* chondrogenesis is dependent upon cell type, initial cell density, scaffold characteristics, and culture conditions. For the research presented here, scaffolds created via the electrospinning fabrication technique and then seeded with chondrocytes were maintained in a bioreactor growth environment to investigate a novel approach to articular cartilage tissue engineering (Figure 14). The specific aim of this study was to achieve tissue that likened the mechanical and biochemical properties of the middle zone of articular cartilage since the scaffolds consist of randomly arranged fibers and would not be degraded by the end of the 6 week duration.
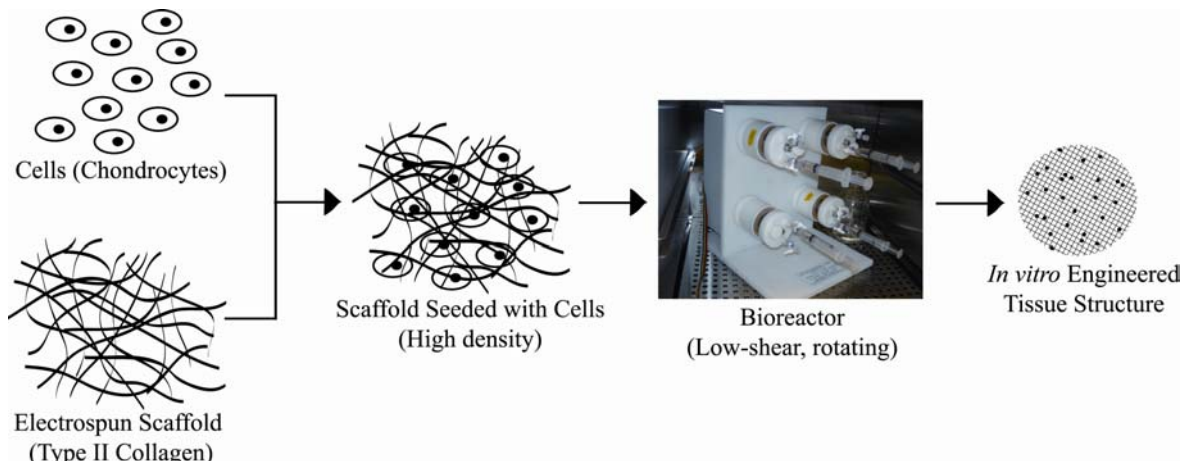
Figure 14. Schematic of the design approach used in this research.

Chondrocytes

In vitro chondrogenesis can be achieved via the seeding of the designed scaffolds with cells capable of synthesizing articular cartilage ECM; these cells are namely chondrocytes or their precursor cells (chondroprogenitor cells derived from marrow, periosteum, or perichondrium). Chondrocytes offer the advantage of already being capable of producing type II collagen and GAGs since they are already of the correct phenotype. Disadvantages include being limited in availability and resulting in donor-site morbidity [45]. Expansion in culture is necessary to obtain sufficient numbers of chondrocytes for seeding, but the main problem is dedifferentiation into a fibroblastic phenotype during culture. This dedifferentiation results in a change in the synthesis of type II collagen to types I and III [43]. Thus, chondroprogenitor cells, and in particular marrow-derived mesenchymal stem cells have been investigated as an alternative [45, 58].

Chondrocytes have been chosen in this research to be seeded onto the scaffolds since these cells are responsible for producing the matrix components (type II collagen and aggrecan) that give the cartilage strength and flexibility. It has been shown that suspension of passaged chondrocytes within a three-dimensional matrix (such as agarose gels and alginate beads) and special culturing techniques (such as suspension cultures, high-density cultures, and co-cultures with primary chondrocytes) can induce redifferentiation from the fibroblastic phenotype back into the chondrocytic phenotype by restoring the spherical shape of the cells [20, 44, 46, 131, 132]. This research will investigate the differentiation status of the chondrocytes on the electrospun type II collagen scaffolds. It still remains to be shown whether chondrocytes that have been passaged several times in monolayer culture can produce tissue of favorable cartilage quality and quantity [46].

Bioreactor

Ideally, since this research is addressing the tissue engineering of the middle zone of articular cartilage, the desired tissue outcome is a uniform spatial distribution of chondrocytes within the three-dimensional scaffold structure. Static culture vessels can result in poor cellular infiltration into the thickness of the scaffold due to poor mass transport of nutrients and wastes; thus, only a layer of cells on one side of the scaffold may develop. Mixed/spinner flasks do provide a well-mixed environment around the cells, but may result in the formation of a fibrous capsule around the scaffold structure because of the turbulent flow and associated shear stress that is too high [57]. On the other hand,

bioreactors are designed to maintain cells and tissue in continuous free fall (simulated microgravity), providing a buoyant, low shear environment (for mechanical stimulation) and high mass transfer of nutrients. The buoyant environment of these devices fosters cell-cell and cell-matrix contacts and the formation of large cell masses. The *in vitro* culture conditions within the bioreactor can be controlled such that the chondrocytes are able to proliferate within the scaffold while degrading and replacing it with new extracellular matrix components. One negative of the bioreactor environment is that cells within the scaffold align in the direction of the shear forces; this is not ideal since the different zones of articular cartilage have cells with different alignments relative to the surface [57]. Other drawbacks to the rotating wall vessel bioreactor include non-uniform growth of tissue and collision of the scaffolds with the vessel wall resulting in cell damage and disturbances with cell attachment and matrix deposition [57]. Despite the disadvantages, the bioreactor growth environment is best for the desired tissue-engineered structure proposed in this particular study [60, 133]. The bioreactor used in this research is the Slow Turning Lateral Vessel (STLV) on the Rotary Cell Culture System (RCCS) (Synthecon™, Inc.), which is a rotating wall vessel in which the scaffolds flow between two concentric cylinders, the inner of which is a silicone gas exchange membrane.

Methods

Collagen Preparation

Type II collagen was extracted from articular cartilage removed from all joints of fetal calf legs [134]. For a detailed checklist of extraction and purification steps, see Appendix B. Unless otherwise stated, all procedures were performed at 4ºC. To a slurry of homogenized cartilage, guanidine (2.5 M final concentration) and Tris (0.025 M final concentration), pH 7.4, were added and stirred overnight. Following four rinses with cold deionized water, the cartilaginous tissue was suspended in 0.5 M acetic acid, pH 2.8. Pepsin (2x, Sigma-Aldrich Chemical Co.) was added to the mixture at 1 g per 1 L solution and incubated overnight. The viscous supernatant containing solubilized collagen was adjusted to pH 7.4; sodium chloride was added to a final concentration of 5 M while stirring slowly. The solution was incubated overnight at room temperature, after which the collagen precipitate was dissolved in 0.05 M Tris/0.2 M sodium chloride, pH 7.4. This solution was dialyzed (Spectrum Spectra/Por 4 RC Dialysis Membrane Tubing 12000-14000 MWCO, Fisher Scientific International Inc.) against a buffer solution containing 0.05 M Tris/0.2 M sodium chloride buffer, pH 7.4, and allowed to equilibrate overnight; this was repeated two additional times. Anion exchange microgranular diethylaminoethyl cellulose separation media, DE-52 (Whatman, Fisher Scientific International Inc.), was added to the collagen solution (at 100 g per liter of solution) and incubated overnight. To

the supernatant, sodium chloride (0.8 M final concentration) and acetic acid (0.1 M final concentration) were added and stirred overnight. The precipitated collagen was dissolved in 0.1 M acetic acid, and the resulting solution was dialyzed against a solution containing 0.01 M acetic acid overnight with stirring; this was repeated six additional times. Finally, the purified collagen solution was frozen and lyophilized until dry product was obtained.

Collagen Purity and Apparent Molecular Weight

Isolated (lyophilized) and electrospun type II collagen were dissolved in 50 mM acetic acid solution at a concentration of 4 mg/mL. These solutions were analyzed by SDS-PAGE gel electrophoresis under denaturing conditions for purity and apparent molecular weight determination. Briefly, 40 µg of purified or electrospun collagen were prepared by the addition of 1X SDS sample buffer and boiled for 3 minutes. The samples were resolved using an 8-16% gradient SDS-PAGE gel (Criterion™ precast gel, BioRad) and visualized using GelCode® blue stain reagent (Pierce).

Electrospinning

The lyophilized collagen was dissolved in 1,1,1,3,3,3 hexafluoro-2-propanol (HFP, TCI America, Portland, OR) at concentrations of 60, 80, 100, and 120 mg/mL at room temperature; this concentration range was previously determined as the electrospinning range for type II collagen [135]. The collagen solution was electrospun to create randomly-oriented, non-woven, fibrous mats. Figure 13 illustrates the electrospinning process. The apparatus used includes a syringe pump (KD Scientific), a high voltage

power supply (Spellman CZE1000R, Spellman High Voltage Electronics Corp.), a syringe (Becton Dickinson, plastic) as the reservoir for the polymer solution to which is attached an 18-gauge blunt-end needle, and a 303 stainless steel mandrel (7.6 cm length x 2.5 cm width x 1.6 cm thickness) as the collection target. All electrospinning parameters were kept constant, including applied voltage (22 kV), distance between the needle and grounded mandrel (12.7 cm), solution dispensing rate (2 mL/hr), translational speed (2 cm/s over a 7.3 cm distance), and rotational speed (500 rpm for random fiber orientation). There was no grounded plate behind the mandrel. For each mat, 5 mL of solution was electrospun.

Cross-linking of Collagen Scaffolds

The carbodiimide cross-linking solution was prepared by dissolving the solid cross-linking agent, N-(3-Dimethylaminopropyl)-N'-ethyl-carbodiimide hydrochloride (EDC, Sigma-Aldrich Chemical Co.), in pure ethanol (Fisher Scientific Inc.) to the desired concentration of 20 mM. Electrospun mats of each of the 4 concentrations (with approximate dimensions 6 cm length x 2 cm width) were submerged in 20 mL of the EDC solution and incubated with shaking for 18 hours. After cross-linking, the mats were placed in 20 mL of 0.1 M sodium phosphate for 2 hours to hydrolyze any unreacted *O*-isoacylurea intermediates. Finally, all samples were rinsed and soaked in sterile phosphate buffered saline (PBS) for at least 2 hours.

Fiber Diameter and Pore Size Measurement of Dry Scaffolds

Fiber and pore morphologies of the dry (uncross-linked) electrospun mats were viewed with scanning electron microscopy (SEM) using a JEOL JSM-820 JE electron microscope (Japanese Electron Optical Ltd., Japan). A micrograph was taken and digitized with a Hewlett-Packard Scanjet 5550c flatbed scanner and then examined with UTHSCSA ImageTool 3.0 imaging software (NIH shareware) to measure fiber diameter and pore size. Mean and standard deviation were determined from 60 fiber diameter measurements and 40 pore area measurements; calibration for each micrograph was made with the scale bar on the micrograph.

Fiber Diameter, and Pore Size Measurement of Hydrated Scaffolds

Environmental scanning electron microscopy (ESEM) was used to take images of the 60 mg/mL cross-linked mat in the hydrated state. The microscope used was a Philips XL30 ESEM TMP (FEI Company, Hillsboro, OR) purchased under the NSF award # DBI-0098534 at the Duke University, Department of Biology, Scanning Electron Microscopy Lab. For improved image quality, the hydrated sample was blotted slightly to remove excess water such that the sample could be fixed to the sample holder. The grayscale of the digital images taken with the ESEM was inverted to allow for improved viewing of the topography of the mat surface. Mean and standard deviation were determined from 60 fiber diameter measurements and 40 pore area measurements; calibration for the measurement was made with the scale bar on the digital image. There have been problems utilizing the ESEM in the Department of Neurobiology and Anatomy Microscopy Facility

at Virginia Commonwealth University; thus, only the 60 mg/mL scaffold will have

morphology data in the dry and hydrated states for comparison.

Porosity Measurement

Porosity, expressed as the percentage void to total volume, was determined by the

following equation:

$$\text{Porosity} = \left(1 - \frac{\rho}{\rho_0}\right) \times 100$$

where ρ is the calculated density of the scaffold determined by dividing the mass

(measured in the dry state) by the overall volume (measured in the hydrated state) of the

mat and ρ_0 is the density of collagen (1.41 g/cm^3). Three samples were used to determine

the porosity of each scaffold of each concentration.

***Permeability Measurement and Fiber Diameter and Pore Size Determination of
Hydrated Scaffolds***

The permeability of three punches (1 cm diameter) from each cross-linked,

electrospun mat of each concentration was measured in the hydrated state (soaked in PBS

for at least 2 hours at room temperature beyond cross-linking protocol). A meter

developed by Scott Sell based on Ogston's theory of flow through systems of long thin

rods was employed for permeability measurement, and the fluid utilized for the testing was

PBS to mimic the physiologic ionic strength [136, 137]. Permeability, represented as the

Darcy constant (τ), is calculated using the following equation:

$$\tau = \frac{Q \eta h}{F t p}$$

where Q is the volume that flows through in time t (mL/sec), η is the viscosity of the fluid,

h is the thickness of the scaffold, F is the cross-sectional area of the scaffold, and p is the

applied pressure (proportional to the height of the meter). The average fiber diameter (d)

can then be calculated from the Darcy constant as follows:

$$d = \sqrt{k \tau \Phi}$$

where k is a constant determined to be equal to 10 [137], and Φ is the volume fraction of

the collagen in the scaffold. The average pore area (using the assumption of a circular pore

shape) can be determined based on the equation for the average pore radius (R) as follows:

$$R = \frac{0.5093}{\tau^{-\frac{1}{2}}}.$$

Tensile Testing (Stress-Strain Relationship) of Hydrated Scaffolds

Mechanical properties of the cross-linked mats were measured in the hydrated state

(soaked in PBS for approximately 2 hours at room temperature) to show behavior under

approximate physiological conditions. Uniaxial tensile testing of the mats on a MTS

Bionix 200 Mechanical Testing System (MTS Systems Corp., Eden Prairie, MN),

incorporating a 50N load cell with an extension rate of 10.0 mm/minute to failure, was

performed on four "dog-bone" shaped samples (2.67 mm wide at their narrowest width and

a gage length of 7.49 mm) punched from each mat of each concentration. The data

acquisition rate was 20 Hz. The mechanical properties recorded include tangential

modulus, peak stress, and strain at failure, which were calculated by the MTS software TestWorks 4.0.

Scaffold Preparation and Disinfection

From each cross-linked, electrospun mat of each concentration, scaffold discs were punched using a 1.0 cm biopsy punch. The scaffold discs were placed in petri dishes, covered with 100% ethanol, and allowed to soak for 10 minutes. The ethanol was removed with a pipette and the scaffold discs were rinsed with sterile PBS four times (10 minutes per rinse). The scaffold discs were stored in sterile PBS until cell-seeding.

General Culture of Chondrocytes

Clonetics™ normal human articular chondrocytes from the knee (NHAC-kn) were purchased from Cambrex Corporation. The cells were cultured in tissue culture plastic flasks in monolayer (until sufficient numbers were attained) under standard culture conditions: 37ºC at 5% CO_2 and constant humidity in an incubator. Sterile technique was followed and all work was performed in a laminar flow workstation. While in monolayer, the growth media used was Dulbecco's Modified Eagle Medium with Nutrient Mixture F-12 (Invitrogen Corporation) supplemented with 10% fetal bovine serum and 1% penicillin-streptomyocin (10,000 Units/mL each). The cells were used at passage three.

Initial Cell-Seeding Investigation

An initial cell-seeding investigation was performed to determine which method would result in attachment of the most cells with the most uniform distribution. Five scaffold discs total, 1.0 cm in diameter, were punched from a 60 mg/mL cross-linked, electrospun mat. Three discs were placed in a 48-well plate for static culture. 0.25 mL of the media and cell mixture was added to two of the discs at a cell density of 5×10^5 cells/mL media, and 0.25 mL of media alone was added to the third disc (the control with no cells); after about 2 hours, another 0.25 mL of media was added on top of all three discs. A media height of approximately 2 mm was maintained above the scaffold surface, and more media was added if evaporation occurred. Two scaffold discs were placed in a 55 mL bioreactor (Slow Turning Lateral Vessel (STLV) on the Rotary Cell Culture System (RCCS) (Synthecon™, Inc.)) for dynamic culture with an initial cell density of 5×10^5 cells/mL media; rotation was started at 15 rpm and increased to 20 rpm after one day. Both cultures were maintained (under standard culture conditions) for three days so that the growth media did not have to be replaced. The media used in this initial investigation was the same as that described for the general culture of chondrocytes. The cell density used was determined based on previous bioreactor studies by Vunjak-Novakovic et al. [60, 138]. After three days of culture, all scaffolds were removed, placed in 10% formalin, and processed for histology (Hematoxylin and Eosin staining).

Scaffold Seeding and Tissue Culture in Bioreactors

Clonetics™ standard chondrocyte growth media (Cambrex Corporation) was prepared by adding the entire amount of each supplement in the BulletKit (CGM SingleQuots CC-4409) to the basal medium (CC-3217); thus, supplementation included 5% fetal bovine serum, 0.1% gentamicin sulfate amphotericin-B, 0.2% bovine insulin, 0.5% r-human fibroblast growth factor-B, 0.1% transferrin, and 0.2% insulin-like growth factor-1. Twelve scaffold discs, 1.0 cm in diameter, were punched from each cross-linked, electrospun mat of each concentration, for a total of 48 scaffold discs, and soaked in media before cell-seeding. Four 55 mL bioreactor chambers (Slow Turning Lateral Vessel (STLV) on the Rotary Cell Culture System (RCCS) (Synthecon™, Inc.)) were conditioned prior to use (i.e. filled with media, bubbles removed, attached to RCCS in incubator, turned on to rotate, and left about 24 hours in incubator to check for leaks). Nine scaffolds of each concentration were transferred under sterile conditions to one bioreactor chamber (Figure 15) and 3 scaffolds of each concentration were placed in media (without cells) to serve as controls; thus, there were 4 bioreactor chambers each with a different concentration of electrospun type II collagen (Figure 15). Chondrocytes were resuspended in media (to a density of 4.3×10^5 cells/mL media) and added to each bioreactor chamber such that the concentration of cells was 2.6×10^6 cells/scaffold. For improved seeding efficiency and uniformity, the cells were seeded on the scaffolds in this dynamic manner within the bioreactor (as opposed to statically). Three full days were allowed for cell seeding before the media was changed. The media was completely changed about every third day. Three scaffolds of each concentration were removed after 2, 4, and 6 week

culture periods (Figure 15). All culturing was performed under standard culture conditions: 37ºC at 5% CO_2 and constant humidity in the incubator. The rates of rotation necessary to suspend the scaffold discs in continuous free fall were determined experimentally. In general, it was found that a rate of 22 rpm was sufficient to maintain the scaffold discs in free fall during tissue development; by the sixth week, the rate was increased to 25 rpm.
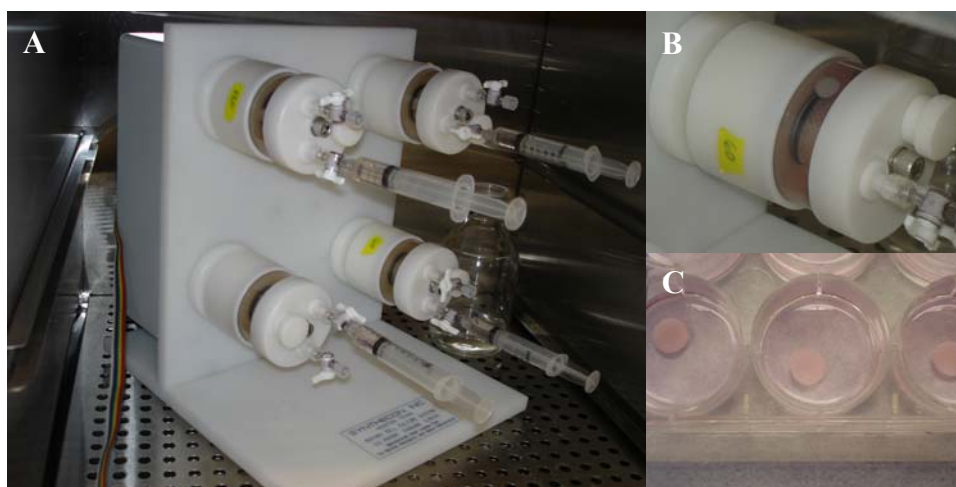

Figure 15. Photographs of the (A) four STLVs on the RCCS in the incubator, (B) a single STLV bioreactor chamber with a scaffold disc rotating within, and (C) the scaffolds removed from the chambers.

Thickness Measurement of Cultured Tissue

After removal from the bioreactor at the 2, 4, and 6 week culture periods, the thicknesses of the scaffold discs were measured with a dial caliper. There were three measurements for each concentration at each time period. These measurements were

compared to the thickness measurements of the scaffolds prior to cell seeding. All scaffold discs were measured in the hydrated state without compression such that fluid was not forced out/removed from the discs.

Stress Relaxation Testing of Cultured Tissue

An indenter (cylindrical, 2 mm diameter, plane-ended, stainless steel) was attached to the MTS Bionix 200 Mechanical Testing System (MTS Systems Corp., Eden Prairie, MN) incorporating a 50N load cell as shown in Figure 16. Indentation was performed in the center of each scaffold disc, perpendicular to the scaffold surface. The discs were placed in a glass petri dish and kept hydrated with growth media. Three discs for each concentration were tested at each time period. The following parameters were used: test speed of 0.5 mm/min, data acquisition rate of 10 Hz, hold time of 200 s, and a preload of 0.015 N for the first run only (to ensure contact); the temperature in the room fluctuated between 75 and 81ºF. The indenter was lowered to contact the scaffold, and five successive ramp-and-hold displacements were applied to achieve 5, 10, 15, 20, and 25% strains. After each ramp-and-hold displacement, stress relaxation was achieved within 200 seconds; the equilibrium stress was calculated with the measured equilibrium load (recorded by the MTS software TestWorks 4.0). An equilibrium stress-strain curve was plotted and the slope of the most linear portion was taken to be the equilibrium stiffness (or indentation stiffness) of the cultured tissue. This method has been used by others investigating the mechanical properties of cartilage [88, 139].
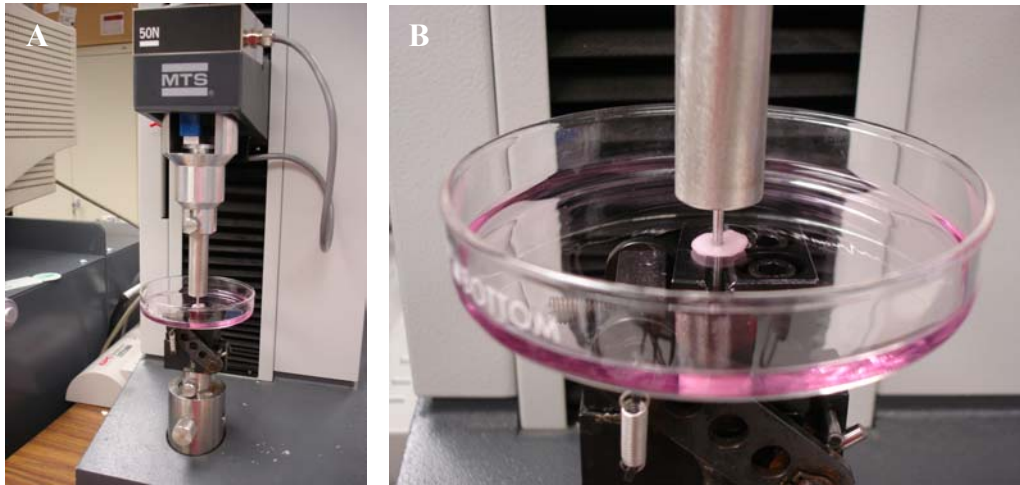
Figure 16. Photographs of the stress relaxation testing with (A) the Mechanical Testing System (MTS) and (B) the indenter.

Cell Density Analysis of Cultured Tissue

The cell density in each scaffold construct per weight (i.e. wet mass) was determined based on DNA concentration via fluorometric analysis with Hoechst 33258 dye [140]. The following chemical preparations were made. Papain was dissolved in sterile PBS at 125 μg/mL, pH 6.0, with 5 mM cysteine·HCl and 5 mM Na$_2$EDTA. A stock solution of Hoechst 33258 dye was made at 1 mg/mL in distilled water and stored in a foil-wrapped container at 4ºC; the working solution of dye was prepared immediately before use by diluting the working solution to 0.2 μg/mL in 10 mM Tris, 1 mM Na$_2$EDTA, 0.1 mM NaCl, pH 7.4, and it was put in an amber bottle. Calf thymus DNA was made at 100 μg/mL in PBS, and dilutions of 0 to 100 μg DNA/mL PBS were prepared for the standard curve. From each of the 3 scaffold discs of each concentration, a 3 mm biopsy punch was taken (see Figure 17). Each biopsy punch was rinsed in PBS, weighed wet with an

analytical balance, placed in a cryovial, and digested in 1 mL papain solution for 13.5 hr at

60ºC. Additionally, cultured chondrocytes (in monolayer) were passaged, counted,

prepared as dilutions, pelleted, and treated the same as the biopsy punches. To 100 μL of

each papain-digested sample, 1 mL of dye solution was added with gentle shaking. 300 μL

of each of these solutions were placed into wells of a 96-well plate. The Hoechst dye

working solution was used as a blank. The FLUOstar fluorometer (BMG Lab

Technologies) with FLUOstar Galaxy software was used in the fluorometric assay in

which the excitation wavelength was 320 nm (ideally would be 365 nm) and the emission

wavelength was 460 nm (ideally would be 458 nm). Eight cycles were run and recorded.

The DNA content per chondrocyte has previously been shown to be 7.7 pg per cell [140].

Figure 17. Photograph of the 3 mm biopsy punches taken from each scaffold disc for cell
density, GAG, type I collagen and type II collagen, and histological analyses.

Glycosaminoglycan (GAG) Analysis of Cultured Tissue

The GAG concentration in each scaffold construct per weight (i.e. wet mass) was determined via use of dimethylmethylene blue dye [86, 141, 142]. The following chemical preparations were made. 16 mg of 1,9-dimethylmethylene blue was dissolved in 1 L of water containing 3.04 g glycine, 2.37 g NaCl, and 95 mL 0.1 M HCl, solution pH 3.0 with an absorbance of 0.31 at 525 nm; the solution was stored in a brown bottle at room temperature. Papain was dissolved at 50 μg/mL in 0.1 M sodium phosphate, 5 mM cysteine·HCl, and 5 mM Na_2EDTA, pH 6.0. Bovine chondroitin sulfate was made at 100 μg/mL in the buffer solution above, and dilutions of 0 to 100 μg/mL were prepared for the standard curve. From each of the 3 scaffold discs of each concentration, a 3 mm biopsy punch was taken (see Figure 17). Each biopsy punch was rinsed in PBS, weighed wet with an analytical balance, placed in a cryovial, and digested in 1 mL papain solution for 2 hr at 60ºC. To a 33 μL aliquot of each papain-digested solution and the standards placed into wells of a 96-well plate, 300 μL of 1,9-dimethylmethylene blue dye solution was added. The buffer solution was used as the blank. The absorbance was measured at 525 nm in the SPECTRAmax® PLUS[384] microplate spectrophotometer (Molecular Devices). Pipetting, mixing, and measurement were performed as quickly as possible due to the instability of the dye color.

Type II Collagen Synthesis in Cultured Tissue

From each of the 3 scaffold discs of each concentration, a 3 mm biopsy punch was taken (see Figure 17). Each biopsy punch was rinsed in cold distilled water, weighed wet

with an analytical balance, placed in a cryovial, and incubated in 1 mL of cold distilled

water at 4°C overnight. The swollen tissue was resuspended in 0.5 mL of 3 M guanidine

hydrochloride/0.05 M Tris-HCl buffer, pH 7.5, and mixed on a rocker at 4°C overnight.

The tissue was centrifuged for 3 min at 10,000 rpm, and the precipitate was washed with

cold distilled water three times and then resuspended in 0.8 mL of 0.05 M acetic acid

containing 0.5 M NaCl, pH 2.9-3.0 (adjusted with formic acid). 0.1 mL of pepsin solution

(10 mg/mL dissolved in 0.05 M acetic acid) was added to each sample and mixed at 4°C

for 48 hours. 0.1 mL of 10X TBS (1.0 M Tris/2.0 M NaCl/50 mM $CaCl_2$) was then added

and the pH was adjusted to 8.0 with 1 N NaOH. Finally, 0.1 mL of pancreatic elastase (1

mg/mL dissolved in 1X TBS, pH 7.8-8.0) was added and mixed at 4°C overnight on a

rocker. The samples were centrifuged at 10,000 rpm for 5 min and the supernatants were

collected (the tissues appeared completely solubilized). Until tested with the type II

collagen ELISA, the samples were kept frozen at -20°C.

The Native Type II Collagen Detection Kit by Chondrex, Inc. (Redmond, WA) was

used to perform an ELISA on the digested tissue samples in order to quantify the amount

of type II collagen in the cultured tissue per weight (i.e. wet mass). Briefly, each of the

following chemicals was consecutively placed in wells of a 96-well plate provided in the

kit, allowed to incubate, and then rinsed away with the wash buffer provided in the kit: a

capture antibody (100 µL per well, incubated at 4 °C overnight), the samples and standards

(dilutions were prepared from the type II collagen standard provided in the kit) (100 µL per

well, incubated at room temperature for 2 hours), a detection antibody (100 µL per well,

incubated at room temperature for 2 hours), and Streptavidin Peroxidase (100 µL per well,

incubated at room temperature for 1 hours). Tablets of urea H_2O_2 and o-phenylenediamine (OPD) chromagen were dissolved in water and added to each well (100 μL per well, incubated at room temperature for 30 min); the reaction was stopped with 2N sulfuric acid (50 μL per well). Optical density values were measured with the SPECTRAmax® PLUS[384] microplate spectrophotometer (Molecular Devices) at 490 nm.

Type II/Type I Collagen Ratio in Cultured Tissue

From each of the 3 scaffold discs of each concentration, a 3 mm biopsy punch was taken (see Figure 17). Each biopsy punch was rinsed in cold distilled water, weighed wet with an analytical balance, placed in a cryovial, and incubated in 1 mL of cold distilled water at 4ºC overnight. These punches were processed exactly the same as described above for the type II collagen analysis. The samples were kept frozen at -20 ºC until tested with the type I collagen ELISA.

The Human Type I Collagen Detection Kit by Chondrex, Inc. (Redmond, WA) was used to perform an ELISA on the digested tissue samples in order to quantify the amount of type I collagen in the cultured tissue per weight (i.e. wet mass). The procedure for this kit is exactly the same as described above for the type II collagen analysis except that the capture and detection antibodies are specific for type I collagen. After quantifying the amounts of type I collagen in each sample, the ratio of type II to type I collagen can be calculated for each electrospun type II collagen concentration.

Histological Evaluation of Cultured Tissue

From each of the 3 scaffold discs of each concentration, two 3 mm biopsy punches were taken (see Figure 17). All of these punches were placed in 10% formalin and processed for histology; one of the two punches from each scaffold disc was stained with Hematoxylin and Eosin (H&E) and the other with Masson's Trichrome. For each punch, a slide with nine cross-sectional slices was prepared for viewing with a light microscope. Cellular distribution within the scaffolds and cellular morphology was assessed qualitatively.

Statistical Analysis

Statistical analysis was performed on all data recorded in the experiments described above. Unless otherwise stated, all statistical analysis was based on a one-way analysis of variance and a Tukey-Kramer pair-wise multiple comparison procedure (with an a priori significance level of $\alpha = 0.05$) performed with the JMP$^{\circledR}$IN 4.0.3 statistical software package (SAS Institute, Inc.). Graphs of the results were constructed with Microsoft Excel 2000. The goals of the statistical analysis were as follows: to determine if the electrospun collagen concentration had significantly different influences on the fiber diameter, pore size, permeability, and mechanical properties of the mats, and to determine if the electrospun collagen concentration (i.e. resulting fiber diameter and pore size) and/or the culture time had any effects on the mechanical properties of and the cellular responses within the cultured tissue.

Results

The results of the following are given in this section: the purity of the type II collagen, the physical characterization of the scaffolds, the biomechanical testing of the electrospun mats and scaffolds (uniaxial tensile and stress relaxation), the biochemical characterization of the scaffolds, and the histological analysis of the scaffolds. Additionally, comments are made regarding the results of the statistical analysis; data from the statistical analysis is given in Appendix C.

Collagen Purity

Type II collagen has successively been extracted and purified from fetal calf legs for use in this research. Figure 18 gives the results of the SDS-PAGE; the apparent molecular weight, determined to be 150 kDa, and the purity of the collagen samples are consistent with the type II collagen standard supplied by the University of Tennessee, RDRCC Collagen Core Center [134]. The stained band for the electrospun sample is a result of a more dilute solution loaded into the gel.
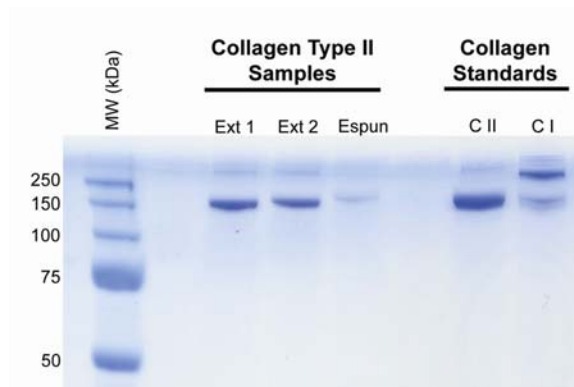
Figure 18. SDS-PAGE analysis of the purified collagen from two different extractions (Ext 1 and Ext 2) and of electrospun collagen (Espun) was conducted to determine the apparent molecular weight and purity. The 150 kDa bands of Ext 1, Ext 2, and Espun are consistent with the molecular weight of the type II collagen standard (C II) and appear to be homogeneous.

Physical Characterization of Dry and Hydrated Scaffolds

Figure 19 gives SEMs of the dry electrospun mats of type II collagen prior to cross-linking, and Figure 20 shows the ESEM of the hydrated 60 mg/mL type II collagen cross-linked, electrospun mat. The handling characteristics of the electrospun mats, immediately removed from the mandrel, are such that the mat can be gently manipulated by hand without permanent deformation to the structure. Table 2 gives the fiber diameter, pore size, porosity, and permeability measurements of the dry (uncross-linked) and hydrated (cross-linked) scaffolds before any culturing was performed. To better illustrate the relationship between electrospinning solution concentration and fiber diameter and pore area, Figure 21 gives the trend lines produced using the data. A linear relationship does exist between concentration and fiber diameter measured using the scanning electron micrographs, but no other linear relationships exist, particularly not between concentration and pore area. At $P<0.0001$, there

is a statistically significant difference between all of the diameter means (for each concentration) measured from the scanning electron micrographs, and there is a significant difference between the 60 mg/mL concentration mean fiber diameter measurements for dry and hydrated mats measured with SEM and ESEM, respectively. For the diameter calculations made using the permeability data, the following significant differences were determined: the 60 mg/mL concentration is different from the 100 mg/mL and the 120 mg/mL concentrations, and the 80 mg/mL concentration is different from the 100 mg/mL and the 120 mg/mL concentrations. The only significant difference calculated within the pore area measurements made with SEM is between the mean pore areas for the 60 mg/mL and the 100 mg/mL concentrations; there is no significant difference between the 60 mg/mL concentration mean pore area measurements for dry and hydrated mats measured with SEM and ESEM, respectively. The mean pore area values determined from the permeability data are all statistically significantly different from one another except for the 60 mg/mL and 80 mg/mL concentrations which are not significantly different from each other. The porosity of all of the electrospun mats falls between 84 and 90%; none of the porosity means for the different concentrations are statistically different from one another. There is a trend toward increasing permeability as concentration increases with the exception of the 120 mg/mL concentration. Additionally, the mean permeability values are all statistically significantly different from one another except for the 60 mg/mL and 80 mg/mL concentrations which are not significantly different from each other.
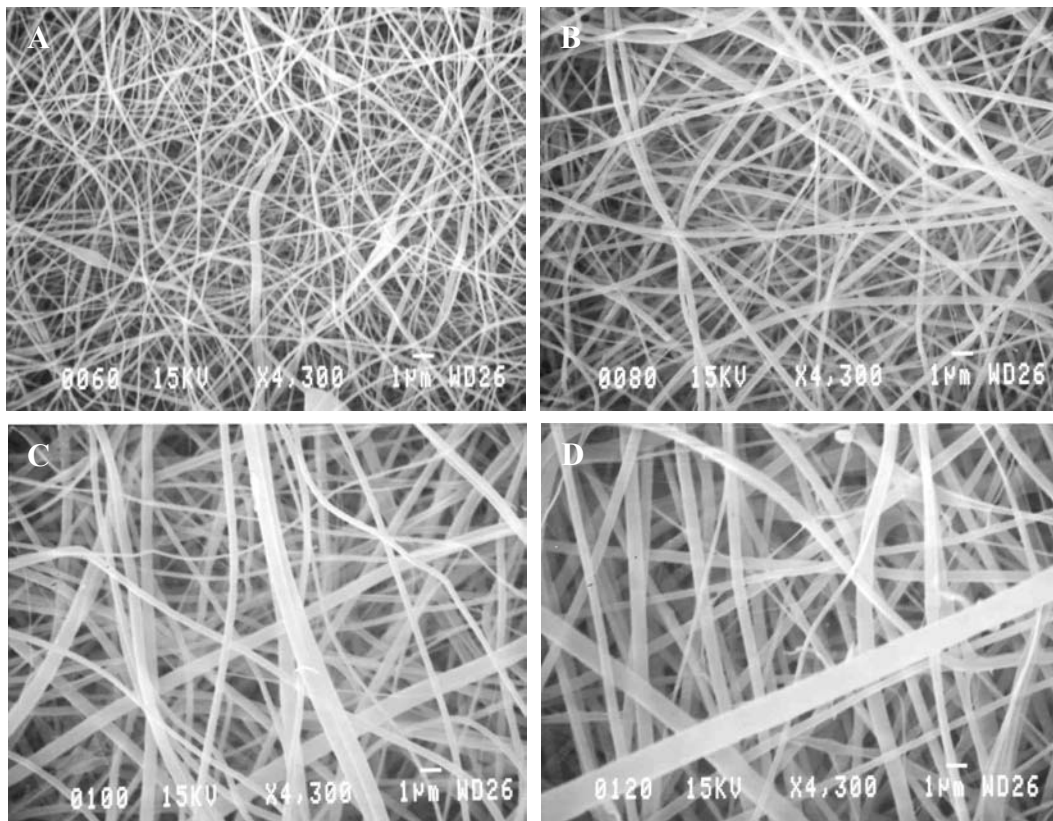
Figure 19. Scanning electron micrographs of dry (uncross-linked) type II collagen electrospun mats at (A) 60 mg/mL, (B) 80 mg/mL, (C) 100 mg/mL, and (D) 120 mg/mL (scale bar is 1 µm).

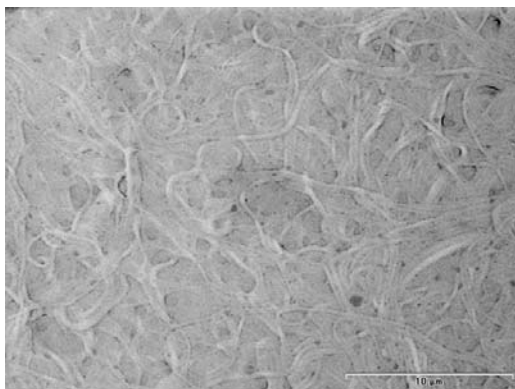Figure 20. Environmental scanning electron micrograph of hydrated (cross-linked) type II collagen electrospun mat at 60 mg/mL (scale bar is 10 µm).

Table 2. Fiber diameter, pore size, porosity, and permeability measurements for the type II collagen electrospun mats; results are given as mean ± standard deviation.

Measurement	Measurement Technique	Electrospun Concentration			
		60 mg/mL	80 mg/mL	100 mg/mL	120 mg/mL
Fiber Diameter (nm)	SEM (dry)	107 ± 38	184 ± 74	309 ± 12	446 ± 232
	ESEM (hydrated)	232 ± 57	—	—	—
	Permeability Meter	289 ± 94	318 ± 41	618 ± 79	592 ± 45
Pore Size (μm²)	SEM (dry)	1.76 ± 1.76	2.12 ± 1.73	3.17 ± 2.44	2.92 ± 2.28
	ESEM (hydrated)	1.68 ± 1.55	—	—	—
	Permeability Meter	0.00055 ± 0.00012	0.00080 ± 0.00030	0.00282 ± 0.00029	0.00181 ± 0.00034
Porosity (%)	Dry mass/wet volume	87.3 ± 6.4	89.1 ± 2.1	88.8 ± 2.6	84.1 ± 0.5
Permeability $\frac{(x10^{-4}\,D)}{(x10^{-13}\,m^4/Ns)}$	Permeability Meter	6.82 ± 1.45 / 7.56 ± 1.61	9.91 ± 3.73 / 11.0 ± 4.1	35.0 ± 3.6 / 38.8 ± 4.0	22.5 ± 4.2 / 24.9 ± 4.6
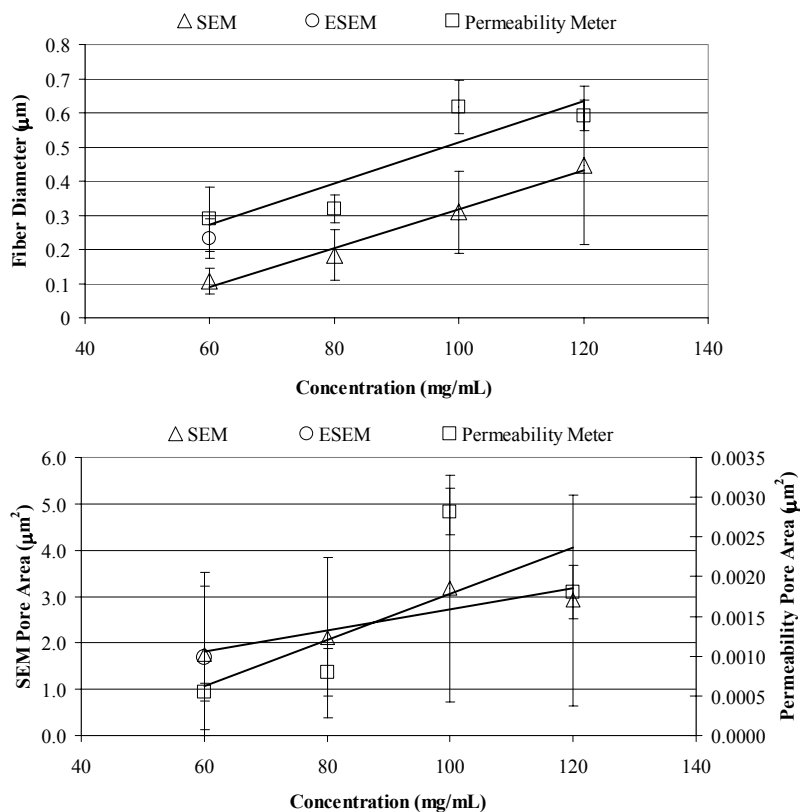
Figure 21. (Top) Fiber diameter versus concentration measured with SEM, ESEM and permeability meter; n = 60 measurements; R^2 values for the trend lines are 0.9854 for SEM and 0.7977 for permeability meter. (Bottom) Pore area versus concentration measured with SEM, ESEM, and permeability meter; n = 40 measurements; R^2 values for the trend lines are 0.7764 for SEM and 0.5214 for permeability meter.

Tensile Testing

Previous uniaxial tensile testing performed on dry and cross-linked (hydrated) samples of a 60 mg/mL type II collagen electrospun mat indicated that a statistically significant difference existed between the dry (no treatment) samples and all of the cross-linked samples for peak stress, strain at break, and tangential modulus [129]. Since the type II collagen scaffolds will only be used in the cross-linked, hydrated state for any tissue engineering purposes, all biomechanical testing in this research was performed in the hydrated state. Figure 22 shows the stress-strain relationships of samples of each concentration of collagen electrospun. These hydrated, cross-linked samples demonstrate uniaxial tensile behavior more characteristic of native tissue than do dry, uncross-linked samples. Table 3 lists the values of the mechanical properties (means and standard deviations) for each electrospun concentration, and Figure 23 is presented to allow a quick comparison between these mechanical parameters. Also shown in Table 3 are the corresponding mechanical properties for native articular cartilage tissue. The values for peak stress and tangential modulus for the electrospun mats are at least an order of magnitude less than the values of these properties for native cartilage, while the values for strain at break for the electrospun mats are at least an order of magnitude greater than the value of this property for native cartilage. At $P<0.0001$, there is a statistically significant difference between the mean values of peak stress for the 60 mg/mL, 80 mg/mL, and 100 mg/mL concentrations and between the mean values of peak stress for 80 mg/mL, 100 mg/mL, and 120 mg/mL concentrations. For strain at break calculations, both the 80 mg/mL and 120 mg/mL concentrations are significantly different from all of the other concentrations, while the 60 mg/mL and 100 mg/mL are not significantly

different from one another. Statistical analysis of the tangential modulus data revealed that the 60 mg/mL and 120 mg/mL concentrations are significantly different from both the 80 mg/mL and 100 mg/mL concentrations.
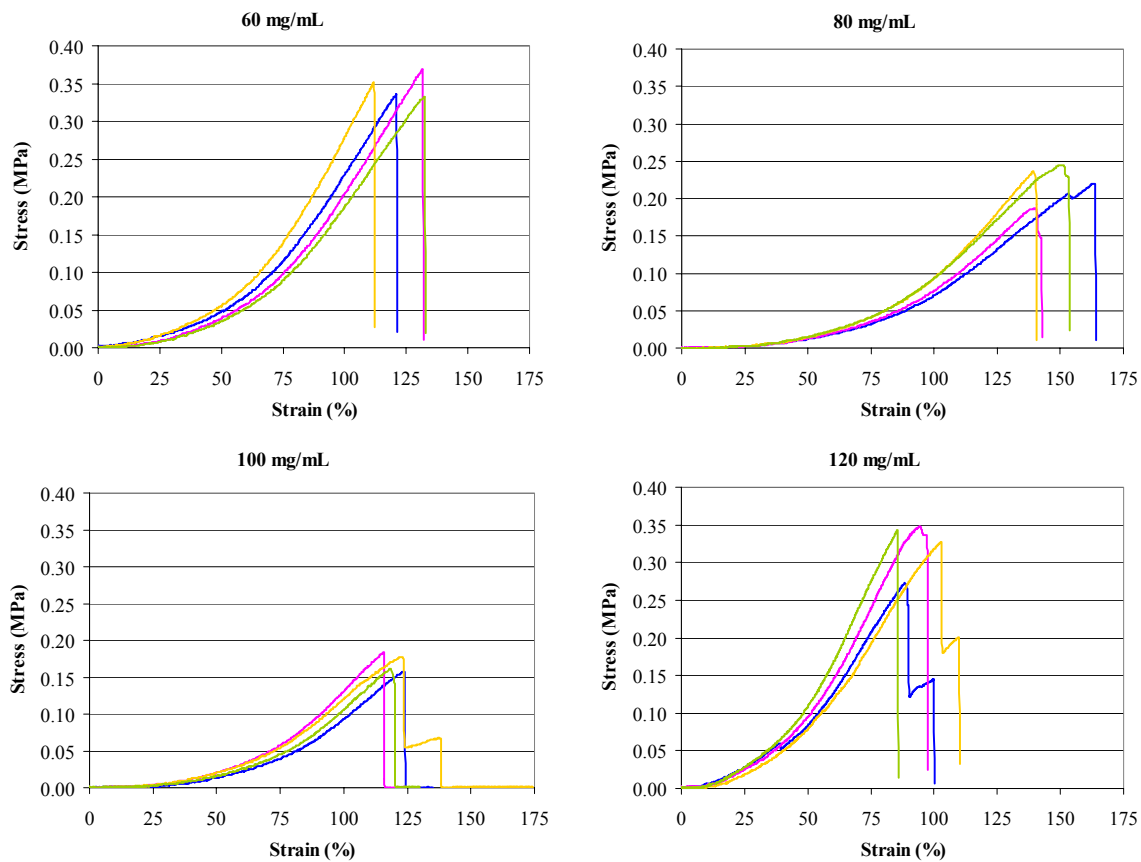

Figure 22. Stress-strain curves for the cross-linked, electrospun mats of each concentration tested in uniaxial tension; n = 4.

Table 3. Mechanical properties from uniaxial tensile testing (given as mean ± standard deviation) for each electrospun mat of type II collagen of each concentration.

	Electrospun Concentration				Native Articular Cartilage
	60 mg/mL	80 mg/mL	100 mg/mL	120 mg/mL	
Peak Stress (MPa)	0.35 ± 0.02	0.22 ± 0.03	0.17 ± 0.01	0.32 ± 0.03	1.3-4.4 [29]
Strain at Break (%)	120 ± 10	150 ± 11	120 ± 4	93 ± 8	9.2-25.9 [29]
Tangential Modulus (MPa)	0.55 ± 0.06	0.34 ± 0.05	0.32 ± 0.03	0.64 ± 0.09	5-25 [27-29]
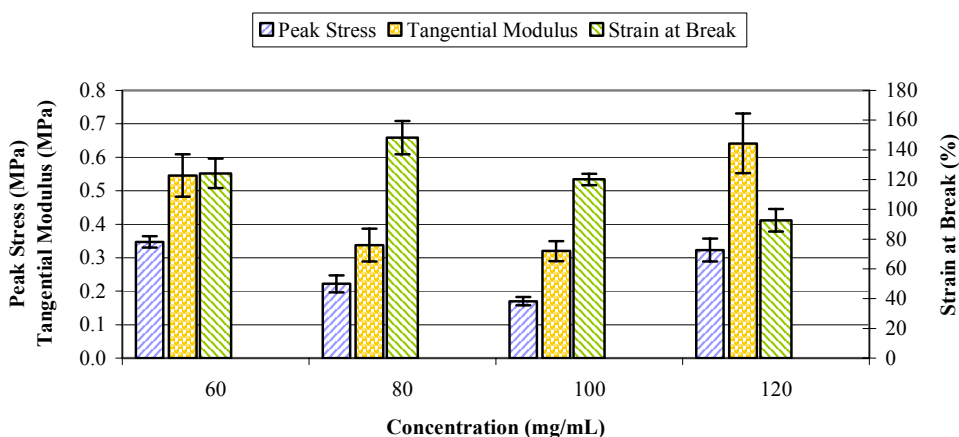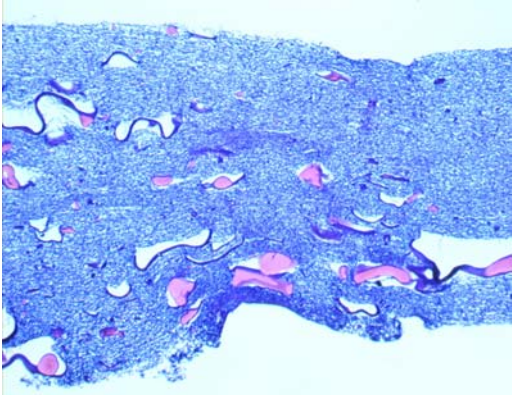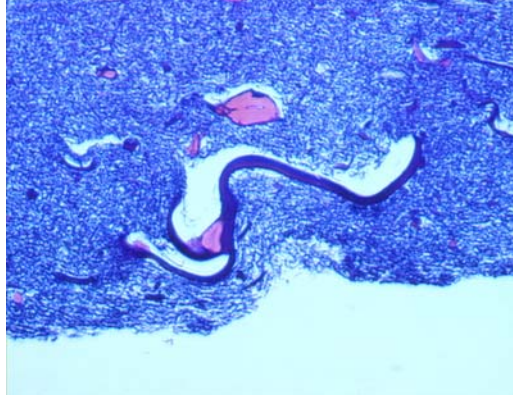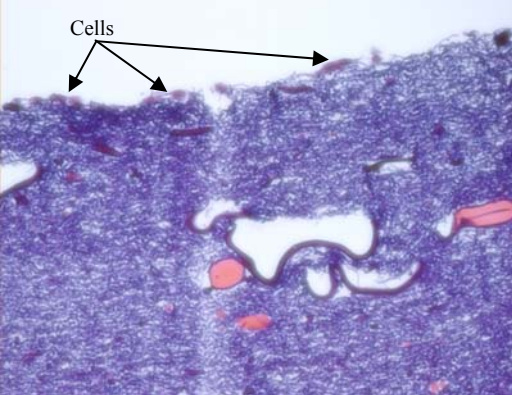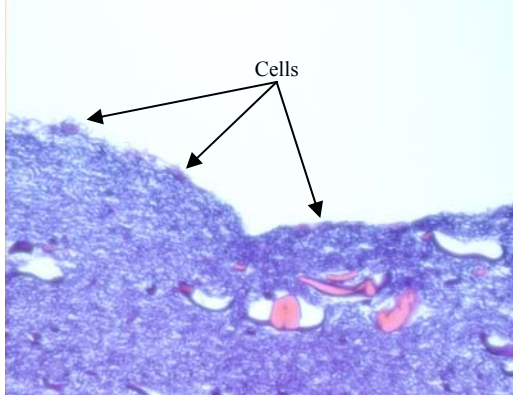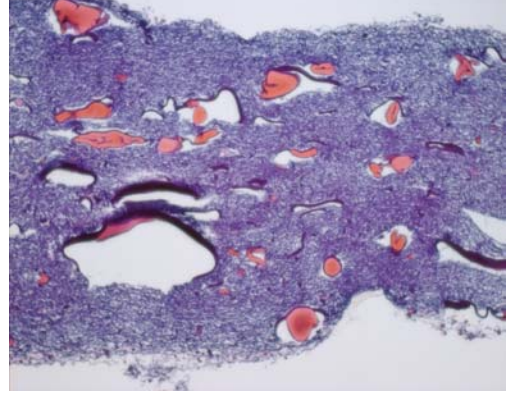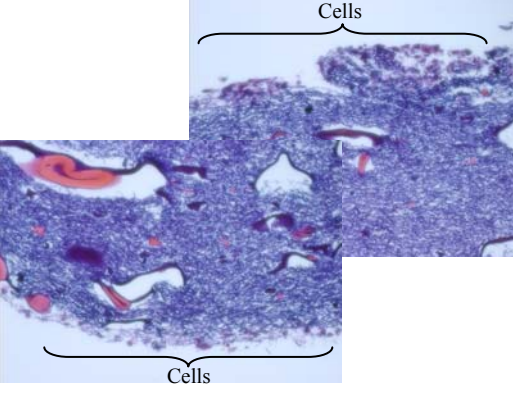
Figure 23. Average peak stress, tangential modulus, and strain at break for the type II collagen cross-linked, electrospun mats of each concentration tested in uniaxial tension; n = 4, error bars show standard deviation.

Initial Cell-Seeding Investigation

The scaffolds placed both in the static culture and in the bioreactor had an initial cell density of 5×10^5 cells/mL media. Photographs of the resulting histology can be seen in Table 4. Though cells do attach to the statically cultured scaffold, the cells do not grow on both sides of that scaffold. However, in the bioreactor, the cells attach to both sides/surfaces of the scaffold and, hence, have more surface area to potentially migrate and proliferate more readily into the thickness of the scaffold. From these results, the cell density used appeared to be

sufficient to obtain at least a monolayer of cells (though maybe not confluent) on most of the

surfaces of the scaffolds within the bioreactor.

Table 4. Histology from the initial cell-seeding investigation; sections are stained with H&E.

No Cells	H&E, 20x	H&E, 40x
Static Culture	H&E, 40x	H&E, 40x
Bioreactor	H&E, 20x	H&E, 40x (top and bottom are opposite sides)

Thickness of Cultured Tissue

The thickness measurements of the scaffold discs are presented in Figure 24. When the thickness measurements of each concentration were analyzed statistically to determine any differences for each culture period, there were no statistical differences found except for the 100 mg/mL concentration in which there was a significant difference between the control (week 0) and week 4 mean values. In other words, the thickness values did not vary significantly over time for each concentration (with the one exception noted). At each time period, there were significant differences determined: at week 0 the 60 mg/mL concentration was different from the 80 mg/mL and 120 mg/mL concentrations, the 80 mg/mL concentration was also different from the 100 mg/mL concentration, and the 100 mg/mL concentration was also different from the 120 mg/mL concentration; at week 2 all of the concentrations were significantly different from each other; at week 4 the 60 mg/mL concentration was different from the 80 mg/mL and 120 mg/mL concentrations, and the 100 mg/mL concentration was different from the 120 mg/mL concentration; and at week 6 the significant differences were determined to be the same as at week 0.
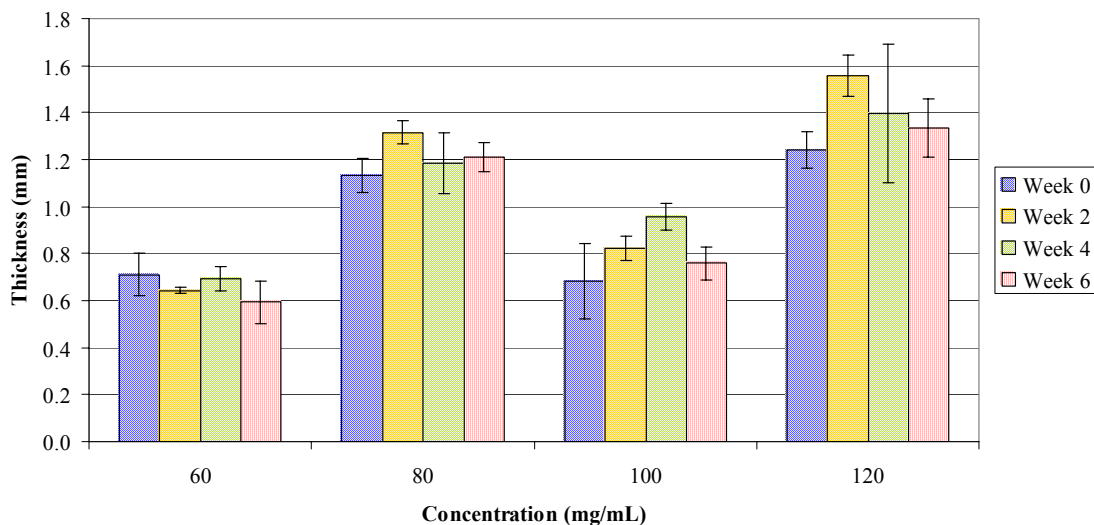
Figure 24. Thickness measurements of the scaffolds of each electrospun concentration before (week 0) and during tissue culture (weeks 2, 4, and 6); n = 3, error bars show standard deviation.

Stress Relaxation

The results of the stress relaxation testing performed on the control samples and on the cultured tissue samples are given in Figure 25. In general, there was a trend for all concentrations in which the equilibrium stiffness decreased from week 2 to week 6 of tissue culture. For the 60 mg/mL concentration, the equilibrium stiffness mean value at week 0 was statistically significantly different from the mean values at week 4 and week 6. There were no significant differences determined between the mean values for the different times periods for the 80 mg/mL and 120 mg/mL concentrations. For the 100 mg/mL concentration, the only significant difference was between the mean values at week 2 and week 6. At week 0 and week 4 there were no statistically significant differences between the concentrations.

However, at week 2 the 60 mg/mL concentration was significantly different from the 100

mg/mL concentration; and at week 6 the 120 mg/mL concentration was significantly different

from the other three concentrations. Also tested in this method of stress relaxation were

cartilage pieces removed from several locations on a calf femur, and the equilibrium stiffness

from those tests was determined to be 0.60 ± 0.69 MPa; this value is about an order of

magnitude greater than the values determined for the scaffolds. The cartilage pieces tested

were taken from different locations on the calf femur (front, back, middle), but there were no

other samples available (i.e. a piece from the same location on the femur could not be tested

multiple times); thus, this data is not included in the statistics. Graphs of load and extension

used to prepare the equilibrium stress versus strain curves (from which the equilibrium

stiffness was determined) are given in Appendix D.
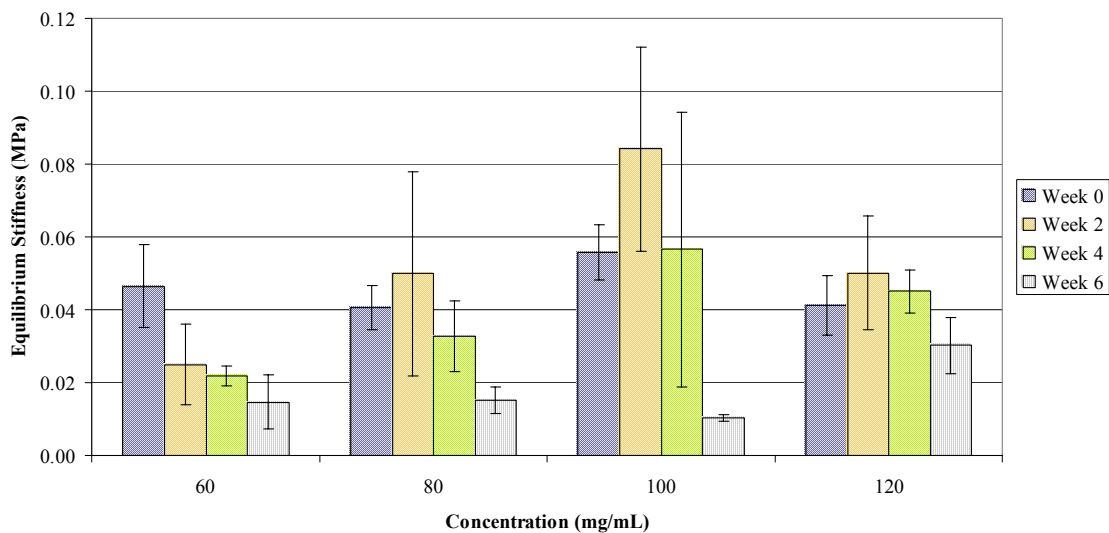
Figure 25. Equilibrium stiffness determined from stress relaxation testing of the scaffolds of
each electrospun concentration before (week 0) and during tissue culture (weeks 2, 4, and 6);
n = 3, error bars show standard deviation.

Biochemical Analysis of Cultured Tissue

The results of the cell density analysis are presented in Figure 26. In general, the trend is such that as concentration increases, cell density (i.e. cell number per mass of scaffold) decreases. Cell density also appears to increase with time for each concentration. From the statistical analysis by concentration, at week 2 the only significant differences are between the mean values of cell density for the 60 mg/mL concentration and the 80 mg/mL and 120 mg/mL concentrations; at week 4 the only significant difference exists between the values for the 60 mg/mL concentration and the 120 mg/mL concentration; and at week 6 the 120 mg/mL concentration is significantly different from the other concentrations, and the 60 mg/mL concentration is also different from the 100 mg/mL concentration. Statistical analysis by time period revealed no significant differences between the mean cell density values at the three time periods for the 60 mg/mL, 100 mg/mL, and 120 mg/mL concentrations; and for the 80 mg/mL concentration the mean value at week 6 was significantly different from the values for week 2 and week 4. The cell number seeded per mg scaffold mass is given in Figure 26. for comparison, but it must be noted that this seeding was performed in the bioreactor media not directly on the surfaces of the scaffolds (refer to Methods section).
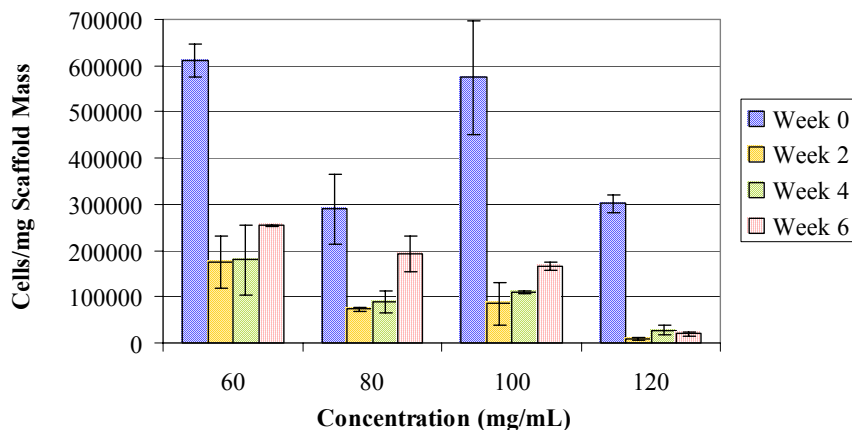
Figure 26. Cell density (cell number per mg scaffold mass) for the scaffolds of differing electrospinning solution concentrations cultured for 2, 4, and 6 weeks; n = 3, error bars show standard deviation. Week 0 is shown to give the number of cells seeded per mg scaffold mass (2.6×10^6 cells per scaffold were seeded in the bioreactors).

Overall, the results of the GAG analysis do not reveal any trends (Figure 27); neither the particular electrospun mat (i.e. a specific concentration) nor any particular time period of culture had any influence on the GAG content (represented as μg GAG per mg scaffold mass). It should be noted that the control scaffolds (week 0) had some GAG content; thus, it is possible that the extraction process was not successful in completely removing all of the GAGs from the type II collagen. From the statistical analysis, there are no significant differences between the mean values of GAG content for the different concentrations at any of the time periods (including week 0), nor are there any significant differences between the mean values of GAG content for each time at any one concentration.
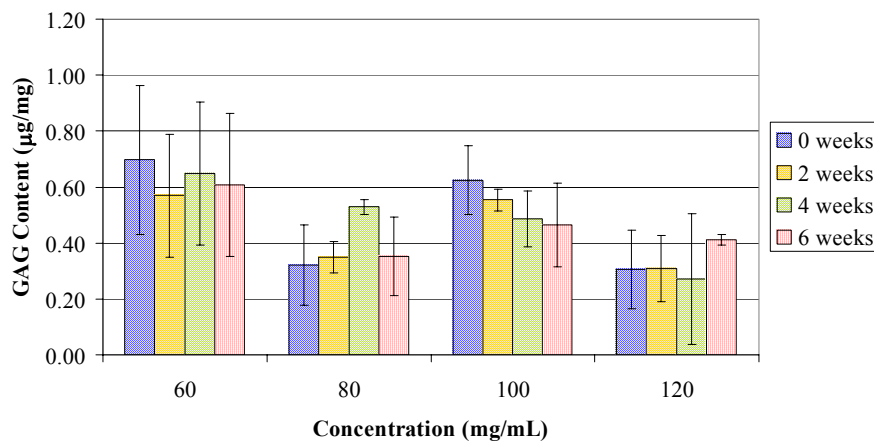
Figure 27. GAG content (μg per mg scaffold mass) for the scaffolds of differing electrospinning solution concentrations cultured for 0 (controls), 2, 4, and 6 weeks; n = 3, error bars show standard deviation.

Table 5 gives the mean values of the collagen content in the scaffolds determined via

ELISA testing. There are no statistically significant differences between any of the mean

values of type I collagen content in the scaffolds in any of the analyses based on time period

or electrospinning solution concentration. For the type II collagen statistical analysis, at week

6 the mean value of type II collagen content in the 100 mg/mL concentration is significantly

different from all of the other concentrations. Furthermore, for the 100 mg/mL concentration,

the mean value of type II collagen content at week 6 is significantly different from the mean

values of the same concentration at weeks 0, 2, and 4. There are no other significant

differences between the type II collagen values. The type II/type I collagen ratio can not be

calculated since there are no values of type II collagen and type I collagen content for

corresponding time periods and concentrations (i.e. in the ratio calculations, either the

numerator or the denominator would always be zero). A spike and recovery study was performed to test the protocol used to detect type II collagen; the standard provided in the ELISA kit was added to several samples without cells and tested alone at a known concentration. The spiked samples gave readings equal to the reading of the standard alone. Thus, the standard is working but the collagen in the samples is either at undetectable levels (unlikely since the scaffolds are composed of type II collagen) or is not being detected by the antibody that was raised against the collagen molecules in the standard.

Table 5. Collagen content (µg per mg scaffold mass) for the scaffolds of differing electrospinning solution concentrations cultured for 0 (controls), 2, 4, and 6 weeks; values are given as mean ± standard deviation, n = 3.

	Concentration (mg/mL)	Week 0	Week 2	Week 4	Week 6
Type II Collagen (µg/mg)	60	0	0	0	0
	80	0.00053 ± 0.00092	0.00112 ± 0.00102	0.00344 ± 0.00296	0.00040 ± 0.00041
	100	0.00027 ± 0.00047	0.00048 ± 0.00022	0.00231 ± 0.00240	0.00638 ± 0.00104
	120	0	0	0	0
Type I Collagen (µg/mg)	60	0	0	0	0.00049 ± 0.00062
	80	0	0	0	0
	100	0	0	0	0
	120	0	0	0.00003 ± 0.00006	0

Histological Analysis of Cultured Tissue

Representative photographs were taken of the histology slides and are given in Table 6, Table **7**, Table **8**, and Table **9** for the 60 mg/mL, 80 mg/mL, 100 mg/mL, and 120 mg/mL concentrations, respectively. For all of the concentrations, pictures were taken of the control scaffolds, without cells, for comparison purposes. Some general comments are given below describing the observations made on all of the scaffolds.

60 mg/mL Concentration

For the 60 mg/mL concentration at week 2, one side of the scaffold usually had more cells on it than the other side; there was not much infiltration of the cells into the scaffolds unless there was a large void or pocket present. Some of the cells were spheroid in shape and some were elongated. It was typical to find clumps of cells especially on the side of the scaffold with more cells. For the most part, there was a solid layer of cells on both sides of the scaffolds. At week 4, the observation was made that when the cells are in clusters, they appeared more spheroid in shape; but when the cells are in a monolayer on the scaffold, they appeared more elongated. Also, the cells that have infiltrated the scaffold appear to be more spheroid than the cells lining the outside of the scaffold. There was very little cellular infiltration unless a path (such as a tear or void) was available. At week 6 there appeared to be an abundance of cells on one side, and only one or two layers of cells on the other side across the entire length of the scaffold. There were numerous spheroid cells, and cellular infiltration into the scaffold did occur though not through the entire thickness; the infiltration

was from the direction with the most cells. There were also a few areas of lighter blue visible in the Masson's Trichrome-stained section possibly indicating new collagen production.

<u>80 mg/mL Concentration</u>

For the 80 mg/mL concentration at week 2, there are some cell clusters and thin layers of cells lining both sides of the scaffolds, with one side having a layer greater than two cells in thickness and the other side having a layer less than or equal to two cells in thickness. The cells tended to follow the contours of the scaffold, and most of the cells appeared elongated. There are some pockets of spheroid cells and some light blue areas seen in the sections stained with Masson's Trichrome (possibly indicating new collagen production). There is some cellular infiltration from the direction of the side with the most cells; most cellular infiltration occurred where there is a path for the cells to move along. Clusters of cells appeared to be moving into openings on the ends of the scaffolds between the layers created by electrospinning; this is interesting because these sections were punched out of the 1 cm disc, so the ends are not exposed before punching (though the punches are made near the edge of the 1 cm disc). At week 4 it was observed that the cells formed a confluent layer on both sides of the scaffold. No cellular infiltration was observed and there were no significant areas of light blue visible in the Masson's Trichrome-stained sections. There were some spheroid cells, but most cells appeared elongated. At week 6 two of the samples displayed clusters of cells on one side of the scaffold and only a thin layer of cells on the other side, while the other sample only had thin layers of cells with no clusters. There was cellular infiltration from the

direction of the side with the most cells (i.e. clusters of cells), and there were areas of light blue seen around the cell clusters in the Masson's Trichrome-stained sections.
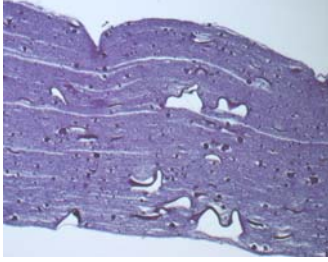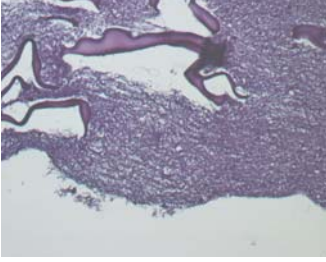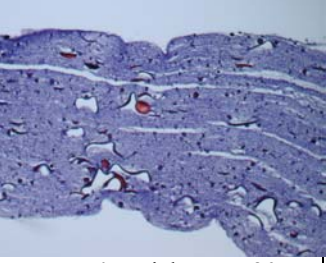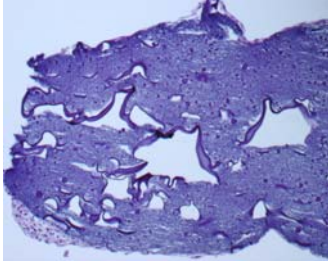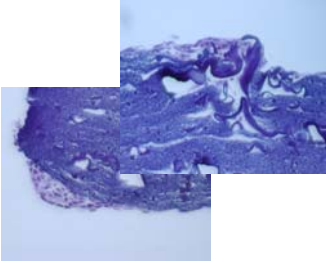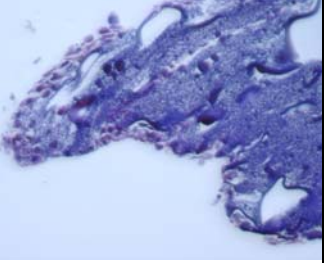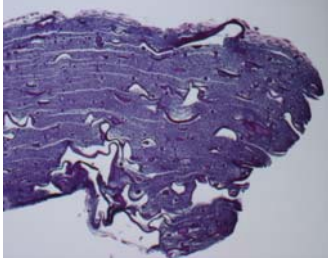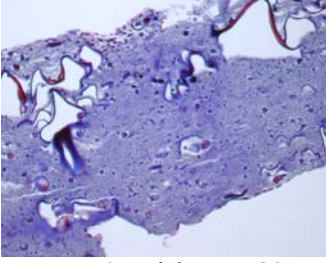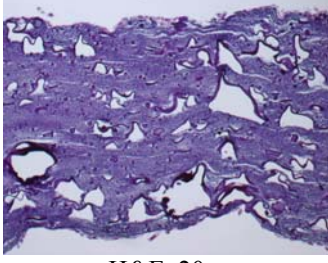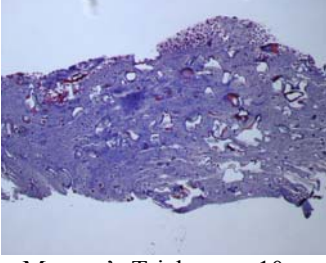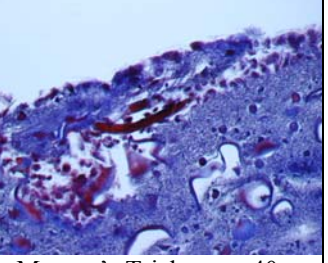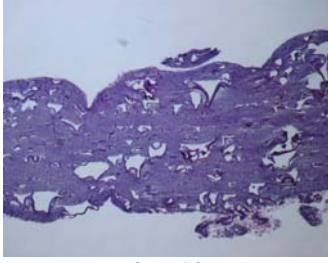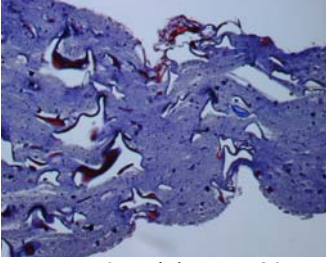
100 mg/mL Concentration

For the 100 mg/mL concentration at week 2, there were thin confluent layers of cells on both sides of the scaffolds that appeared spheroid in shape and more evenly distributed (i.e. there were no clusters of cells visible). There was very little to no cellular infiltration seen but there were cells lining the delaminated surfaces of the scaffold, and there were a few light blue areas in the Masson's Trichrome-stained sections (possibly indicating new collagen production). At week 4 there were still somewhat thin cell layers on both sides of the scaffold with a few cell clusters and very little cellular infiltration. Both spheroid and elongated cells were seen, and some blue areas are visible in the Masson's Trichrome-stained sections. Where there were larger gaps or crevices on the surface, more cells aggregated. On one sample there were cells in the middle of the scaffold as well as in thin layers on the top and bottom of the scaffold; this was interesting because there was no clear path through the thickness of the scaffold for the cells to have migrated into the middle of the scaffold. At week 6 the sections contained numerous cell clusters and some cellular infiltration especially where the scaffold geometry was not solid; the rest of the scaffold surfaces (both sides) were covered by thin layers of cells (several cells in thickness) with much less cellular infiltration. The amount of spheroid cells outnumbered the elongated cells. There were some blue areas seen in the Masson's Trichrome-stained sections.

<u>120 mg/mL Concentration</u>

For the 120 mg/mL concentration at week 2, there were very thin layers of cells lining the top and bottom surfaces of the scaffolds, with the cell layer on one surface slightly thicker than the layer on the other surface. One sample did delaminate and there may have been a few cells on the delaminated surfaces. Cellular infiltration was almost nonexistent except for the one Masson's Trichrome-stained sample in which cells appeared in the middle of the scaffold with no clear path of migration from either side (i.e. top or bottom) of the scaffold; these cells had a spheroid appearance. At week 4 there appeared to be confluent cell layers on both sides of the scaffold with one layer several cells in thickness and the other layer only a monolayer of cells. Several samples have very contoured surfaces. The cell shape was difficult to determine, though most appeared to be elongated, and there did not appear to be any cellular infiltration. One sample had a small cluster of cells on one surface with very minimal infiltration into the scaffold at that cluster. There were a few cells observed in the middle of two sections stained with Masson's Trichrome. At week 6 the samples had thin, mostly confluent layers of cells on both sides of the scaffolds, either a monolayer or several cells in thickness. There were some spheroid cells, but the majority appeared elongated. There was a sample with cells in the middle of the scaffold with an opening on one edge of the scaffold (a possible path for cellular migration). Only a very small area of the light blue staining was visible in one sample stained with Masson's Trichrome.

Table 6. Histology for the 60 mg/mL concentration for each culture period; H&E and Masson's Trichrome stains are represented at 10x, 20x, or 40x magnifications.

WEEK 0 No cells		H&E, 20x	H&E, 40x	Masson's Trichrome, 20x
WEEK 2	Sample 1	H&E, 20x	H&E, 40x	Masson's Trichrome, 40x
	Sample 2	H&E, 20x	Masson's Trichrome, 20x	
	Sample 3	H&E, 20x	Masson's Trichrome, 10x	Masson's Trichrome, 40x
WEEK 4	Sample 1	H&E, 10x	Masson's Trichrome, 20x	
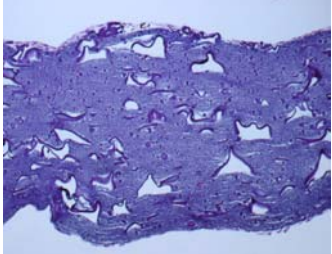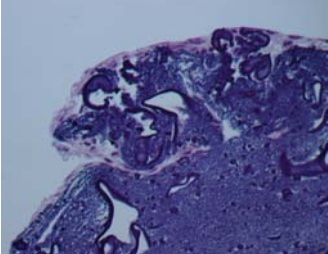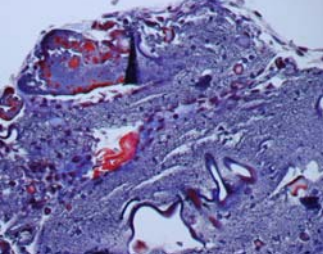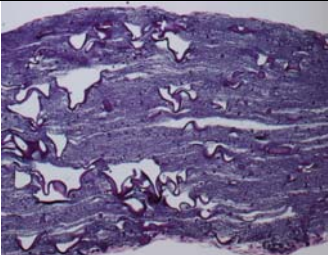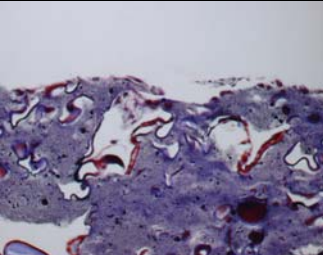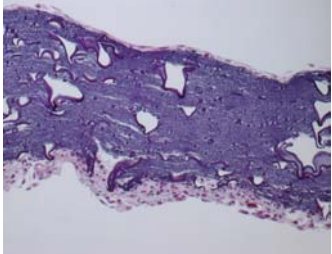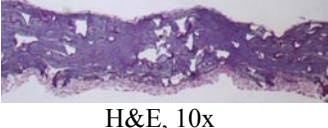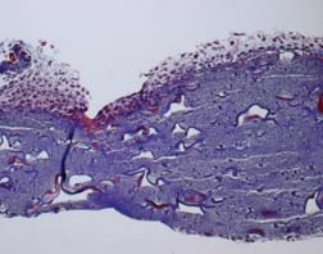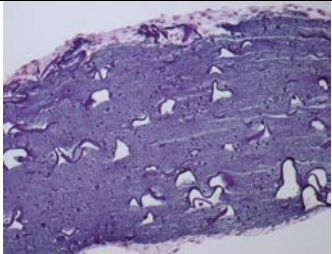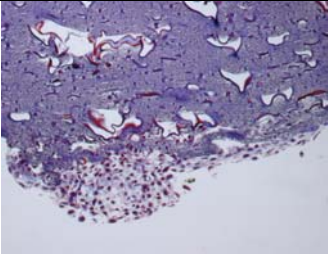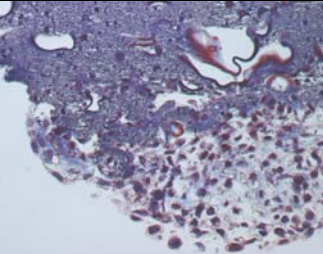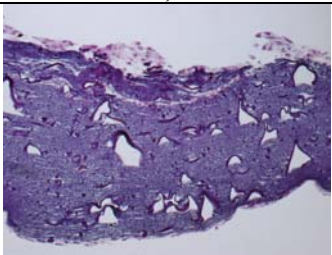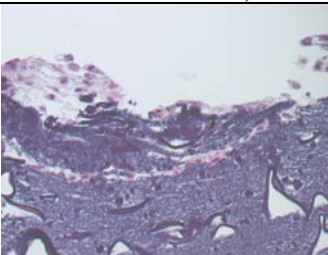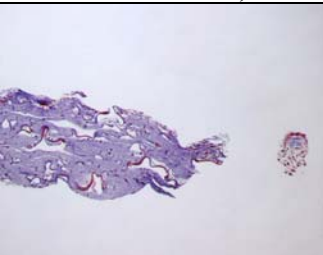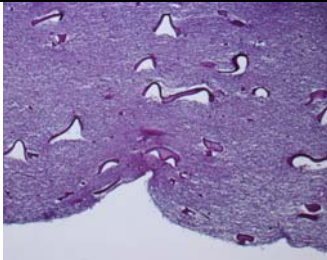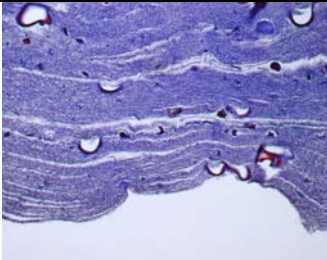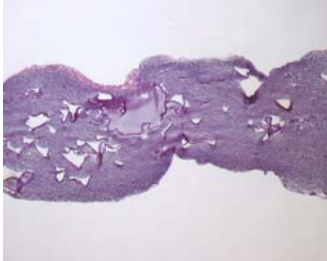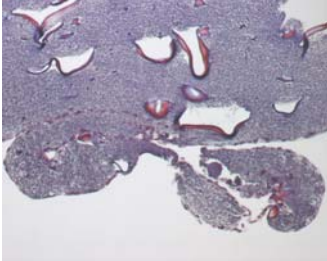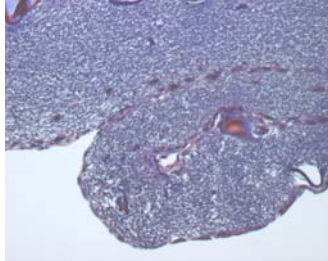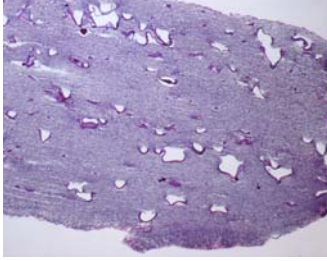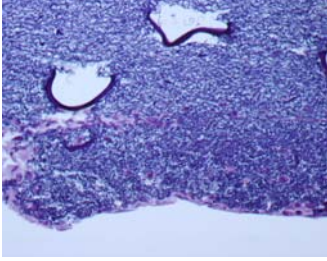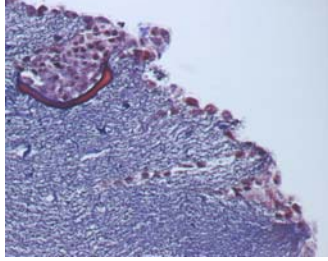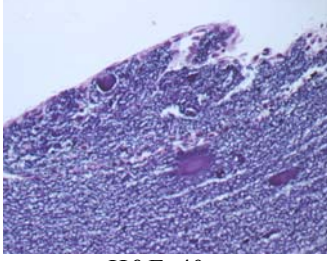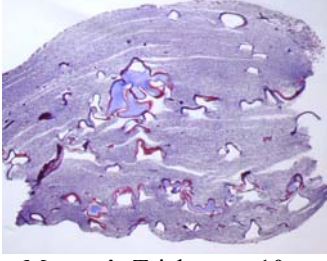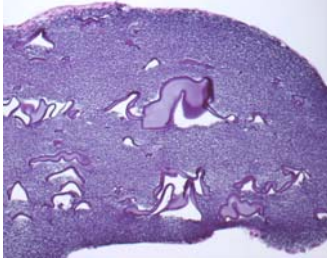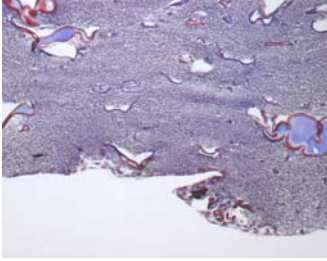
	Sample 2	H&E, 20x	H&E, 40x	Masson's Trichrome, 40x
	Sample 3	H&E, 20x	H&E, 20x	Masson's Trichrome, 20x
WEEK 6	Sample 1	H&E, 20x	H&E, 10x / H&E, 40x	Masson's Trichrome, 20x
	Sample 2	H&E, 20x	Masson's Trichrome, 20x	Masson's Trichrome, 40x
	Sample 3	H&E, 20x	H&E, 40x	Masson's Trichrome, 10x

Table 7. Histology for the 80 mg/mL concentration for each culture period; H&E and
Masson's Trichrome stains are represented at 10x, 20x, or 40x magnifications.

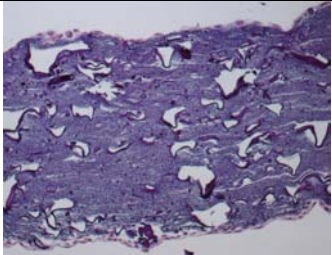| WEEK 0 No cells	H&E, 20x	Masson's Trichrome, 20x	
WEEK 2 Sample 1	H&E, 10x	Masson's Trichrome, 20x	Masson's Trichrome, 40x
Sample 2	H&E, 10x	H&E, 40x	Masson's Trichrome, 20x
Sample 3	H&E, 40x	Masson's Trichrome, 10x	
WEEK 4 Sample 1	H&E, 20x	Masson's Trichrome, 20x	
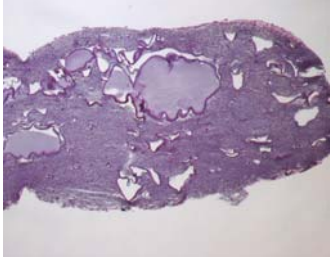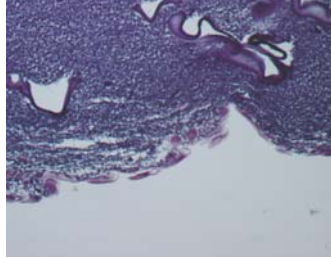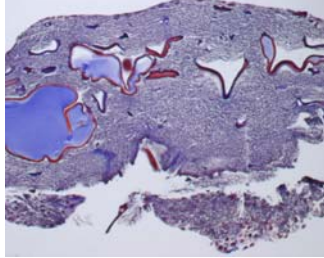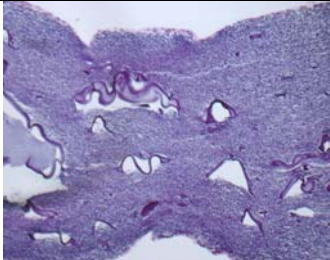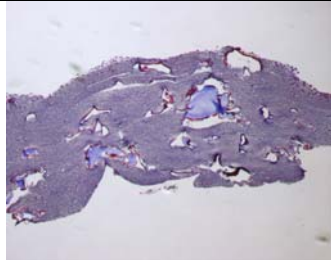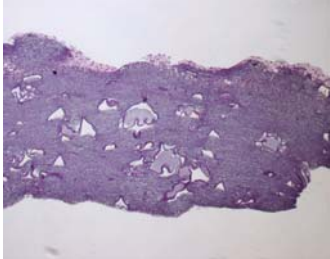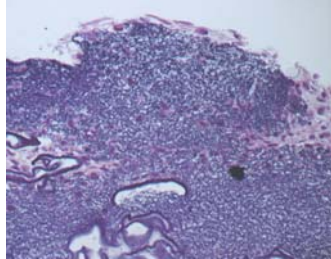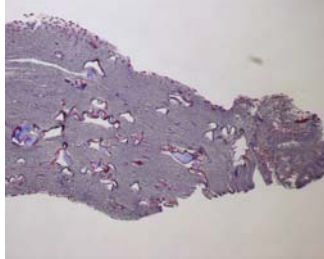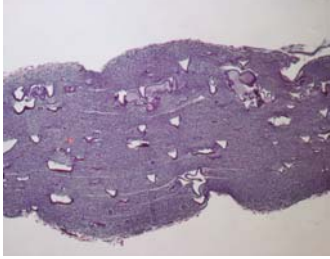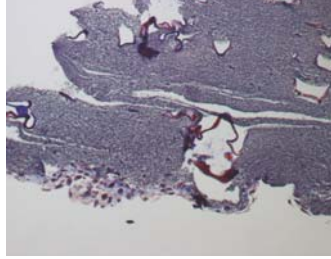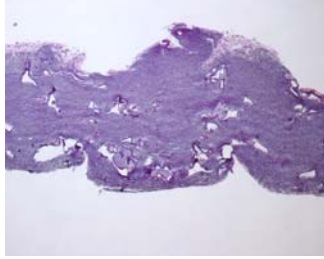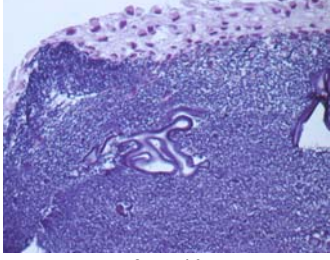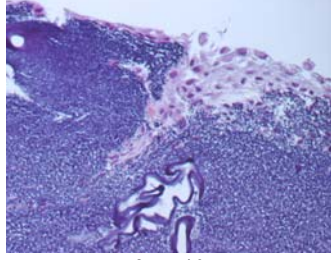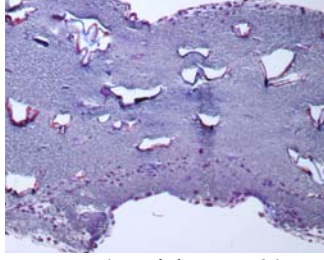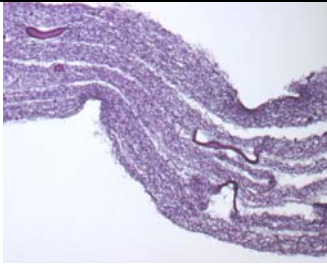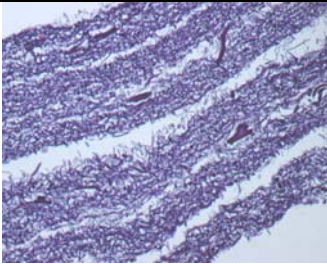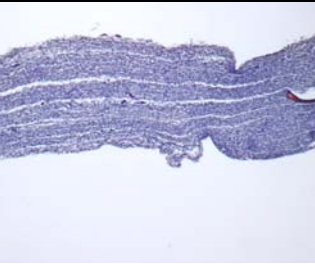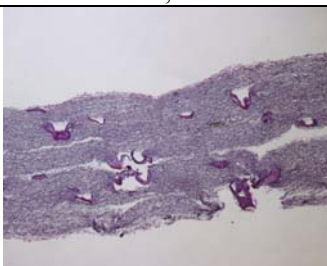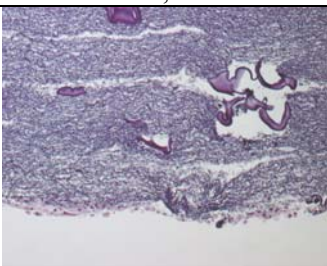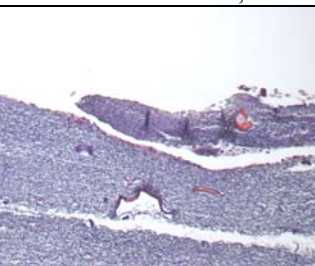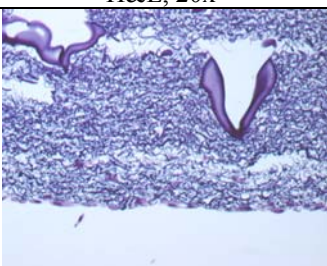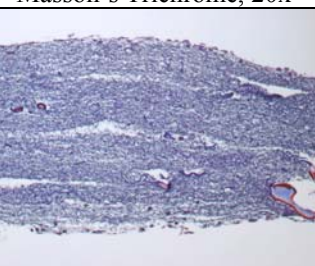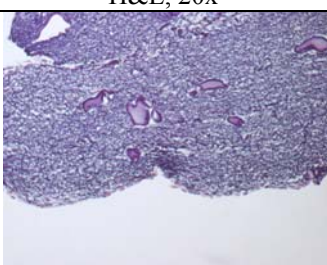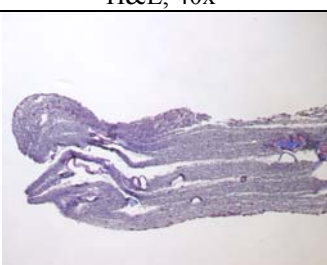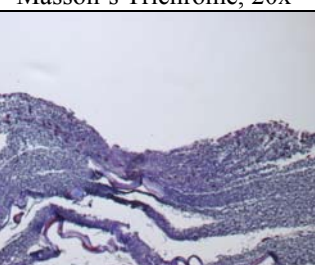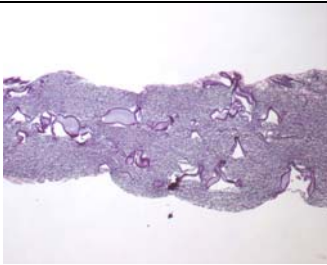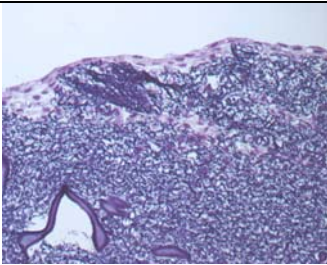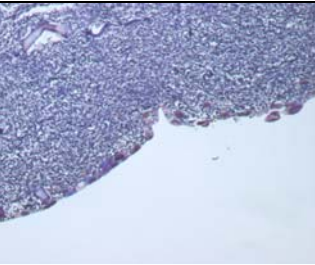
	Sample 2	H&E, 10x	H&E, 40x	Masson's Trichrome, 20x
	Sample 3	H&E, 20x	Masson's Trichrome, 10x	
WEEK 6	Sample 1	H&E, 10x	H&E, 40x	Masson's Trichrome, 10x
	Sample 2	H&E, 10x	Masson's Trichrome, 20x	Sample 3: H&E, 10x
	Sample 3	H&E, 40x	H&E, 40x	Masson's Trichrome, 20x

Table 8. Histology for the 100 mg/mL concentration for each culture period; H&E and Masson's Trichrome stains are represented at 10x, 20x, or 40x magnifications.

WEEK 0 No cells		H&E, 20x	H&E, 40x	Masson's Trichrome, 20x
WEEK 2	Sample 1	H&E, 10x	H&E, 20x	Masson's Trichrome, 20x
	Sample 2	H&E, 20x	H&E, 40x	Masson's Trichrome, 20x
	Sample 3	H&E, 20x	Trichrome, 10x	Masson's Trichrome, 20x
WEEK 4	Sample 1	H&E, 10x	H&E, 40x	Masson's Trichrome, 40x
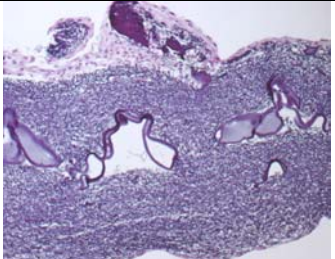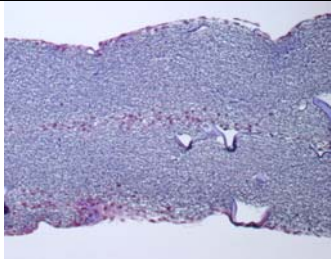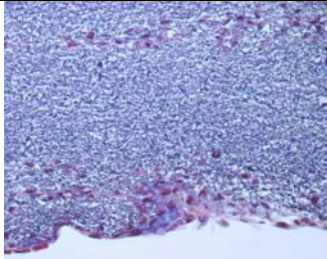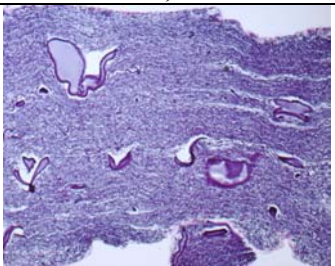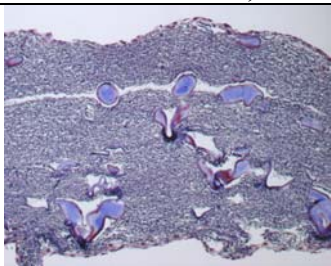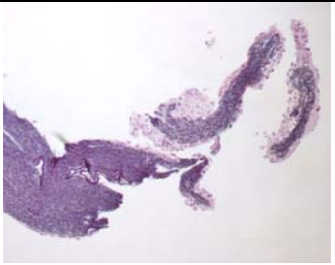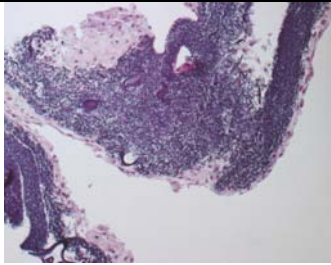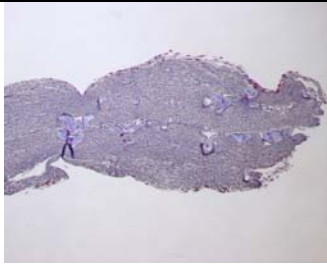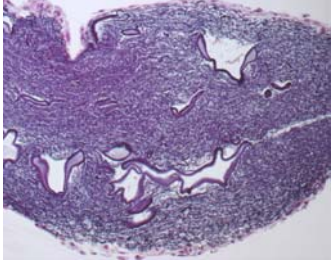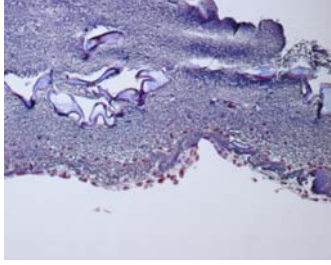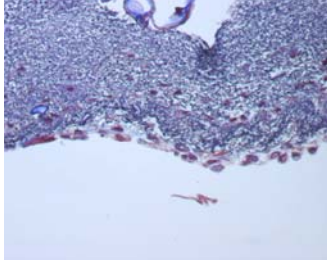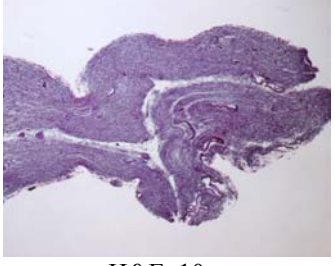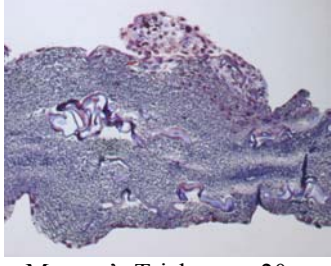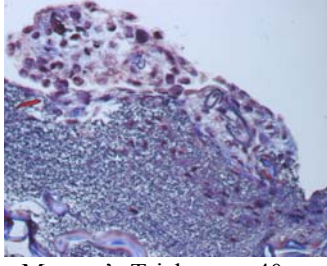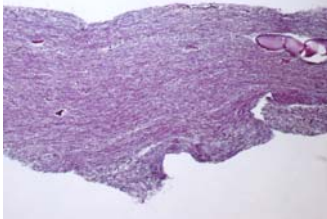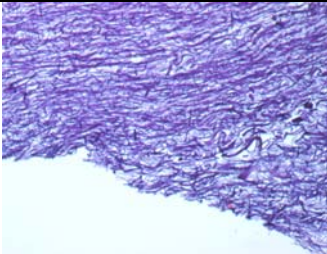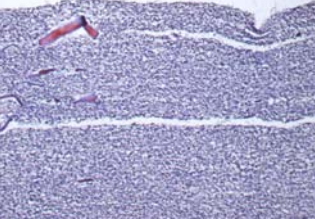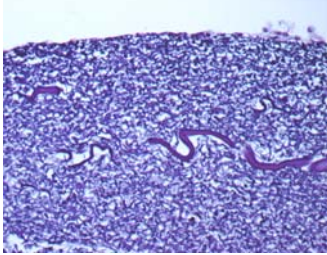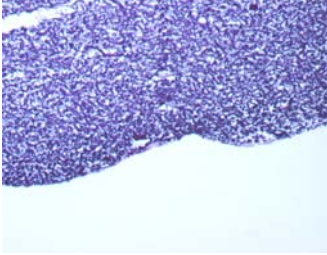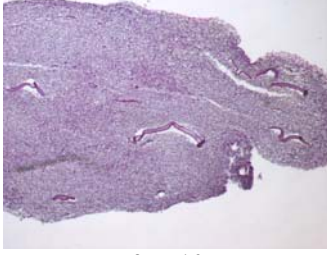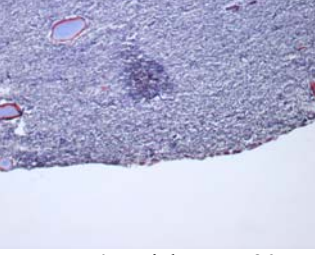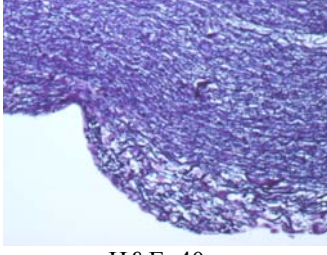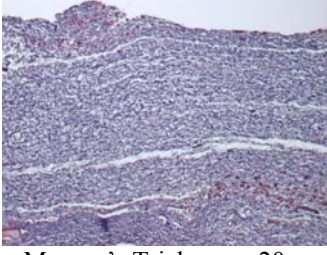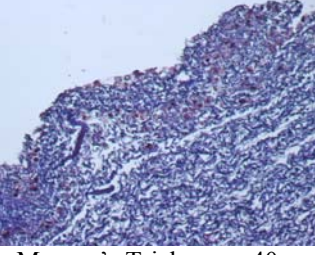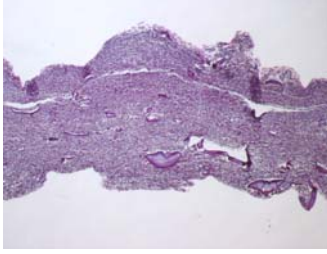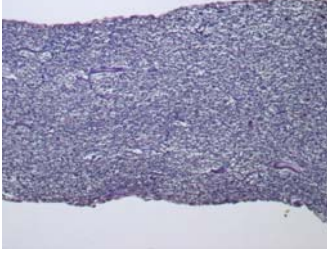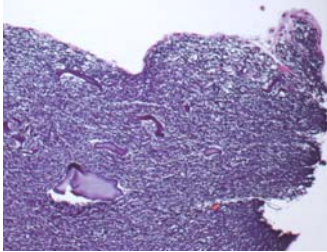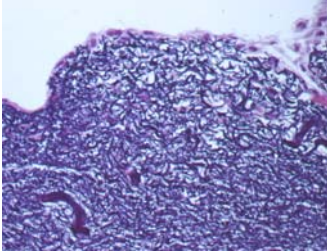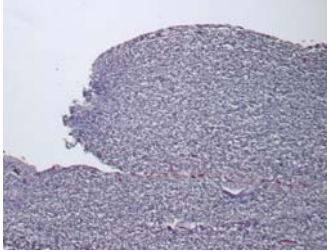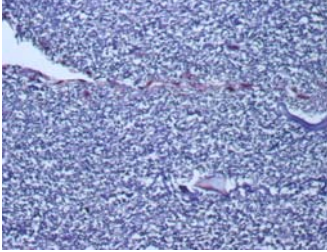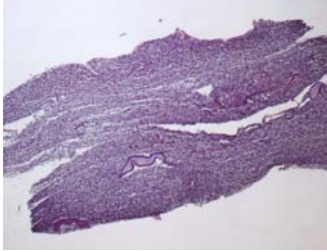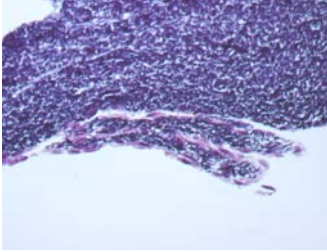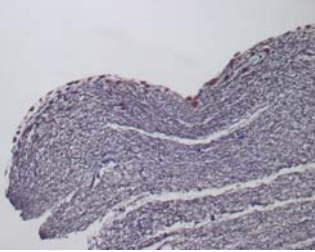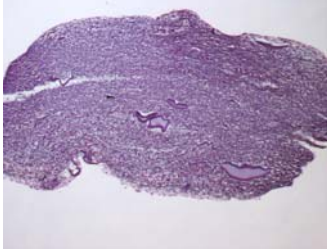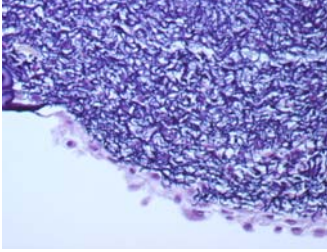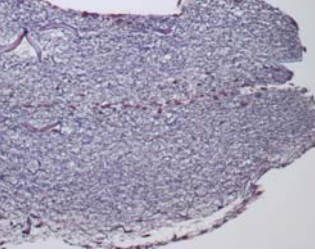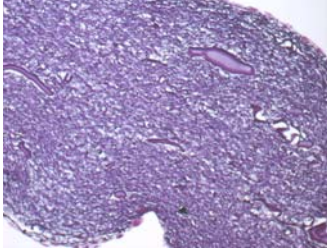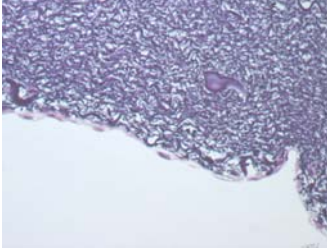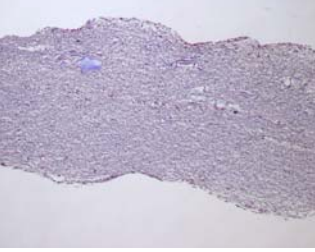
	Sample 2	H&E, 20x	Masson's Trichrome, 20x	Masson's Trichrome, 40x
	Sample 3	H&E, 20x	Masson's Trichrome, 20x	
WEEK 6	Sample 1	H&E, 10x	H&E, 20x	Masson's Trichrome, 10x
	Sample 2	H&E, 20x	Masson's Trichrome, 20x	Masson's Trichrome, 40x
	Sample 3	H&E, 10x	Masson's Trichrome, 20x	Masson's Trichrome, 40x

Table 9. Histology for the 120 mg/mL concentration for each culture period; H&E and Masson's Trichrome stains are represented at 10x, 20x, or 40x magnifications.

WEEK 0 No cells		H&E, 10x (half, delaminated)	H&E, 40x	Masson's Trichrome, 20x
WEEK 2	Sample 1	H&E, 40x (one side)	H&E, 40x (opposite side)	Masson's Trichrome, 20x
	Sample 2	H&E, 10x	H&E, 40x	Masson's Trichrome, 20x
	Sample 3	H&E, 40x	Masson's Trichrome, 20x	Masson's Trichrome, 40x
WEEK 4	Sample 1	H&E, 10x	Masson's Trichrome, 20x	

	Sample 2	H&E, 20x	H&E, 40x	Masson's Trichrome, 20x
	Sample 3	Trichrome, 20x	Masson's Trichrome, 40x	
WEEK 6	Sample 1	H&E, 10x	H&E, 40x	Masson's Trichrome, 20x
	Sample 2	H&E, 10x	H&E, 40x	Masson's Trichrome, 20x
	Sample 3	H&E, 20x	H&E, 40x	Masson's Trichrome, 10x

Discussion

Cross-linking Electrospun Collagen

Electrospun collagen fibers consist of reconstituted collagen fibrils (i.e. acid soluble collagen extracted from fetal calf cartilage) that are formed via both the electrospinning fabrication process and possibly via the spontaneous organization of collagen molecules [143]. These electrospun collagen fibers are potentially similar in ultrastructure to native collagen; however, the fibers are fragile, possibly due to a lack of native cross-links resulting in weakly bonded fragments of collagen molecules. Thus, the electrospun structures need further treatment to stabilize the material. Further cross-linking, beyond what little weak bonding may have spontaneously occurred, is necessary in order to work with an electrospun collagen scaffold in a hydrated state for tissue engineering applications. The heterobifunctional reagent EDC was used to introduce synthetic cross-links that form a bridge between two amino acids without imparting any other chemistry to the collagen molecule. Within the triple helical structure of collagen, there are a large number of opportunities for lysine interactions with aspartic acid and with glutamic acid residues; thus, cross-links created by EDC can be formed within an α chain, between α chains, between collagen molecules, or between collagen fibrils [127].

To avoid the disintegration or fragmentation of the electrospun structures, ethanol was utilized as the cross-linking solvent and the proton donor for the EDC reaction instead

of a buffered solution; this is the unique aspect of the cross-linking protocol used in this research. Ethanol molecules in concentrated solutions associate via hydrogen bonding, the energy of which is comparable to that of the hydrogen bonding of water [144]. Furthermore, the ethanol molecule has little steric hindrance and can interact with and hydrogen bond to chemical groups in tissues, including carbonyl oxygen, amine, and amide nitrogen, i.e. the O and N atoms in peptide bonds [144, 145]. Additionally, solvents of a lower dielectric constant (35 for ethanol compared to a value of 81 for water) reduce the dipolar forces resulting in a change in the bonding; the salt bridges (due to oppositely charged groups) of fibrous proteins in an aqueous solution will be converted to hydrogen bonds when immersed in alcohol solutions [144, 145], which may be advantageous in maintaining the electrospun collagen mat structure. Further support for the greater performance of the electrospun collagen mats immersed in ethanol compared to water is that ethanol molecules in concentrated solutions hydrogen bond to one another and can form polymeric chains [144], which may help stabilize the electrospun collagenous structure. Also, the ethyl group of the solvent could interact through hydrophobic interactions with the collagen surface [146, 147]; the hydroxyl group is then available to interact with other ethanol molecules or other residues in the protein to again stabilize the electrospun collagenous mat structure. The critical issue involved in this study was not to provide better reactivity of groups, but to provide the condition that maintained the proper structure of the mat. Ethanol provided that condition since it was not possible to use a buffered solution.

Some shrinkage in overall dimensions of the electrospun mats was observed with the EDC cross-linking treatment. This shrinkage (between 12 and 33% decrease in dimensions) is probably due to the absorption of moisture by the agents during measurement of the solids prior to cross-linking and the subsequent reaction of the fibrous collagen to slight hydration.

Scaffold Morphology and the Interaction with Chondrocytes

The type II collagen electrospun scaffolds supported chondrocyte attachment and possible proliferation on the surface of the scaffolds. Cell adhesion, spreading, and shape have been shown to be influenced by scaffold morphology; thus, fiber diameter, porosity, pore size, and pore interconnectivity and tortuosity in a scaffold can influence cell behavior and serve to orient cells [148]. The average diameters of the fibers in the scaffolds of all concentrations ranged between about 100 to 620 nm; this scale is comparable to that of the native ECM. Thus, the electrospun collagen provided the size and chemical composition the cells would see *in vivo*.

There was a statistically significant difference found in the fiber diameter measurements of the 60 mg/mL concentration in the dry, untreated state (measurement made using a digitized image of a scanning electron micrograph) and in the hydrated, cross-linked state (measurement made using a digital picture). This could be a result of the cross-linking procedure binding collagen fibrils together to increase fiber diameter or a result of some swelling due to the hydration or a combination of both. Further investigation is needed.

A large pore volume (i.e. porosity) allows sufficient space for cells to grow into tissues and for nutrients and wastes to diffuse in and out, respectively. The average porosity of the scaffolds used in this research ranged between 84 and 89%. These values are just below the suggested minimum porosity of 90% (considered highly porous, and there has been suggestion of a 95% or greater porosity needed for chondrocytes [91]), which is believed to provide sufficient space for cellular infiltration where the cells perform actively and exchange nutrients and wastes with the environment [84, 149]. This parameter must be considered in conjunction with the other scaffold design parameters.

It has traditionally been thought that the minimum pore size is dependent on the diameter of the cell in the tissue to be regenerated [150]. Pores smaller in diameter than 2 nm only allow small molecules such as gases to penetrate; small proteins are able to pass through pores with diameters between 2 nm and 50 nm; larger proteins and molecules can penetrate pores with diameters greater than 50 nm; and cells can migrate when pore sizes exceed 1 μm [113]. Mooney and Langer state that pores greater than 10 μm in diameter are necessary for a scaffold to become incorporated into the host tissue, though Matthews et al. have shown that an electrospun scaffold, with pore sizes 50 times smaller than that described by Mooney and Langer, resulted in migration and dense population of aortic smooth muscle cells throughout the scaffold [99]. However, the behavior of chondrocytes in such a scaffold may not be the same as that seen with smooth muscle cells. On an additional note regarding pores, a uniform pore structure and distribution has been shown to have better mechanical properties [91].

Pores in an electrospun scaffold constitute the spaces formed between the fibers that collect on the target during the electrospinning process. Because the mat that is created is nonwoven, it is believed that there is the potential for cells to push the fibers around during migration such that the cells essentially dictate the pore size and distribution desirable for a particular cell behavior [84]. In this research, approximate pore diameters of the electrospun mats were calculated from the average pore areas measured using the imaging software on the scanning electron micrographs, and these values ranged between 1.5 and 2.0 μm for the dry and hydrated mats of varying concentrations. These values are significantly greater than the pore diameters determined using the permeability data, which ranged between 0.02 and 0.06 μm. The pore area measurement from the scanning electron micrographs is very subjective; it is quite difficult to determine actual pores in a two-dimensional picture; thus, the calculations from the permeability data may be more accurate.

The pore sizes determined from the permeability data (0.02 to 0.06 μm) more closely match but are still greater in size than the pores formed by collagen and proteoglycans in healthy articular cartilage, the size of which ranges from 25 to 75 Å [14]. Though this pore-size scale will limit what passes through the scaffold (more like the native tissue), perhaps this pore-size scale is too small for chondrocytes to infiltrate the scaffolds. As seen in the histology photographs, the scaffolds do appear as dense mats of collagen with a few large voids and some areas of delamination (depending on the concentration), but in general there is very little cellular infiltration perhaps due to the relatively small pore size.

Healthy articular cartilage has a very low permeability, which ranges from 10^{-16} to 10^{-15} m^4/N·sec [12, 14, 32]. The mean values of electrospun mat permeability calculated in this research range from 0.000682 to 0.00350 D or from 7.6×10^{-13} to 3.9×10^{-12} m^4/N·sec, which are at least 2 orders of magnitude greater than the permeability of normal articular cartilage. In fact, the permeability of the electrospun mats is closer to but still greater than that for degenerated cartilage (which is on the order of 10^{-14} m^4/N·sec) [12, 14, 32]. The permeability of the type II collagen electrospun mats in this study is comparable to the mean permeability (about 1.25×10^{-12} m^4/N·sec) determined for non-woven mesh PGA scaffolds commonly used in cartilage tissue engineering [151].

On an additional note, prior to seeding, the scaffold dry weights (all collagen) were (on average) approximately 10% of the scaffold wet weights. This illustrates the sponge-like capacity of the electrospun scaffolds; in other words, the scaffolds displayed a swollen behavior upon hydration. Furthermore, to compare the unseeded scaffolds to native articular cartilage tissue, water constitutes greater than 60% of the tissue by wet weight and type II collagen about 20% by wet weight.

Histology and Biochemical Analyses

Chondrocytes cultured in monolayer did take on the fibroblast-like, flattened morphology. Thus, there is the possibility of dedifferentiation during the static culture. Upon transfer of the chondrocytes to the bioreactor for dynamic culture on the scaffolds, redifferentiation media was not used. The hypothesis being tested was that growing the cells on the three-dimensional electrospun type II collagen fibrous scaffolds would result

in the cells reexpressing, and possibly redifferentiating into, the chondrocytic phenotype and their spheroid morphology. The tissue structure created in this research resembled the superficial zone more than the middle zone. The collagen fibrils are oriented tangentially to the scaffold surfaces (with no fibers oriented perpendicular to the surfaces) and some cells are elongated in shape, both are characteristics of the superficial zone.

The results of the histology give some insight into the effects of scaffold morphology on cell growth and cellular infiltration. There were numerous cell aggregates (cell clusters) especially in crevices on the surfaces of the scaffolds. The cells in these clusters appeared more spheroid in shape whereas the cells in the thin layers (one to only a few cells in thickness) usually appeared elongated. The formation of such cell clusters has been observed inside tissue-engineered matrices by others studying the *in vitro* regeneration of articular cartilage [90].

It has been shown by Vunjak-Novakovic et al. that dynamic cell seeding results in a more uniform distribution of cells throughout the scaffold, and higher seeding cell numbers have been associated with high rates of cartilage matrix production (partially attributed to greater opportunities for cell-to-cell and cell-to-matrix interactions) [138, 152]. It is believed that an uneven distribution of cells may lead to an inhomogeneous repair tissue which is unacceptable in cartilage repair. To date a homogeneous cell distribution has been best achieved in the gel matrix [153]. The initial cell seeding study performed as part of this research demonstrated that cells attached to both sides of the scaffolds with dynamic cell seeding in the bioreactor environment. However, the histology results here show that there were always more cells on one side/surface of the scaffolds than on the

other side/surface. In a few sections, there is some cellular infiltration from the direction of the side with the most cells. The seeding density used in this research definitely resulted in the attachment of cells to all scaffolds, but no conclusions can be made at this point about the effects on matrix production (as described below).

There was only one statistically significant change in thickness over time and that was for the 100 mg/mL concentration between week 0 and week 4, though this finding can not sufficiently be explained by the other results (biochemical, mechanical, or histological). The reason for the lower thickness of the 100 mg/mL concentration compared to the 80 mg/mL concentration could be explained by the loss of fibers during the electrospinning process (which is known to be affected by changes in temperature, humidity, and extraneous electrical interferences).

The main observation made regarding cell migration is that most cellular infiltration into the scaffold occurred where there is a path for the cells to move along. Such a path could be a tear or a large void or pocket along the surface of the scaffold or an area of delamination (separation of the layers of fibers sometimes created during electrospinning) on the edge of the scaffold disc. Clusters of cells appeared to be moving into the openings on the edges of some of the 3 mm diameter scaffolds. This is interesting because these sections were punched out of the 1 cm cultured disc, so the ends are not exposed before punching; however, these 3 mm discs are punched from near or on the edge of the 1 cm disc so it is possible the cells had time to migrate into the scaffolds from the edge over the 2, 4, or 6 week culture period. Migration occurring from the edges of the scaffolds may also be because the matrix is a layering of fibers in two dimensions; cells

moving in from the edge can follow one fiber into the scaffold rather than moving from fiber to fiber (as the cells would during migration from the surface into the thickness).

The number of chondrocytes per mg of cartilage (wet mass) has been shown to be between 26,000 and 78,000 chondrocytes/mg [154]. This finding is much lower than most of the cell density values determined in this research with the exception of the 120 mg/mL concentration and the 80 mg/mL and 100 mg/mL concentrations at week 2. In viewing the histological slides, there did appear to be more cells in the 60 mg/mL, 80 mg/mL, and 100 mg/mL concentrations; this finding does correlate with the DNA analysis results which showed that the 120 mg/mL concentration over all three culture periods resulted in the lowest cell density. The general trend is that cell density increased over time, thereby indicating proliferation on the collagen scaffolds. This trend does seem to be supported by the histology. Several of the cell density mean values have quite large standard deviations, possibly indicating poor uniformity of cell distribution. One note needs to be made regarding cell density: in measuring the DNA content in the scaffold samples, an excitation wavelength of 320 nm had to be used even though the Hoechst 33258 dye excites at 365 nm and an emission wavelength of 460 nm had to be used despite an emission peak at 458 nm for the Hoechst 33258 dye. This was due to the limitations of the instrument available. Though the wavelengths used are not exactly at the peaks of the spectra for this dye, the widths of the spectra are such that analysis was still possible.

The GAG content measured in this research represents that deposited on/within the collagen scaffold, and was much lower than a reported range of GAG content in articular cartilage found to be between 22 and 38 μg/mg of cartilage (wet mass) [154]. The GAG

content did not increase over time in any of the concentrations as was expected. In fact, there are no statistically significant differences between any of the GAG contents in any one concentration over the different culture periods, nor are there any differences between the GAG contents in any one culture period over the different concentrations. Thus, it may be possible that the cells did not reexpress the chondrocytic phenotype despite the appearance of spheroid-shaped cells particularly in the 60 mg/mL, 80 mg/mL, and 100 mg/mL concentrations. There is an explanation for the appearance of GAGs in the control scaffolds that contain no cells. Though the purity of the collagen samples was consistent with the type II collagen standard supplied by the University of Tennessee, RDRCC Collagen Core Center [134], there may still be the presence of proteoglycans that were not removed in the collagen extraction process. The molecular weight of the backbone core protein is around 250,000 and that of chondroitin sulfate is about 20,000; there is an average of 80 chondroitin sulfate chains present in a typical cartilage proteoglycan [155]. Thus, this high molecular weight would not appear on the gel used in the SDS-PAGE in this research.

The collagen synthesis detected by the ELISA tests was minimal. Only the 80 mg/mL and 100 mg/mL concentrations showed any type II collagen present. From those results, the values of type II collagen content that aren't essentially zero are those values for the 80 mg/mL concentration at weeks 2 and 4 and those for the 100 mg/mL concentration at weeks 4 and 6. The histology (Masson's trichrome-stained sections) revealed the presence of collagen, by way of light blue staining, in the 80 mg/mL concentration at weeks 2 and 6 and in the 100 mg/mL concentration at weeks 4 and 6;

these results do correlate with the results of the type II collagen ELISA test. Very slight

areas of blue staining were seen in the 60 mg/mL concentration at week 6 and in the 120

mg/mL concentration at week 6. The type I collagen ELISA test did detect type I collagen

in these two concentrations (60 mg/mL and 120 mg/mL) though the mean values are very

close to zero. Though type II collagen was not produced in large quantities, it is good that

type I collagen was not produced. This could potentially mean that the cells have not

changed phenotypes; however, they are not actively making their own matrix.

It is very interesting that the type II collagen ELISA did not detect the collagen that

comprised the scaffold itself – this is shown by the zero reading (or essentially zero) for

the control scaffolds at week 0. The lyophilized collagen (at the stage prior to dissolution

in HFP and subsequent electrospinning) is detected by the ELISA and, in fact, results in a

standard curve closely matching that created by running the standard provided in the kit.

Further tests are underway to understand if the electrospinning process or possibly the

cross-linking process transforms the collagen in such a manner as to mask the epitopes

detected by the ELISA kit antibodies. Type II collagen dissolved in HFP as well as

electrospun type II collagen were detected by the ELISA kit though the concentrations

(including the standards run in this particular test) were not what were expected (i.e.

known concentrations were prepared and tested) – since an already-opened kit was used, it

is possible that the thawed, re-frozen, and thawed antibodies were no longer stable. The

spike and recovery test revealed that the spiked samples gave readings equal to the reading

of the standard alone. Thus, the standard is working but the collagen in the samples is

either at undetectable levels (unlikely since the scaffolds are composed of type II collagen)

or is not being detected by the antibody that was raised against the collagen molecules in the standard. This test showed that the sample preparation is sufficient since the standard was recovered from the samples (i.e. nothing in the preparation is hindering the binding of the standard), but the collagen molecules in the samples won't bind to the kit antibody. The cross-linking effect of EDC could have rendered a conformational change (to the type II collagen in the electrospun mat) that has hindered/inhibited the binding to the epitopes by the antibodies (provided in the ELISA kit) that are specific to those epitopes of native type II collagen. Such a conclusion was made with porcine dermal collagen membranes treated with glutaraldehyde [156]. An interesting study would be to recharacterize the cross-linked, electrospun type II collagen scaffolds by developing a new antibody for these scaffolds that would recognize and bind to the new epitopes/surface residues available in these scaffolds. Testing the new antibody versus the original antibody (from the kit, that recognizes native type II collagen epitopes) may prove to be insightful.

Scaffold Mechanical Properties

In native tissue, at small extensions, there is a non-linear toe region in which collagen fibers are realigning, and at larger extensions, the aligned collagen fibers are stretched collectively thereby contributing to the stiffness observed in the curve [27]. The same phenomenon is occurring in the cross-linked, electrospun, non-woven mats, in which the randomly-oriented collagen fibers first align themselves at small extensions and are collectively strained at larger extensions.

The stiffness of the structure as a whole depends on fiber diameter and orientation, number of fibers, and the strength of covalent cross-links and noncovalent bonds (i.e. type and amount). The tensile material properties do not follow a particular trend in this research. The diameter and pore area measurements determined from the permeability meter show that the mean values increase with concentration with the exception of the 120 mg/mL concentration, which showed a decrease to values below that of the 100 mg/mL concentration. There may be a concentration threshold at which the collagen molecules can no longer form fibers of larger diameters. Additionally, alignment was not controlled because a random arrangement of fibers was the desired effect. Though no control efforts were made, the increasing diameters may have had an effect on the arrangement of the fibers; this alignment needs to be measured in future work. All of the cross-linked, electrospun mats tested in this research demonstrated values of peak stress and tangential modulus at least an order of magnitude less than those reported for cartilage tissue, and the strain at break values of the electrospun mats were at least an order of magnitude greater than the value of this property for native cartilage tissue. Though it must be kept in mind that these differences reflect variances between a simulated ECM alone versus whole tissue, it does bode well for the use of electrospun type II collagen mats in the tissue engineering of cartilage in that during tissue regeneration *in vitro*, the stiffness of the electrospun scaffold should not inhibit chondrocyte mobility, and the electrospun fibers should be free to be moved by the cells themselves [101]. However, this was not the case in this research; the cells did not appear to move the fibers so that cellular infiltration could occur rapidly.

The cross-linked, electrospun scaffolds maintained their structural integrity during the 6 weeks of culture such that they could still be easily manipulated with forceps. Such capacity to maintain strength favors these scaffolds over collagen gels for use in cartilage tissue engineering.

In the stress relaxation test, a constant displacement is applied to the specimen surface and the resulting stress within the tissue is measured. During the ramp phase of the displacement, the tissue is compressed at a constant rate, fluid exudation occurs and the solid ECM is compacted. During the relaxation phase, once the desired displacement is attained and the compressive strain is held constant, fluid and stress redistribution occurs within the specimen until an equilibrium is achieved (i.e. a homogeneous state of compression is achieved). This method (with indentation) was selected because of the anticipated limited thickness of the cultured tissue and the requirement to not disturb the surrounding tissue since it was to be used in other biochemical testing and histology. There were no statistically significant differences between the equilibrium stiffness values of the controls (week 0); thus, the electrospinning solution concentration (and hence the fiber diameter and pore size) did not have an influence on the equilibrium stiffness. Culture time also had little to no influence as shown by the few statistical differences that do not follow any particular pattern. One point of interest is that at week 6 the 120 mg/mL concentration is significantly different from all of the other concentrations; this correlates well with the finding that the 120 mg/mL concentration had the lowest cell density, which was significantly different from the cell densities of all of the other concentrations. The trend that the mean equilibrium stiffness decreases from week 2 to week 6 may be related

to the cell density trend in which the mean cell density increases from week 2 to week 6 (with the exception of the 120 mg/mL concentration). Thus, a decrease in equilibrium stiffness may be related to an increase in cell density. Very little degradation, if any, is suspected over the 6 week culture period because the pore structure appeared the same at week 6 as at week 0 per the histological analysis. However, it is possible that there was some slight degradation occurring in the scaffolds which may account for the general decreasing trend in equilibrium stiffness over time. The exact degradation rate has yet to be determined.

Mechanical stimulation via hydrodynamic forces in the rotating chambers of the bioreactor during *in vitro* cultivation is proposed to more closely resemble some of the aspects of the dynamic loading on cartilage *in vivo* and has been shown to result in the production of the cartilaginous matrix components GAG and type II collagen with uniform distribution in some tissue-engineered constructs [56]. In the research presented here it is not clear if the dynamic bioreactor environment had any influences on the mechanical properties or biochemical compositions of the scaffolds. It is possible that greater hydrodynamic loading is necessary to stimulate the cells on these scaffolds that were found to be stiffer than native cartilage. In any case, the benefits of being able to control the conditions of cell seeding and culture environment more easily in the bioreactor were appreciated in this research.

Conclusions and Future Work

The electrospun type II collagen mats created for this research have the desired fibrous structure (on the scale of native ECM) and possess mechanical properties (following cross-linking) that enable handling and use in culture conditions. Based on the biochemical results in conjunction with the histology, the cell proliferation and biosynthetic activity of the chondrocytes was not influenced (to a statistically significant level) by electrospinning solution concentration (i.e. fiber diameter and pore size) or by time in culture. In fact, very little if any biosynthetic activity (GAG and collagen synthesis) was observed in this research. While the cells are still proliferating, there will be minimal production of matrix components.

It is possible that, following the extraction process involving the use of pepsin that digests and removes the telopeptide ends, the product remaining is type II atelocollagen [90]; this is no longer the ordered fibril form that existed before the extraction process. After electrospinning, the mat may be more of a filamentous structure rather than composed of collagen fibrils (of an ordered structure) because of a lack of native crosslinks. Hence, the structure may be in the monomeric form. The EDC is used to cross-link the electrospun mat such that it has sufficient mechanical integrity to withstand tissue culture conditions. It would be of interest to know if the lack of native crosslinks, which in turn does not allow the formation of purely native type II collagen fibrils,

interferes with cell signaling in any way. Thus, further investigation into the exact chemical structure of the cross-linked, electrospun type II collagen molecules should be performed in an effort to better understand the cell-matrix interactions.

Though the chemical composition may not be exactly native type II collagen, the first action item for future work should be investigating the scaffold design. The electrospun mats that underwent the studies in culture were used in the physical state they were in when removed from the mandrel (with cross-linking and subsequent swelling upon hydration). The results of this research showed very little cellular migration into the scaffold thickness and very little matrix biosynthetic activity, which could be because the cells remained on the surface of the scaffolds and grew outward from the scaffold, thereby really only participating in cell-to-cell interactions.

Most of the studies that have had some successes in stimulating the production of cartilaginous tissue (i.e. engineered cartilage) have utilized scaffolds with large interconnected pores, in the range of 50 to 300 μm. The electrospun scaffolds achieve pore interconnectivity, but the pore size is very small. Additionally, this research did not reveal an ability of the chondrocytes to move the fibers in order to migrate into the scaffolds (in fact, most cellular infiltration only occurred at open paths into the thickness/cross-section of the scaffolds). A design proposition would be to actually punch uniformly distributed holes, on the 100 μm scale, into the hydrated scaffold (following cross-linking) to provide direct paths large enough for the cells to easily migrate through and into the thickness of the scaffold. Exact geometries, and the consequential effects on the mechanical properties, would have to be investigated. Additionally, cells could be sprayed into the scaffold

during the electrospinning fabrication process. This would create a scaffold with cells already distributed within the scaffold; however, sterile conditions must be maintained.

On an additional design note, the tissue structure created in this research more closely resembles the superficial zone than the middle zone at this point. Though the collagen fibers are randomly organized within the electrospun mat, the fibers are essentially only in two dimensions and run tangential to the mat surfaces. Thought needs to be given as to how to create fibers that run perpendicular to the mat surfaces such that fibers are oriented randomly in three dimensions.

Several modifications can be made to the methods in future work to improve the analysis of GAGs and collagen, such as using the stains safranin-O or alcian blue for histochemical visualization of proteoglycans or picrosirius red to stain for collagen, or using SEM to visualize the cells on the surface of the scaffolds (to better show spherical versus elongated). Additionally, instead of the ELISA for detection of collagen, several other techniques could be used including fluorescence immunostaining, probing the cells via in situ hybridization, or de novo synthesis with radioactive proline. It could be possible that the cells need longer culture periods to degrade the existing scaffold, migrate into the scaffold, and replace the scaffold with their own ECM. Though spherical cells were observed, the chondrocytes may need to be redifferentiated or freshly isolated chondrocytes could be used instead of chondrocytes cultured in monolayer prior to seeding. The passaged cells could be combined with primary chondrocytes when seeded onto the scaffolds; such a co-culture approach has proven successful in increasing cartilage tissue formation [132]. Fabricating a scaffold out of another material or a mixture of

materials (i.e. natural and synthetic polymers) may stimulate the cells to make their own matrix; the type II collagen could be electrospun with another polymer, either from the same mixture or from multiple nozzles. It has been shown that chondrocytes respond to decreases in the amount of matrix surrounding them by increasing their rate of matrix deposition [152]. Thus, tailoring the degradation rate (e.g. via cross-linking or modifying the materials) of the scaffold to be more rapid may cause the chondrocytes to respond with increased synthesis.

From the results of this research, there did not appear to be extensive cell-matrix interactions. In articular cartilage, there is an interdependence between the two components in which the chondrocytes synthesize and degrade the ECM, and the ECM protects the chondrocytes from mechanical damage, transmits and stores such molecules as cytokines and growth factors for the chondrocytes, and acts as a signal transducer for the chondrocytes to help maintain their phenotype. Though the chondrocytes attached to the surfaces of the scaffolds, the cell layers grew outward from the scaffolds and formed cell clusters in many areas. There was very little cellular infiltration unless there was an opening of significant size (typically larger than the size of the cell). The author believes that the first item to address given these results is to reevaluate the scaffold design.

Literature Cited

Literature Cited

1.   Buckwalter, J.A. and H.J. Mankin, *Instructional Course Lectures, The American Academy of Orthopaedic Surgeons - Articular cartilage. Part II: Degeneration and osteoarthrosis, repair, regeneration, and transplantation.* Journal of Bone and Joint Surgery Am., 1997. **79**(4): p. 612-632.

2.   Arthritis_Foundation, *Disease Center: Osteoarthritis, http://www.arthritis.org/disease-center.php?disease_id=32. Accessed July 27, 2007.* 2007.

3.   Pearle, A.D., R.F. Warren, and S.A. Rodeo, *Basic science of articular cartilage and osteoarthritis.* Clinics In Sports Medicine, 2005. **24**(1): p. 1-+.

4.   Nesic, D., et al., *Cartilage tissue engineering for degenerative joint disease.* Advanced Drug Delivery Reviews, 2006. **58**(2): p. 300-322.

5.   Hunziker, E.B., *Articular cartilage repair: Basic science and clinical progress. A review of the current status and prospects.* Osteoarthritis and Cartilage, 2002. **10**(6): p. 432-463.

6.   Bell, E., *Tissue engineering: a perspective.* Journal of Cellular Biochemistry, 1991. **45**(3): p. 239-41.

7.   Langer, R. and J.P. Vacanti, *Tissue engineering.* Science., 1993. **260**(5110): p. 920-6.

8.   Marler, J.J., et al., *Transplantation of cells in matrices for tissue regeneration.* Advanced Drug Delivery Reviews, 1998. **33**(1-2): p. 165-182.

9.   Buckwalter, J.A., L.C. Rosenberg, and E.B. Hunziker, *Articular cartilage: Composition, structure, response to injury, and methods of facilitating repair*, in *Articular Cartilage and Knee Joint Function: Basic Science and Arthroscopy*, J.W. Ewing, Editor. 1990, Raven Press: New York. p. 19-56.

10.   Mow, V.C., D.C. Fithian, and M.A. Kelly, *Fundamentals of articular cartilage and meniscus biomechanics*, in *Articular Cartilage and Knee Joint Function: Basic Science and Arthroscopy*, J.W. Ewing, Editor. 1990, Raven Press: New York. p. 1-18.

11.   Fung, Y.C., *Bone and cartilage*, in *Biomechanics: Mechanical Properties of Living Tissues*. 1993, Springer-Verlag: New York. p. 500-544.

12.   Hasler, E.M., et al., *Articular cartilage biomechanics: Theoretical models, material properties, and biosynthetic response.* Critical Reviews in Biomedical Engineering, 1999. **27**(6): p. 415-488.

13.   Temenoff, J.S. and A.G. Mikos, *Review: Tissue engineering for regeneration of articular cartilage.* Biomaterials, 2000. **21**(5): p. 431-440.

14. Mow, V.C., W. Zhu, and A. Ratcliffe, *Structure and function of articular cartilage and meniscus*, in *Basic Orthopaedic Biomechanics*, V.C. Mow and W.C. Hayes, Editors. 1991, Raven Press: New York. p. 143-198.

15. Almarza, A.J. and K.A. Athanasiou, *Design characteristics for the tissue engineering of cartilaginous tissues.* Annals of Biomedical Engineering, 2004. **32**(1): p. 2-17.

16. Birk, D.E. and P. Bruckner, *Collagen suprastructures*, in *Topics in Current Chemistry: Collagen*, J. Brinckmann, H. Notbohm, and P.K. Muller, Editors. 2005, Springer-Verlag: Berlin. p. 185-205.

17. Koide, T. and K. Nagata, *Collagen biosynthesis*, in *Topics in Current Chemistry: Collagen*, J. Brinckmann, H. Notbohm, and P.K. Muller, Editors. 2005, Springer-Verlag: Berlin. p. 85-114.

18. Silver, F.H., I. Horvarth, and D.J. Foran, *Mechanical implications of the domain structure of fiber-forming collagens: Comparison of the molecular and fibrillar flexibilities of the alpha 1-chains found in types I-III collagen.* Journal of Theoretical Biology, 2002. **216**(2): p. 243-254.

19. Zimmermann, B.K., et al., *Cross-linkages in collagen - Demonstration of 3 different intermolecular bonds.* European Journal of Biochemistry, 1970. **16**(2): p. 217-225.

20. Lin, Z., et al., *The chondrocyte: Biology and clinical application.* Tissue Engineering, 2006. **12**(7): p. 1971-1984.

21. Buckwalter, J.A. and H.J. Mankin, *Instructional Course Lectures, The American Academy of Orthopaedic Surgeons - Articular cartilage. Part I: Tissue design and chondrocyte-matrix interactions.* Journal of Bone and Joint Surgery Am., 1997. **79**(4): p. 600-611.

22. Meachim, G. and R.A. Stockwell, *The chondrocytes*, in *Adult Articular Cartilage*, M.A.R. Freeman, Editor. 1973, Grune & Stratton: New York. p. 51-99.

23. Meachim, G. and R.A. Stockwell, *The matrix*, in *Adult Articular Cartilage*, M.A.R. Freeman, Editor. 1973, Grune & Stratton: New York. p. 1-50.

24. Mow, V.C. and C.C.B. Wang, *Some bioengineering considerations for tissue engineering of articular cartilage.* Clinical Orthopaedics and Related Research, 1999(367): p. S204-S223.

25. Buckwalter, J.A. and E.B. Hunziker, *Articular cartilage morphology and biology*, in *Biology of the Synovial Joint*, C.W. Archer, et al., Editors. 1999, Harwood Academic Publishers: Amsterdam. p. 75-100.

26. Laasanen, M.S., et al., *Biomechanical properties of knee articular cartilage.* Biorheology, 2003. **40**(1-3): p. 133-140.

27. Mow, V. and X.E. Guo, *Mechano-electrochemical properties of articular cartilage: Their inhomogeneities and anisotropies.* Annual Review of Biomedical Engineering, 2002. **4**: p. 175-209.

28. Akizuki, S., et al., *Tensile properties of human knee-joint cartilage.1. Influence of ionic conditions, weight bearing, and fibrillation on the tensile modulus.* Journal of Orthopaedic Research, 1986. **4**(4): p. 379-392.

29. Yamada, H., *Tensile properties of human hyaline cartilage*, in *Strength of Biological Materials*, F.G. Evans, Editor. 1970, Robert E. Krieger Publishing Company: Huntington, New York. p. 80-81.

30. Abbott, W.M. and R.P. Cambria, *Control of physical characteristics (elasticity and compliance) of vascular grafts*, in *Biological and Synthetic Vascular Prostheses*, J.C. Stanley, Editor. 1982, Grune and Stratton: New York, NY. p. 189-220.

31. Mak, A.F., W.M. Lai, and V.C. Mow, *Biphasic indentation of articular cartilage. 1. Theoretical analysis.* Journal of Biomechanics, 1987. **20**(7): p. 703-714.

32. Mow, V.C., C.S. Proctor, and M.A. Kelly, *Biomechanics of articular cartilage*, in *Basic Biomechanics of the Musculoskeletal System*, M. Nordin and V.H. Frankel, Editors. 1989, Lea & Febiger: Philadelphia. p. 31-58.

33. Nehrer, S., et al., *Chondrocyte-seeded collagen matrices implanted in a chondral defect in a canine model.* Biomaterials, 1998. **19**(24): p. 2313-2328.

34. Mow, V.C. and L.J. Soslowsky, *Friction, lubrication, and wear of diarthrodial joints*, in *Basic Orthopaedic Biomechanics*, V.C. Mow and W.C. Hayes, Editors. 1991, Raven Press: New York. p. 245-292.

35. Darling, E.M. and K.A. Athanasiou, *Biomechanical strategies for articular cartilage regeneration.* Annals of Biomedical Engineering, 2003. **31**(9): p. 1114-1124.

36. Frenkel, S.R. and P.E. Di Cesare, *Scaffolds for articular cartilage repair.* Annals of Biomedical Engineering, 2004. **32**(1): p. 26-34.

37. Vunjak-Novakovic, G., *The fundamentals of tissue engineering: Scaffolds and bioreactors*, in *Tissue Engineering of Cartilage and Bone*, G. Bock and J. Goode, Editors. 2003, Wiley: Chichester, West Sussex. p. 34-51.

38. Cancedda, R., et al., *Tissue engineering and cell therapy of cartilage and bone.* Matrix Biology, 2003. **22**(1): p. 81-91.

39. Lindahl, A., M. Brittberg, and L. Peterson, *Cartilage repair with chondrocytes: clinical and cellular aspects*, in *Tissue Engineering of Cartilage and Bone*, G. Bock and J. Goode, Editors. 2003, Wiley: Chichester, West Sussex. p. 175-189.

40. Beris, A.E., et al., *Advances in articular cartilage repair.* Injury, Int. J. Care Injured, 2005. **36**(Suppl 4): p. S14-23.

41. Kuo, C.K., et al., *Cartilage tissue engineering: its potential and uses.* Current Opinion In Rheumatology, 2006. **18**(1): p. 64-73.

42. Yang, F. and J.H. Elisseeff, *Cartilage tissue engineering*, in *Tissue Engineering and Artificial Organs*, J.D. Bronzino, Editor. 2006, Taylor and Francis Group: Boca Raton. p. 51-1-51-11.

43. Kino-Oka, M., et al., *A kinetic modeling of chondrocyte culture for manufacture of tissue-engineered cartilage.* Journal of Bioscience and Bioengineering, 2005. **99**(3): p. 197-207.

44. Thirion, S. and F. Berenbaum, *Culture and phenotyping of chondrocytes in primary culture*, in *Cartilage and Osteoarthritis*, M. Sabatini, P. Pastoureau, and F.D. Ceuninck, Editors. 2004, Humana Press: Totowa, NJ. p. 1-14.

45.   Capito, R.M. and M. Spector, *Scaffold-based articular cartilage repair.* IEEE Eng Med Biol Mag., 2003. **22**(5): p. 42-50.

46.   Randolph, M.A., K. Anseth, and M.J. Yaremchuk, *Tissue engineering of cartilage.* Clinics in Plastic Surgery, 2003. **30**(4): p. 519-537.

47.   Grande, D.A., et al., *Evaluation of matrix scaffolds for tissue engineering of articular cartilage grafts.* Journal of Biomedical Materials Research, 1997. **34**(2): p. 211-220.

48.   Huckle, J., et al., *Differentiated chondrocytes for cartilage tissue engineering*, in *Tissue Engineering of Cartilage and Bone*, G. Bock and J. Goode, Editors. 2003, Wiley: Chichester, West Sussex. p. 103-117.

49.   Buschmann, M.D., et al., *Chondrocytes in agarose culture synthesize a mechanically functional extracellular-matrix.* Journal of Orthopaedic Research, 1992. **10**(6): p. 745-758.

50.   Boland, E.D., et al., *Tissue engineering scaffolds*, in *The Encyclopedia of Biomaterials and Biomedical Engineering*, G.L. Bowlin and G.E. Wnek, Editors. 2004, Marcel Dekker, Inc.: New York. p. 1630-1638.

51.   Lee, J.H., J. Kisiday, and A.J. Grodzinsky, *Tissue-engineered versus native cartilage: linkage between cellular mechano-transduction and biomechanical properties*, in *Tissue Engineering of Cartilage and Bone*, G. Bock and J. Goode, Editors. 2003, Wiley: Chichester, West Sussex. p. 52-69.

52.   Li, K.W., et al., *In vitro physical stimulation of tissue-engineered and native cartilage*, in *Cartilage and Osteoarthritis*, M. Sabatini, P. Pastoureau, and F.D. Ceuninck, Editors. 2004, Humana Press: Totowa, NJ. p. 325-351.

53.   Buschmann, M.D., et al., *Mechanical compression modulates matrix biosynthesis in chondrocyte agarose culture.* Journal of Cell Science, 1995. **108**: p. 1497-1508.

54.   Carver, S.E. and C.A. Heath, *Increasing extracellular matrix production in regenerating cartilage with intermittent physiological pressure.* Biotechnology And Bioengineering, 1999. **62**(2): p. 166-174.

55.   Freed, L.E. and G. Vunjak-Novakovic, *Tissue engineering of cartilage*, in *The Biomedical Engineering Handbook: Second Edition*, J.D. Bronzino, Editor. 2000, CRC Press LLC: Boca Raton.

56.   Vunjak-Novakovic, G., et al., *Bioreactor studies of native and tissue engineered cartilage.* Biorheology, 2002. **39**(1-2): p. 259-268.

57.   Chen, H.C. and Y.C. Hu, *Bioreactors for tissue engineering.* Biotechnology Letters, 2006. **28**(18): p. 1415-1423.

58.   Athanasiou, K.A., et al., *Basic science of articular cartilage repair.* Clinics in Sports Medicine, 2001. **20**(2): p. 223-247.

59.   Vunjak-Novakovic, G., et al., *Bioreactor cultivation conditions modulate the composition and mechanical properties of tissue-engineered cartilage.* Journal Of Orthopaedic Research, 1999. **17**(1): p. 130-138.

60.   Freed, L.E. and G. Vunjak-Novakovic, *Cultivation of cell-polymer tissue constructs in simulated microgravity.* Biotechnology and Bioengineering, 1995. **46**(4): p. 306-313.

61.   Gooch, K.J., et al., *Effects of mixing intensity on tissue-engineered cartilage.* Biotechnology and Bioengineering, 2001. **72**(4): p. 402-407.

62.   Reneker, D.H. and I. Chun, *Nanometre diameter fibres of polymer, produced by electrospinning.* Nanotechnology, 1996. **7**(3): p. 216-223.

63.   Doshi, J. and D.H. Reneker, *Electrospinning process and applications of electrospun fibers.* Journal of Electrostatics, 1995. **35**(2-3): p. 151-160.

64.   Huang, Z.M., et al., *A review on polymer nanofibers by electrospinning and their applications in nanocomposites.* Composites Science and Technology, 2003. **63**(15): p. 2223-2253.

65.   Shenoy, S.L., et al., *Role of chain entanglements on fiber formation during electrospinning of polymer solutions: good solvent, non-specific polymer-polymer interaction limit.* Polymer, 2005. **46**(10): p. 3372-3384.

66.   Kidoaki, S., I.K. Kwon, and T. Matsuda, *Mesoscopic spatial designs of nano- and microfiber meshes for tissue-engineering matrix and scaffold based on newly devised multilayering and mixing electrospinning techniques.* Biomaterials, 2005. **26**(1): p. 37-46.

67.   Matthews, J.A., et al., *Electrospinning of collagen type II: A feasibility study.* Journal of Bioactive and Compatible Polymers, 2003. **18**(2): p. 125-134.

68.   Shields, K.J., et al., *Mechanical properties and cellular proliferation of electrospun collagen type II.* Tissue Engineering, 2004. **10**(9-10): p. 1510-1517.

69.   Bhattarai, N., et al., *Alginate-based nanofibrous scaffolds: Structural, mechanical, and biological properties.* Advanced Materials, 2006. **18**(11): p. 1463-1467.

70.   Li, W.J., et al., *Biological response of chondrocytes cultured in three-dimensional nanofibrous poly(epsilon-caprolactone) scaffolds.* Journal of Biomedical Materials Research Part A, 2003. **67A**(4): p. 1105-1114.

71.   Li, W.J., et al., *A three-dimensional nanofibrous scaffold for cartilage tissue engineering using human mesenchymal stem cells.* Biomaterials, 2005. **26**(6): p. 599-609.

72.   Li, W.J., et al., *Fabrication and characterization of six electrospun poly(alpha-hydroxy ester)-based fibrous scaffolds for tissue engineering applications.* Acta Biomaterialia, 2006. **2**(4): p. 377-385.

73.   Shin, H.J., et al., *Electrospun PLGA nanofiber scaffolds for articular cartilage reconstruction: mechanical stability, degradation and cellular responses under mechanical stimulation in vitro.* Journal of Biomaterials Science-Polymer Edition, 2006. **17**(1-2): p. 103-119.

74.   Subramanian, A., et al., *Preparation and evaluation of the electrospun chitosan/PEO fibers for potential applications in cartilage tissue engineering.* Journal of Biomaterials Science-Polymer Edition, 2005. **16**(7): p. 861-873.

75.   Martins-Green, M., *Dynamics of cell-ECM interactions*, in *Principles of Tissue Engineering*, R.P. Lanza, R. Langer, and J. Vacanti, Editors. 2000, Academic Press: San Diego. p. 33-55.

76.   Humphries, M.J., *The molecular basis and specificity of integrin-ligand interactions.* J Cell Sci., 1990. **97**(Pt 4): p. 585-92.

77. Palsson, B.O. and S.N. Bhatia, *Coordination of cellular-fate processes*, in *Tissue Engineering*. 2004, Pearson Prentice Hall: Upper Saddle River, NJ. p. 105-130.

78. Olsen, B.R., *Matrix molecules and their ligands*, in *Principles of Tissue Engineering*, R.P. Lanza, R. Langer, and J. Vacanti, Editors. 2000, Academic Press: San Diego. p. 57-71.

79. Greisler, H.P., et al., *Biointeractive polymers and tissue engineered blood vessels*. Biomaterials, 1996. **17**(3): p. 329-336.

80. How, T.V., R. Guidoin, and S.K. Young, *Engineering design of vascular prostheses*. Proceedings of the Institution of Mechanical Engineers. Part H, Journal of Engineering in Medicine, 1992. **206**(2): p. 61-71.

81. Mooney, D. and R. Langer, *Engineering biomaterials for tissue engineering: The 10 - 100 micron size scale*, in *The Biomedical Engineering Handbook*, J. Bronzino, Editor. 1995, CRC Press: Boca Raton. p. 1609-1618.

82. Starke, G.R., A.S. Douglas, and D.J. Conway, *An integral mathematical approach to tissue engineering of vascular grafts*, in *Tissue Engineering of Prosthetic Vascular Grafts*, P. Zilla and H.P. Greisler, Editors. 1999, R.G. Landes Company. p. 441-459.

83. Hsu, S. and H. Kambic, *On matching compliance between canine carotid arteries and polyurethane grafts*. Artificial Organs, 1997. **21**(12): p. 1247-1254.

84. Li, W.J., et al., *Electrospun nanofibrous structure: A novel scaffold for tissue engineering*. Journal of Biomedical Materials Research, 2002. **60**(4): p. 613-621.

85. Grinnell, F., *Cell-collagen interactions: Overview*. Methods in Enzymology, 1982. **82**(Pt A): p. 499-503.

86. Nehrer, S., et al., *Canine chondrocytes seeded in type I and type II collagen implants investigated in vitro*. Journal of Biomedical Materials Research, 1997. **38**(2): p. 95-104.

87. Nehrer, S., et al., *Matrix collagen type and pore size influence behaviour of seeded canine chondrocytes*. Biomaterials, 1997. **18**(11): p. 769-776.

88. Lee, C.R., et al., *Effects of a cultured autologous chondrocyte-seeded type II collagen scaffold on the healing of a chondral defect in a canine model*. Journal of Orthopaedic Research, 2003. **21**(2): p. 272-281.

89. Dorotka, R., et al., *Marrow stimulation and chondrocyte transplantation using a collagen matrix for cartilage repair*. Osteoarthritis And Cartilage, 2005. **13**(8): p. 655-664.

90. Pieper, J.S., et al., *Crosslinked type II collagen matrices: Preparation, characterization, and potential for cartilage engineering*. Biomaterials, 2002. **23**(15): p. 3183-3192.

91. Shi, D.H., et al., *Development and potential of a biomimetic chitosan/type II collagen scaffold for cartilage tissue engineering*. Chinese Medical Journal, 2005. **118**(17): p. 1436-1443.

92. Yang, K.G.A., et al., *Impact of expansion and redifferentiation conditions on chondrogenic capacity of cultured chondrocytes*. Tissue Engineering, 2006. **12**(9): p. 2435-2447.

93.   Auger, F.A., et al., *Tissue-engineered skin substitutes: from in vitro constructs to in vivo applications.* Biotechnology and Applied Biochemistry, 2004. **39**: p. 263-275.

94.   Wallace, D.G. and J. Rosenblatt, *Collagen gel systems for sustained delivery and tissue engineering.* Advanced Drug Delivery Reviews, 2003. **55**(12): p. 1631-1649.

95.   Nerem, R.M. and D. Seliktar, *Vascular tissue engineering.* Annual Review of Biomedical Engineering, 2001. **3**: p. 225-243.

96.   Bell, E., *Organotypic and histiotypic models of engineered tissues*, in *Principles of Tissue Engineering*, R.P. Lanza, R. Langer, and J. Vacanti, Editors. 2000, Academic Press: San Diego, CA. p. 181-194.

97.   Mueller, S.M., et al., *Meniscus cells seeded in type I and type II collagen-GAG matrices in vitro.* Biomaterials, 1999. **20**(8): p. 701-709.

98.   Itoh, H., et al., *A honeycomb collagen carrier for cell culture as a tissue engineering scaffold.* Artificial Organs, 2001. **25**(3): p. 213-217.

99.   Matthews, J.A., et al., *Electrospinning of collagen nanofibers.* Biomacromolecules, 2002. **3**(2): p. 232-8.

100.   Buttafoco, L., et al., *Electrospinning of collagen and elastin for tissue engineering applications.* Biomaterials, 2006. **27**(5): p. 724-734.

101.   Boland, E.D., et al., *Electrospinning collagen and elastin: Preliminary vascular tissue engineering.* Frontiers in Bioscience, 2004. **9**: p. 1422-1432.

102.   Li, M.Y., et al., *Electrospun protein fibers as matrices for tissue engineering.* Biomaterials, 2005. **26**(30): p. 5999-6008.

103.   Rho, K.S., et al., *Electrospinning of collagen nanofibers: effects on the behavior of normal human keratinocytes and early-stage wound healing.* Biomaterials, 2006. **27**(8): p. 1452-61.

104.   Koob, T.J., *Collagen fixation*, in *Encyclopedia of Biomaterials and Biomedical Engineering*, G.E. Wnek and G.L. Bowlin, Editors. 2004, Marcel Dekker: New York. p. 335-347.

105.   Jayaraman, K., et al., *Recent advances in polymer nanofibers.* Journal of Nanoscience and Nanotechnology, 2004. **4**(1-2): p. 52-65.

106.   Smith, L.A. and P.X. Ma, *Nano-fibrous scaffolds for tissue engineering.* Colloids And Surfaces B-Biointerfaces, 2004. **39**(3): p. 125-131.

107.   Zhang, S.G., et al., *Design of nanostructured biological materials through self-assembly of peptides and proteins.* Current Opinion In Chemical Biology, 2002. **6**(6): p. 865-871.

108.   Whitesides, G.M. and B. Grzybowski, *Self-assembly at all scales.* Science, 2002. **295**(5564): p. 2418-2421.

109.   Hartgerink, J.D., E. Beniash, and S.I. Stupp, *Self-assembly and mineralization of peptide-amphiphile nanofibers.* Science, 2001. **294**(5547): p. 1684-1688.

110.   Ma, Z.W., et al., *Potential of nanofiber matrix as tissue-engineering scaffolds.* Tissue Engineering, 2005. **11**(1-2): p. 101-109.

111.   Zhang, R.Y. and P.X. Ma, *Synthetic nano-fibrillar extracellular matrices with predesigned macroporous architectures.* Journal of Biomedical Materials Research, 2000. **52**(2): p. 430-438.

112. Ma, P.X. and R.Y. Zhang, *Synthetic nano-scale fibrous extracellular matrix.* Journal of Biomedical Materials Research, 1999. **46**(1): p. 60-72.

113. Mooney, D.J. and R.S. Langer, *Engineering biomaterials for tissue engineering: The 10-100 micron size scale*, in *The Biomedical Engineering Handbook*, J.D. Bronzino, Editor. 2000, CRC Press: Boca Raton, FL.

114. Jayakrishnan, A. and S.R. Jameela, *Glutaraldehyde as a fixative in bioprostheses and drug delivery matrices.* Biomaterials, 1996. **17**(5): p. 471-484.

115. Badylak, S.F., *Modification of natural polymers: Collagen*, in *Methods of Tissue Engineering*, A. Atala and R. Lanza, Editors. 2002, Academic Press: San Diego, CA. p. 505-514.

116. Khor, E., *Methods for the treatment of collagenous tissues for bioprostheses.* Biomaterials, 1997. **18**(2): p. 95-105.

117. Schmidt, C.E. and J.M. Baier, *Acellular vascular tissues: Natural biomaterials for tissue repair and tissue engineering.* Biomaterials, 2000. **21**(22): p. 2215-2231.

118. Simmons, D.M. and J.N. Kearney, *Evaluation of collagen cross-linking techniques for the stabilization of tissue matrices.* Biotechnology and Applied Biochemistry, 1993. **17**: p. 23-29.

119. Eyre, D.R. and J.-J. Wu, *Collagen cross-links*, in *Topics in Current Chemistry: Collagen*, J. Brinckmann, H. Notbohm, and P.K. Muller, Editors. 2005, Springer-Verlag: Berlin. p. 207-229.

120. Barnes, C.P. *Feasibility study of electrospun collagen type III*. in *8th Annual Meeting of Tissue Engineering Society International*. 2005. Shanghai, China.

121. Tanzer, M.L., *Cross-linking*, in *Biochemistry of Collagen*, G.N. Ramachandran and A.H. Reddi, Editors. 1976, Plenum Press: New York. p. 137-162.

122. Olde Damink, L.H.H., et al., *Cross-linking of dermal sheep collagen using a water-soluble carbodiimide.* Biomaterials, 1996. **17**(8): p. 765-773.

123. Pieper, J.S., et al., *Preparation and characterization of porous crosslinked collagenous matrices containing bioavailable chondroitin sulphate.* Biomaterials, 1999. **20**(9): p. 847-858.

124. Angele, P., et al., *Influence of different collagen species on physico-chemical properties of crosslinked collagen matrices.* Biomaterials, 2004. **25**(14): p. 2831-2841.

125. Sung, H.W., et al., *Crosslinking of biological tissues using genipin and/or carbodiimide.* Journal of Biomedical Materials Research Part A, 2003. **64A**(3): p. 427-438.

126. Gratzer, P.F. and J.M. Lee, *Control of pH alters the type of cross-linking produced by 1-ethyl-3-(3-dimethylaminopropyl)-carbodiimide (EDC) treatment of acellular matrix vascular grafts.* Journal of Biomedical Materials Research, 2001. **58**(2): p. 172-179.

127. Lee, J.M., et al., *Crosslinking of tissue-derived biomaterials in 1-ethyl-3-(3-dimethylaminopropyl)-carbodiimide (EDC).* Journal of Materials Science-Materials In Medicine, 1996. **7**(9): p. 531-541.

128.   Miller, E.J. and L.G. Lunde, *Isolation and characterization of cyanogen bromide peptides from alpha-1(II) chain of bovine and human cartilage collagen.* Biochemistry, 1973. **12**(17): p. 3153-3159.

129.   Barnes, C.P., et al., *Cross-linking electrospun type II collagen tissue engineering scaffolds with carbodiimide in ethanol.* Tissue Engineering, 2007. **13**(7): p. 1593-1605.

130.   Vyavahare, N.R., et al., *Prevention of calcification of glutaraldehyde-crosslinked porcine aortic cusps by ethanol preincubation: Mechanistic studies of protein structure and water-biomaterial relationships.* Journal Of Biomedical Materials Research, 1998. **40**(4): p. 577-585.

131.   Schulze-Tanzil, G., et al., *Redifferentiation of dedifferentiated human chondrocytes in high-density cultures.* Cell and Tissue Research, 2002. **308**(3): p. 371-379.

132.   Gan, L. and R.A. Kandel, *In vitro cartilage tissue formation by co-culture of primary and passaged chondrocytes.* Tissue Engineering, 2007. **13**(4): p. 831-842.

133.   Vunjak-Novakovic, G., et al., *Effects of mixing on the composition and morphology of tissue-engineered cartilage.* Aiche Journal, 1996. **42**(3): p. 850-860.

134.   Brand, D.D., *Protocols: Acid extraction of fetal bovine collagen.* 2005: Memphis, TN. p. University of Tennessee, RDRCC Collagen Core Center.

135.   Knapp, D.C., *The extraction of type II collagen and the electrospinning of nano-fibrous scaffolds*, in *Department of Biomedical Engineering*. 2005, Virginia Commonwealth University: Richmond.

136.   Sell, S.A., *Scaffold permeability as a means to determine fiber diameter and pore size of electrospun fibrinogen*, in *Department of Biomedical Engineering*. 2006, Virginia Commonwealth University: Richmond.

137.   Carr, M.E., Jr. and C.L. Hardin, *Fibrin has larger pores when formed in the presence of erythrocytes.* Am J Physiol., 1987. **253**(5 Pt 2): p. H1069-73.

138.   Vunjak-Novakovic, G., et al., *Dynamic cell seeding of polymer scaffolds for cartilage tissue engineering.* Biotechnology Progress, 1998. **14**(2): p. 193-202.

139.   Hyttinen, M.M., et al., *Inactivation of one allele of the type II collagen gene alters the collagen network in murine articular cartilage and makes cartilage softer.* Annals of the Rheumatic Diseases, 2001. **60**(3): p. 262-268.

140.   Kim, Y.J., et al., *Fluorometric assay of DNA in cartilage explants using Hoechst-33258.* Analytical Biochemistry, 1988. **174**(1): p. 168-176.

141.   Farndale, R.W., D.J. Buttle, and A.J. Barrett, *Improved quantitation and discrimination of sulfated glycosaminoglycans by use of dimethylmethylene blue.* Biochimica Et Biophysica Acta, 1986. **883**(2): p. 173-177.

142.   Homicz, M.R., et al., *Effects of serial expansion of septal chondrocytes on tissue-engineered neocartilage composition.* Otolaryngology-Head and Neck Surgery, 2002. **127**(5): p. 398-408.

143.   Yuan, L. and A. Veis, *Self-assembly of collagen molecules.* Biopolymers, 1973. **12**(6): p. 1437-1444.

144.   Puchtler, H., et al., *Carnoy fixation - Practical and theoretical considerations.* Histochemie, 1968. **16**(4): p. 361-371.

145. Gustavson, K.H., *The internal linking of the collagen molecule*, in *The Chemistry and Reactivity of Collagen*. 1956, Academic Press Inc.: New York, NY. p. 133-154.

146. Usha, R., et al., *Structural influence of mono and polyhydric alcohols on the stabilization of collagen.* Colloids and Surfaces B: Biointerfaces, 2006. **48**(2): p. 101-105.

147. Lins, L. and R. Brasseur, *The hydrophobic effect in protein-folding.* Faseb Journal, 1995. **9**(7): p. 535-540.

148. Salem, A.K., et al., *Interactions of 3T3 fibroblasts and endothelial cells with defined pore features.* Journal of Biomedical Materials Research, 2002. **61**: p. 212-217.

149. Karande, T.S., J.L. Ong, and C.M. Agrawal, *Diffusion in musculoskeletal tissue engineering scaffolds: Design issues related to porosity, permeability, architecture, and nutrient mixing.* Annals Of Biomedical Engineering, 2004. **32**(12): p. 1728-1743.

150. Yang, S., et al., *The design of scaffolds for use in tissue engineering. Part I. Traditional factors.* Tissue Engineering, 2001. **7**(6): p. 679-689.

151. Detamore, M.S. and K.A. Athanasiou, *Use of a rotating bioreactor toward tissue engineering the temporomandibular joint disc.* Tissue Engineering, 2005. **11**(7-8): p. 1188-1197.

152. Freed, L.E., et al., *Composition of cell-polymer cartilage implants.* Biotechnology and Bioengineering, 1994. **43**(7): p. 605-614.

153. Gavenis, K., et al., *In vitro comparison of six different matrix systems for the cultivation of human chondrocytes.* In Vitro Cellular & Developmental Biology-Animal, 2006. **42**(5-6): p. 159-167.

154. Hoemann, C.D., *Molecular and biochemical assays of cartilage components*, in *Cartilage and Osteoarthritis: Structure and In Vivo Analysis*, F. DeCeuninck, M. Sabatini, and P. Pastoureau, Editors. 2004, Humana Press: Totowa, NJ. p. 127-156.

155. Hascall, V.C. and G.K. Hascall, *Proteoglycans*, in *Cell Biology of Extracelluar Matrix*, E.D. Hay, Editor. 1981, Plenum Press: New York. p. 39-64.

156. Wu, K.-J., C.-Y. Wang, and H.-K. Lu, *Effect of glutaraldehyde on the humoral immunogenicity and structure of porcine dermal collagen membranes.* Archives of Oral Biology, 2004. **49**: p. 305-311.

APPENDIX A: Comparison of Materials Used *In Vivo*

A summary of *in vivo* findings of the performance of various materials (autologous, natural, and synthetic) used in articular cartilage tissue engineering [36].

Scaffold	Positive findings	Negative findings
I. Autologous scaffolds		
Perichondrium, periosteum	• Contain progenitor cells • Best results in young patients • Uncomplicated surgical handling	• Incomplete filling of defects • Unsatisfactory results, age >40 years • Graft detachment
Autologous chondrocyte transplants	• Repair appears hyaline-like • Graft matures over time • High percentage of patient satisfaction, with pain relief and recovery of function	• Creates defects in non-weight-bearing areas • Requires two surgical procedures (harvest, implantation) • Autologous cells must be expanded *in vitro* • Technically difficult surgical technique
Mosaicplasty	• Pain relief, recovery of function • Implantation procedure may damage implant surface	• Creates defects in non-weight-bearing areas
II. Natural scaffolds, carrying cells, and/or growth factors		
Fibrin	• Improved histological appearance, but not to normal levels • As carrier of growth factor cDNAs, produced good result in rat defect	• Poor mechanical properties • May evoke immune response • Does not permit host cell ingrowth
Agarose, alginate	• Cells uniformly distributed within implant • Injectible • Good histological result in rabbit	• Foreign body giant cell reaction (agarose) • Does not resorb well • Biochemical properties significantly inferior to native tissue
Collagen	• Native to joints • Excellent histological result when carrying cells or BMP-2	• Good early repair may thin over time • Incomplete integration with host tissues • Possible transmission of prion-induced disease?
Hyaluronan	• Native to joints • Good integration with host tissues	• May induce chondrolysis • Repair cartilage is thinner than native tissue
III. Synthetic scaffolds, carrying cells, and/or growth factors		
Polylactic acid (PLA)	• Excellent retention at implantation site • With BMP-2, good integration with host tissues	• Biochemical properties inferior to native tissue • Inconsistent bone regeneration
Polyglycolic acid (PGA)	• Good short-term result in pigs	
PLA-PGA Copolymer, Polylactie-coglycolide	• Allows controlled polymer degradation • Good early histological result in rabbit and goat	

APPENDIX B: Type II Collagen Extraction and Purification

Protocol for Preparation of Type II Collagen from Fetal Bovine Articular Cartilage

Expected yield: ~50:1 ratio of cartilage to CII if all goes well; therefore, a 150g bag of cartilage chips should yield ~3g of CII

Cartilage Aquisition

☐ From fetal calf legs, remove articular cartilage from front and back limbs, all joints. Be careful to avoid collecting non-cartilaginous material (non-cartilaginous tissues contain other types of collagen that are difficult to separate from type II collagen). NOTE: All operations must be performed at 4 ˚C, unless otherwise specified.

Day 1	Date	Amount
☐ Obtain the wet weight of cartilage.		
☐ Cut cartilage into small pieces with a razor blade and blend in a Waring CB10T 3hp blender using ice and cold distilled water. Three pulses at Maximum setting - one minute per pulse.		
☐ Add an equal volume of cold (4˚C) 5 M guanidine/0.05 M Tris, pH 7.4 to the homogenate. [Guanidine extracts proteoglycan]		
☐ Check pH of entire mixture, pH to 7.4.		
☐ Stir overnight in the cold.		
Day 2	**Date**	**Amount**
☐ Centrifuge at 12250 g for 30 min at 4˚C. Discard the supernate.		
☐ Resuspend the cartilage pellet in cold distilled water and homogenize as before in blender if necessary.		
☐ Collect the cartilage pellet by centrifugation (12250 g for 30 min at 4˚C) and wash with cold distilled water 3 more times. Allow at least 1-2 hour of stirring in cold distilled water for each wash. [It is important to remove guanidine completely, because guanidine may interfere with pepsin action at the next step]		

	☐ Wash #2		
	☐ Wash #3		
	☐ Wash #4		
☐	After the last wash, suspend the cartilage pellet in a suitable volume of cold 0.5 M acetic acid (HAc), and adjust the pH of the suspension to 2.8 by using concentrated formic acid.		
☐	Let solution equilibrate to room temperature.		
☐	Add 2x pepsin (Sigma chemical company - highest quality available) – 10 g/10 L of homogenate. Note: You can dissolve pepsin in a small volume of cold distilled water or 0.5 M HAc for a few minutes and add to the cartilage homogenate with stirring. [It is important to use pepsin as soon as it is dissolved because pepsin begins to autolyze as soon as it is in solution]		
☐	Stir overnight in the cold.		
Day 3		**Date**	**Amount**
Appearance: after overnight, the suspension should be viscous with minimal cartilage pieces.			
☐	Centrifuge (12250 g for 60 min in at 4˚C) and collect the viscous supernate containing solubilized collagen. If necessary, the cartilage pellet may be re-extracted with pepsin.		
☐	Adjust the pH of the pepsin-extracted collagen supernate to 7.4:		
	☐ First add 10 mL/L of 1 M Tris, pH 7.4		
	☐ Use 10 M NaOH to bring the pH to 7.4.		
☐	Add an equal volume of 5 M NaCl slowly and with good stirring		
☐	Allow it to stand overnight at room temperature. [This step precipitates collagen and also inactivates pepsin]		
Day 4		**Date**	**Amount**
☐	Collect the collagen precipitate by centrifugation (12250 g for 60 min in at 4˚C).		
☐	Discard supernate.		
☐	Dissolve the collagen precipitate in a suitable volume of 0.05M Tris/0.2 M NaCl, pH 7.4.		

☐ Stir overnight (or longer) in the cold.			
Day 5-7		**Date**	**Amount**
☐ Dialyze the collagen solution vs. the 0.05M Tris/0.2 M NaCl, pH 7.4 buffer (at least 10 volumes) in the cold with stirring.			
☐ 1st change			
☐ 2nd change			
Day 8		**Date**	**Amount**
☐ Centrifuge and collect supernate containing solubilized collagen.			
☐ Add approximately 500 g of DE 52			
☐ Stir gently in the cold overnight.			
Day 9		**Date**	**Amount**
☐ Centrifuge and collect the supernate. Discard the pellet.			
☐ To the supernate, add while stirring the correct volume of 5 M NaCl to make the final concentration of NaCl to be 0.8 M, and the correct volume of HAc to make the final concentration of HAc to be 0.1 M. [collagen will precipitate] – use Molarity Calculator			
☐ Stir overnight in the cold.			
Day 10		**Date**	**Amount**
☐ Centrifuge and collect the collagen precipitate. Discard the supernate.			
☐ Dissolve collagen precipitate in 0.1 M HAc.			
☐ Stir overnight (or longer) in the cold.			
Day 11-15		**Date**	**Amount**
☐ Centrifuge and collect the supernate. Discard the pellet.			
☐ Put collagen supernate into dialysis bags, and dialyze vs. 0.01 M Na$_2$HPO$_4$ (10 volumes) in the cold with stirring. [collagen will precipitate]			
☐ 1st change			
☐ 2nd change			
☐ 3rd change			
☐ 4th change			

Day 16	Date	Amount
☐ Centrifuge and collect collagen precipitate.		
☐ Dissolve the precipitate in 0.1 M HAc.		
☐ Stir overnight (or longer) in the cold.		

Day 17-23	Date	Amount
☐ Centrifuge to obtain collagen solution.		
☐ Place solution in dialysis bags and dialyze vs. 0.01 M HAc (at least 10 volumes) in the cold with stirring.		
☐ 1st change		
☐ 2nd change		
☐ 3rd change		
☐ 4th change		
☐ 5th change		
☐ 6th change		

Day 24+	Date	Amount
☐ Freeze collagen solution in ice cube trays.		
☐ Place cubes in lyophilizer flasks and lyophilize until dry product is obtained.		
☐ Test purity of collagen with SDS-PAGE.		

% Yield: $\dfrac{\text{\# grams CII obtained}}{\text{\# grams cartilage}}$ x 100% = _____ x 100% = _____%

∴   _____ ratio cartilage to type II collagen

Chemicals to make on Day 1

1 M Tris: 1 M x 121.14 MW x 1 L = 121.14 g, then fill to 1 L with dH2O
            pH to 7.4 with HCl

5 M Guanidine/0.05 M Tris: 5 M x 95.53 MW x 1 L = 477.65 g, then fill to 950 mL with dH2O
                             Add 50 mL 1 M Tris
                             pH to 7.4

APPENDIX C: Statistical Analysis

Oneway Analysis of SEM Diameter By Concentration
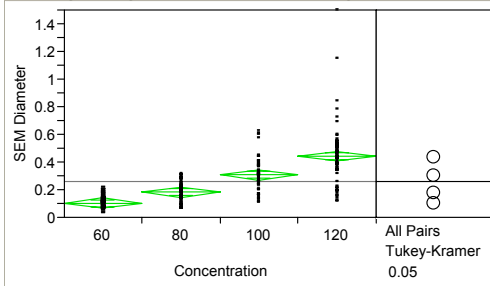
Oneway Anova

Source	DF	Sum of Squares	Mean Square	F Ratio	Prob > F
Concentration	3	3.9574679	1.31916	70.2046	<.0001
Error	236	4.4344806	0.01879		
C. Total	239	8.3919485			

Means Comparisons

Dif=Mean[i]-Mean[j]	120	100	80	60
120	0.000000	0.136717	0.261500	0.338467
100	-0.13672	0.000000	0.124783	0.201750
80	-0.2615	-0.12478	0.000000	0.076967
60	-0.33847	-0.20175	-0.07697	0.000000

Alpha=0.05

Comparisons for all pairs using Tukey-Kramer HSD

q^*
2.58745

Abs(Dif)-LSD	120	100	80	60
120	-0.06476	0.071961	0.196744	0.273711
100	0.071961	-0.06476	0.060028	0.136994
80	0.196744	0.060028	-0.06476	0.012211
60	0.273711	0.136994	0.012211	-0.06476

Positive values show pairs of means that are significantly different.

Oneway Analysis of Diameter By Technique for 60 mg/mL
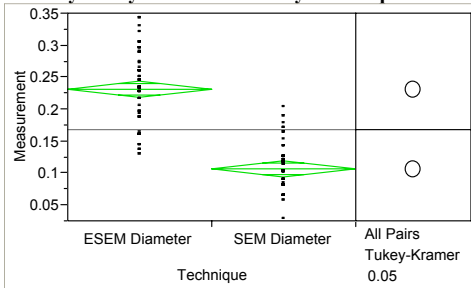
Oneway Anova

Source	DF	Sum of Squares	Mean Square	F Ratio	Prob > F
Technique	1	0.46538108	0.465381	199.7761	<.0001
Error	118	0.27488252	0.002330		
C. Total	119	0.74026359			

Means Comparisons

Dif=Mean[i]-Mean[j]	ESEM Diameter	SEM Diameter
ESEM Diameter	0.000000	0.124550
SEM Diameter	-0.12455	0.000000

Alpha=0.05

Comparisons for all pairs using Tukey-Kramer HSD

```
              q*
           1.98027
```

Abs(Dif)-LSD	ESEM Diameter	SEM Diameter
ESEM Diameter	-0.01745	0.107100
SEM Diameter	0.107100	-0.01745

Positive values show pairs of means that are significantly different.

Oneway Analysis of SEM Pore Area By Concentration
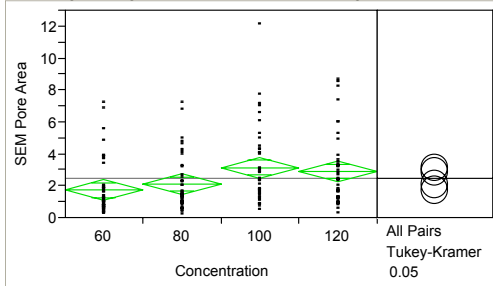
Oneway Anova

Source	DF	Sum of Squares	Mean Square	F Ratio	Prob > F
Concentration	3	52.88905	17.6297	4.0904	0.0079
Error	156	672.35568	4.3100		
C. Total	159	725.24474			

Means Comparisons

Dif=Mean[i]-Mean[j]	100	120	80	60
100	0.00000	0.25750	1.05165	1.41703
120	-0.25750	0.00000	0.79415	1.15953
80	-1.05165	-0.79415	0.00000	0.36538
60	-1.41703	-1.15953	-0.36538	0.00000

Alpha=0.05

Comparisons for all pairs using Tukey-Kramer HSD

```
              q*
           2.59695
```

Abs(Dif)-LSD	100	120	80	60
100	-1.20555	-0.94805	-0.15390	0.21147
120	-0.94805	-1.20555	-0.41140	-0.04603
80	-0.15390	-0.41140	-1.20555	-0.84018
60	0.21147	-0.04603	-0.84018	-1.20555

Positive values show pairs of means that are significantly different.

Oneway Analysis of Pore Area By Technique for 60 mg/mL
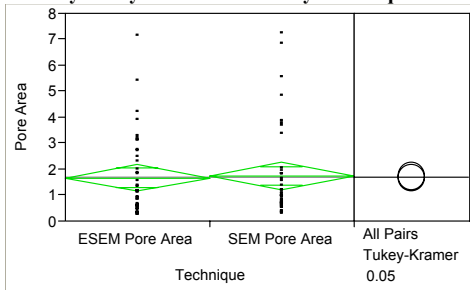
Oneway Anova

Source	DF	Sum of Squares	Mean Square	F Ratio	Prob > F
Technique	1	0.12090	0.12090	0.0438	0.8348
Error	78	215.27934	2.75999		
C. Total	79	215.40024			

Means Comparisons

Dif=Mean[i]-Mean[j]	SEM Pore Area	ESEM Pore Area
SEM Pore Area	0.000000	0.077750
ESEM Pore Area	-0.07775	0.000000

Alpha=0.05

Comparisons for all pairs using Tukey-Kramer HSD

```
                q*
              1.99085
```

Abs(Dif)-LSD	SEM Pore Area	ESEM Pore Area
SEM Pore Area	-0.73957	-0.66182
ESEM Pore Area	-0.66182	-0.73957

Positive values show pairs of means that are significantly different.

Oneway Analysis of Porosity (%) By Concentration (mg/mL)
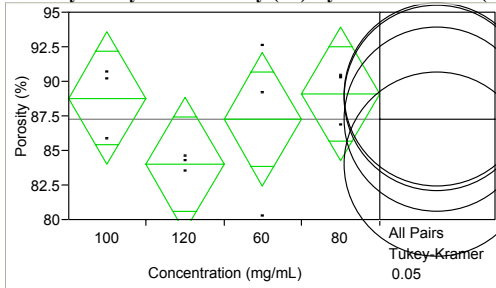
Oneway Anova

Source	DF	Sum of Squares	Mean Square	F Ratio	Prob > F
Concentration (mg/mL)	3	48.57007	16.1900	1.2390	0.3578
Error	8	104.53720	13.0672		
C. Total	11	153.10727			

Means Comparisons

Dif=Mean[i]-Mean[j]	80	100	60	120
80	0.00000	0.31333	1.86333	5.07667
100	-0.31333	0.00000	1.55000	4.76333
60	-1.86333	-1.55000	0.00000	3.21333
120	-5.07667	-4.76333	-3.21333	0.00000

Alpha=0.05

Comparisons for all pairs using Tukey-Kramer HSD

```
                q*
              3.20238
```

Abs(Dif)-LSD	80	100	60	120
80	-9.45186	-9.13853	-7.58853	-4.37520
100	-9.13853	-9.45186	-7.90186	-4.68853
60	-7.58853	-7.90186	-9.45186	-6.23853
120	-4.37520	-4.68853	-6.23853	-9.45186

Positive values show pairs of means that are significantly different.

Oneway Analysis of Permeability (D) By Concentration (mg/mL)
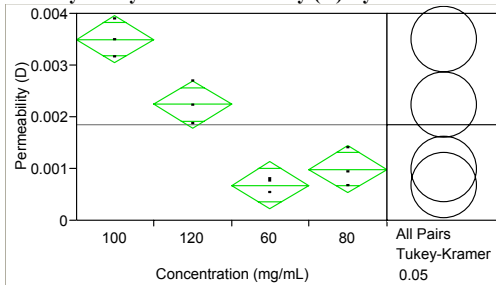
Oneway Anova

Source	DF	Sum of Squares	Mean Square	F Ratio	Prob > F
Concentration (mg/mL)	3	0.00001497	0.000005	42.7107	<.0001
Error	8	0.00000093	0.0000001		
C. Total	11	0.00001590			

Means Comparisons

Dif=Mean[i]-Mean[j]	100	120	80	60
100	0.000000	0.001253	0.002510	0.002820
120	-0.00125	0.000000	0.001258	0.001567
80	-0.00251	-0.00126	0.000000	0.000310
60	-0.00282	-0.00157	-0.00031	0.000000

Alpha=0.05
Comparisons for all pairs using Tukey-Kramer HSD

	q*			
	3.20238			
Abs(Dif)-LSD	100	120	80	60
100	-0.00089	0.000359	0.001617	0.001926
120	0.000359	-0.00089	0.000364	0.000674
80	0.001617	0.000364	-0.00089	-0.00058
60	0.001926	0.000674	-0.00058	-0.00089

Positive values show pairs of means that are significantly different.

Oneway Analysis of Diameter (um) By Concentration (mg/mL) – Permeability Data
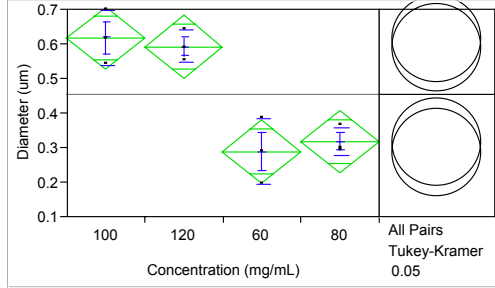
Oneway Anova

Source	DF	Sum of Squares	Mean Square	F Ratio	Prob > F
Concentration (mg/mL)	3	0.27523097	0.091744	19.4504	0.0005
Error	8	0.03773442	0.004717		
C. Total	11	0.31296539			

Means Comparisons

Dif=Mean[i]-Mean[j]	100	120	80	60
100	0.000000	0.025773	0.300032	0.329035
120	-0.02577	0.000000	0.274259	0.303262
80	-0.30003	-0.27426	0.000000	0.029003
60	-0.32903	-0.30326	-0.029	0.000000

Alpha=0.05
Comparisons for all pairs using Tukey-Kramer HSD

	q*			
	3.20238			
Abs(Dif)-LSD	100	120	80	60
100	-0.17958	-0.1538	0.120455	0.149458
120	-0.1538	-0.17958	0.094682	0.123685
80	0.120455	0.094682	-0.17958	-0.15057
60	0.149458	0.123685	-0.15057	-0.17958

Positive values show pairs of means that are significantly different.

Oneway Analysis of Pore Area (um2) By Concentration (mg/mL) – Permeability Data
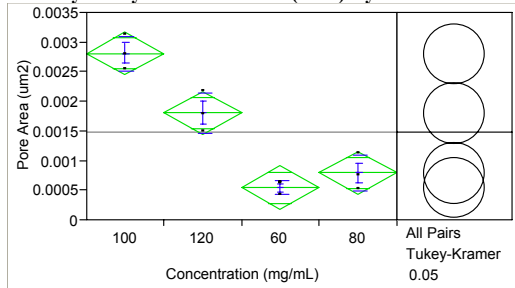
Oneway Anova

Source	DF	Sum of Squares	Mean Square	F Ratio	Prob > F
Concentration (mg/mL)	3	0.00000968	0.0000032	42.7156	<.0001
Error	8	0.00000060	7.5545e-8		
C. Total	11	0.00001029			

Means Comparisons

Dif=Mean[i]-Mean[j]	100	120	80	60

Dif=Mean[i]-Mean[j]	100	120	80	60
100	0.000000	0.001007	0.002019	0.002268
120	-0.00101	0.000000	0.001012	0.001261
80	-0.00202	-0.00101	0.000000	0.000249
60	-0.00227	-0.00126	-0.00025	0.000000

Alpha=0.05
Comparisons for all pairs using Tukey-Kramer HSD

q*
3.20238

Abs(Dif)-LSD	100	120	80	60
100	-0.00072	0.000288	0.001300	0.001549
120	0.000288	-0.00072	0.000293	0.000542
80	0.001300	0.000293	-0.00072	-0.00047
60	0.001549	0.000542	-0.00047	-0.00072

Positive values show pairs of means that are significantly different.

Oneway Analysis of 60 Thickness By Week #
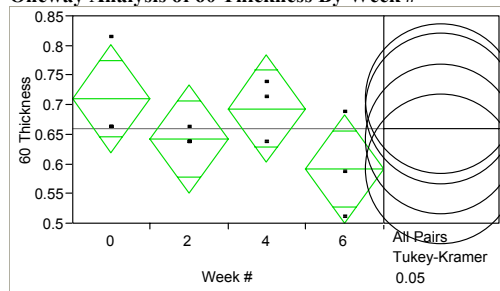
Oneway Anova

Source	DF	Sum of Squares	Mean Square	F Ratio	Prob > F
Week #	3	0.02577267	0.008591	1.8280	0.2201
Error	8	0.03759600	0.004699		
C. Total	11	0.06336867			

Means Comparisons

Dif=Mean[i]-Mean[j]	0	4	2	6
0	0.000000	0.016667	0.067667	0.118333
4	-0.01667	0.000000	0.051000	0.101667
2	-0.06767	-0.051	0.000000	0.050667
6	-0.11833	-0.10167	-0.05067	0.000000

Alpha=0.05
Comparisons for all pairs using Tukey-Kramer HSD

q*
3.20238

Abs(Dif)-LSD	0	4	2	6
0	-0.17925	-0.16258	-0.11158	-0.06091
4	-0.16258	-0.17925	-0.12825	-0.07758
2	-0.11158	-0.12825	-0.17925	-0.12858
6	-0.06091	-0.07758	-0.12858	-0.17925

Positive values show pairs of means that are significantly different.

Oneway Analysis of 80 Thickness By Week #
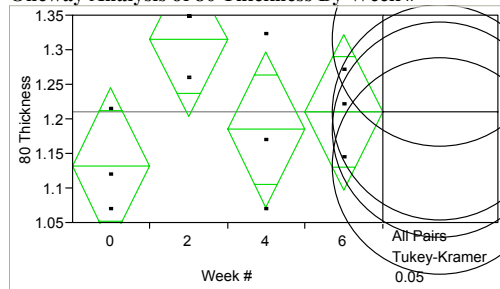
Oneway Anova

Source	DF	Sum of Squares	Mean Square	F Ratio	Prob > F

Source	DF	Sum of Squares	Mean Square	F Ratio	Prob > F
Week #	3	0.05366958	0.017890	2.5048	0.1330
Error	8	0.05713867	0.007142		
C. Total	11	0.11080825			

Means Comparisons

Dif=Mean[i]-Mean[j]	2	6	4	0
2	0.000000	0.105667	0.131000	0.183667
6	-0.10567	0.000000	0.025333	0.078000
4	-0.131	-0.02533	0.000000	0.052667
0	-0.18367	-0.078	-0.05267	0.000000

Alpha=0.05

Comparisons for all pairs using Tukey-Kramer HSD

q*
3.20238

Abs(Dif)-LSD	2	6	4	0
2	-0.22098	-0.11531	-0.08998	-0.03731
6	-0.11531	-0.22098	-0.19564	-0.14298
4	-0.08998	-0.19564	-0.22098	-0.16831
0	-0.03731	-0.14298	-0.16831	-0.22098

Positive values show pairs of means that are significantly different.

Oneway Analysis of 100 Thickness By Week #
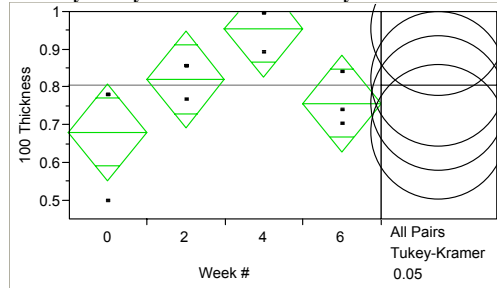
Oneway Anova
Analysis of Variance

Source	DF	Sum of Squares	Mean Square	F Ratio	Prob > F
Week #	3	0.12236967	0.040790	4.3622	0.0425
Error	8	0.07480533	0.009351		
C. Total	11	0.19717500			

Means Comparisons

Dif=Mean[i]-Mean[j]	4	2	6	0
4	0.000000	0.135667	0.199000	0.275333
2	-0.13567	0.000000	0.063333	0.139667
6	-0.199	-0.06333	0.000000	0.076333
0	-0.27533	-0.13967	-0.07633	0.000000

Alpha=0.05

Comparisons for all pairs using Tukey-Kramer HSD

q*
3.20238

Abs(Dif)-LSD	4	2	6	0
4	-0.25284	-0.11717	-0.05384	0.022492
2	-0.11717	-0.25284	-0.18951	-0.11317
6	-0.05384	-0.18951	-0.25284	-0.17651
0	0.022492	-0.11317	-0.17651	-0.25284

Positive values show pairs of means that are significantly different.

Oneway Analysis of 120 Thickness By Week #
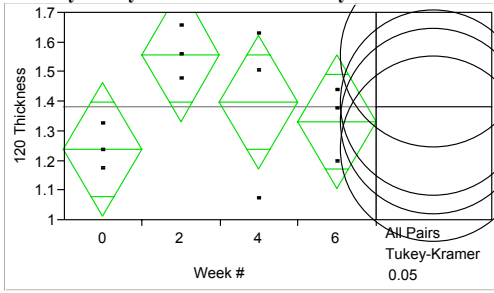
Oneway Anova

Source	DF	Sum of Squares	Mean Square	F Ratio	Prob > F
Week #	3	0.16257620	0.054192	1.8794	0.2114
Error	8	0.23067361	0.028834		
C. Total	11	0.39324981			

Means Comparisons

Dif=Mean[i]-Mean[j]	2	4	6	0
2	0.000000	0.162300	0.225967	0.319300
4	-0.1623	0.000000	0.063667	0.157000
6	-0.22597	-0.06367	0.000000	0.093333
0	-0.3193	-0.157	-0.09333	0.000000

Alpha=0.05

Comparisons for all pairs using Tukey-Kramer HSD

q*
3.20238

Abs(Dif)-LSD	2	4	6	0
2	-0.444	-0.2817	-0.21803	-0.1247
4	-0.2817	-0.444	-0.38033	-0.287
6	-0.21803	-0.38033	-0.444	-0.35066
0	-0.1247	-0.287	-0.35066	-0.444

Positive values show pairs of means that are significantly different.

Oneway Analysis of Week 0 Thickness By Concentration
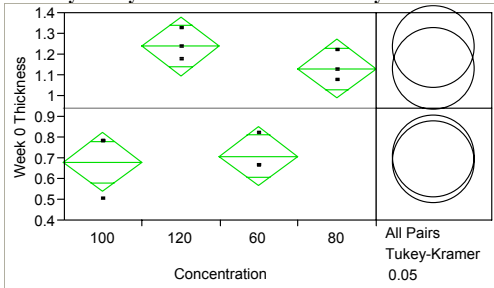
Oneway Anova

Source	DF	Sum of Squares	Mean Square	F Ratio	Prob > F
Concentration	3	0.73946892	0.246490	21.7502	0.0003
Error	8	0.09066200	0.011333		
C. Total	11	0.83013092			

Means Comparisons

Dif=Mean[i]-Mean[j]	120	80	60	100
120	0.000000	0.107667	0.529333	0.558667
80	-0.10767	0.000000	0.421667	0.451000
60	-0.52933	-0.42167	0.000000	0.029333
100	-0.55867	-0.451	-0.02933	0.000000

Alpha=0.05

Comparisons for all pairs using Tukey-Kramer HSD

q*
3.20238

Abs(Dif)-LSD	120	80	60	100
120	-0.27835	-0.17069	0.250981	0.280314
80	-0.17069	-0.27835	0.143314	0.172648

	q*				
60		0.250981	0.143314	-0.27835	-0.24902
100		0.280314	0.172648	-0.24902	-0.27835

Positive values show pairs of means that are significantly different.

Oneway Analysis of Week 2 Thickness By Concentration
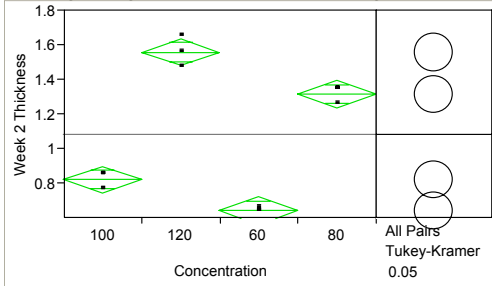
Oneway Anova

Source	DF	Sum of Squares	Mean Square	F Ratio	Prob > F
Concentration	3	1.6301441	0.543381	161.8796	<.0001
Error	8	0.0268536	0.003357		
C. Total	11	1.6569977			

Means Comparisons

Dif=Mean[i]-Mean[j]	120	80	100	60
120	0.000000	0.243300	0.738300	0.916300
80	-0.2433	0.000000	0.495000	0.673000
100	-0.7383	-0.495	0.000000	0.178000
60	-0.9163	-0.673	-0.178	0.000000

Alpha=0.05
Comparisons for all pairs using Tukey-Kramer HSD

q*
3.20238

Abs(Dif)-LSD	120	80	100	60
120	-0.15149	0.091810	0.586810	0.764810
80	0.091810	-0.15149	0.343510	0.521510
100	0.586810	0.343510	-0.15149	0.026510
60	0.764810	0.521510	0.026510	-0.15149

Positive values show pairs of means that are significantly different.

Oneway Analysis of Week 4 Thickness By Concentration
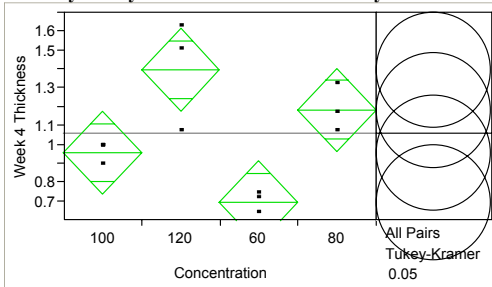
Oneway Anova

Source	DF	Sum of Squares	Mean Square	F Ratio	Prob > F
Concentration	3	0.8214430	0.273814	10.0942	0.0043
Error	8	0.2170080	0.027126		
C. Total	11	1.0384510			

Means Comparisons

Dif=Mean[i]-Mean[j]	120	80	100	60
120	0.000000	0.212000	0.440333	0.703000
80	-0.212	0.000000	0.228333	0.491000
100	-0.44033	-0.22833	0.000000	0.262667
60	-0.703	-0.491	-0.26267	0.000000

Alpha=0.05
Comparisons for all pairs using Tukey-Kramer HSD

q*				
3.20238				
Abs(Dif)-LSD	120	80	100	60
120	-0.43065	-0.21865	0.009688	0.272355
80	-0.21865	-0.43065	-0.20231	0.060355
100	0.009688	-0.20231	-0.43065	-0.16798
60	0.272355	0.060355	-0.16798	-0.43065

Positive values show pairs of means that are significantly different.

Oneway Analysis of Week 6 Thickness By Concentration
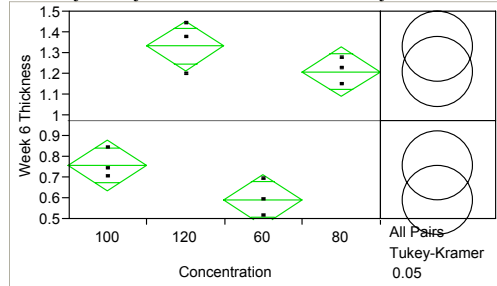
Oneway Anova

Source	DF	Sum of Squares	Mean Square	F Ratio	Prob > F
Concentration	3	1.1323263	0.377442	45.9665	<.0001
Error	8	0.0656900	0.008211		
C. Total	11	1.1980163			

Means Comparisons

Dif=Mean[i]-Mean[j]	120	80	100	60
120	0.000000	0.123000	0.575667	0.741000
80	-0.123	0.000000	0.452667	0.618000
100	-0.57567	-0.45267	0.000000	0.165333
60	-0.741	-0.618	-0.16533	0.000000

Alpha=0.05

Comparisons for all pairs using Tukey-Kramer HSD

q*				
3.20238				
Abs(Dif)-LSD	120	80	100	60
120	-0.23694	-0.11394	0.338730	0.504064
80	-0.11394	-0.23694	0.215730	0.381064
100	0.338730	0.215730	-0.23694	-0.0716
60	0.504064	0.381064	-0.0716	-0.23694

Positive values show pairs of means that are significantly different.

Oneway Analysis of Week 0 Eq Stiffness By Concentration
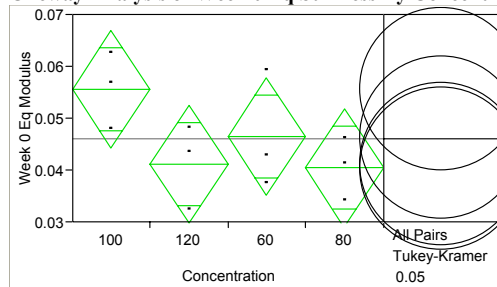
Oneway Anova

Source	DF	Sum of Squares	Mean Square	F Ratio	Prob > F
Concentration	3	0.00044189	0.000147	2.0375	0.1872
Error	8	0.00057833	0.000072		
C. Total	11	0.00102022			

Means Comparisons

Dif=Mean[i]-Mean[j]	100	60	120	80
100	0.000000	0.009267	0.014433	0.015233
60	-0.00927	0.000000	0.005167	0.005967

Dif=Mean[i]-Mean[j]	100	60	120	80
120	-0.01443	-0.00517	0.000000	0.000800
80	-0.01523	-0.00597	-0.0008	0.000000

Alpha=0.05
Comparisons for all pairs using Tukey-Kramer HSD

q*
3.20238

Abs(Dif)-LSD	100	60	120	80
100	-0.02223	-0.01296	-0.0078	-0.007
60	-0.01296	-0.02223	-0.01706	-0.01626
120	-0.0078	-0.01706	-0.02223	-0.02143
80	-0.007	-0.01626	-0.02143	-0.02223

Positive values show pairs of means that are significantly different.

Oneway Analysis of Week 2 Eq Stiffness By Concentration
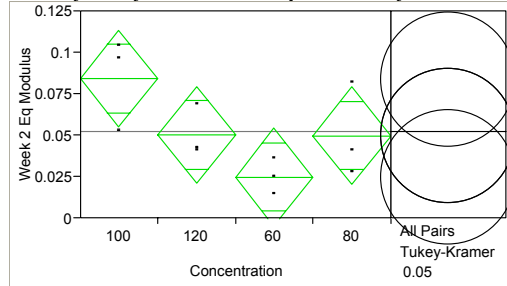
Oneway Anova

Source	DF	Sum of Squares	Mean Square	F Ratio	Prob > F
Concentration	3	0.00531321	0.001771	3.6573	0.0633
Error	8	0.00387406	0.000484		
C. Total	11	0.00918727			

Means Comparisons

Dif=Mean[i]-Mean[j]	100	120	80	60
100	0.000000	0.034033	0.034233	0.059167
120	-0.03403	0.000000	0.000200	0.025133
80	-0.03423	-0.0002	0.000000	0.024933
60	-0.05917	-0.02513	-0.02493	0.000000

Alpha=0.05
Comparisons for all pairs using Tukey-Kramer HSD

q*
3.20238

Abs(Dif)-LSD	100	120	80	60
100	-0.05754	-0.02351	-0.02331	0.001627
120	-0.02351	-0.05754	-0.05734	-0.03241
80	-0.02331	-0.05734	-0.05754	-0.03261
60	0.001627	-0.03241	-0.03261	-0.05754

Positive values show pairs of means that are significantly different.

Oneway Analysis of Week 4 Eq Stiffness By Concentration
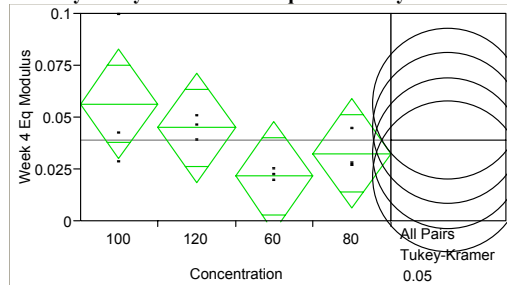
Oneway Anova

Source	DF	Sum of Squares	Mean Square	F Ratio	Prob > F
Concentration	3	0.00204270	0.000681	1.7441	0.2353
Error	8	0.00312322	0.000390		

Source	DF	Sum of Squares	Mean Square	F Ratio	Prob > F
C. Total	11	0.00516592			

Means Comparisons

Dif=Mean[i]-Mean[j]	100	120	80	60
100	0.000000	0.011467	0.023833	0.034767
120	-0.01147	0.000000	0.012367	0.023300
80	-0.02383	-0.01237	0.000000	0.010933
60	-0.03477	-0.0233	-0.01093	0.000000

Alpha=0.05

Comparisons for all pairs using Tukey-Kramer HSD

q*
3.20238

Abs(Dif)-LSD	100	120	80	60
100	-0.05166	-0.0402	-0.02783	-0.0169
120	-0.0402	-0.05166	-0.0393	-0.02836
80	-0.02783	-0.0393	-0.05166	-0.04073
60	-0.0169	-0.02836	-0.04073	-0.05166

Positive values show pairs of means that are significantly different.

Oneway Analysis of Week 6 Eq Stiffness By Concentration
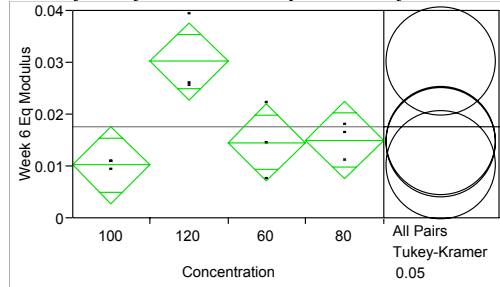
Oneway Anova

Source	DF	Sum of Squares	Mean Square	F Ratio	Prob > F
Concentration	3	0.00068615	0.000229	7.1653	0.0118
Error	8	0.00025536	0.000032		
C. Total	11	0.00094151			

Means Comparisons

Dif=Mean[i]-Mean[j]	120	80	60	100
120	0.000000	0.015133	0.015567	0.020000
80	-0.01513	0.000000	0.000433	0.004867
60	-0.01557	-0.00043	0.000000	0.004433
100	-0.02	-0.00487	-0.00443	0.000000

Alpha=0.05

Comparisons for all pairs using Tukey-Kramer HSD

q*
3.20238

Abs(Dif)-LSD	120	80	60	100
120	-0.01477	0.000361	0.000794	0.005227
80	0.000361	-0.01477	-0.01434	-0.00991
60	0.000794	-0.01434	-0.01477	-0.01034
100	0.005227	-0.00991	-0.01034	-0.01477

Positive values show pairs of means that are significantly different.

Oneway Analysis of 60 Eq Stiffness By Week #
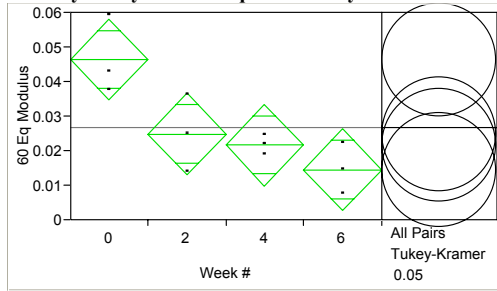
Oneway Anova

Source	DF	Sum of Squares	Mean Square	F Ratio	Prob > F
Week #	3	0.00168734	0.000562	7.1684	0.0118
Error	8	0.00062770	0.000078		
C. Total	11	0.00231504			

Means Comparisons

Dif=Mean[i]-Mean[j]	0	2	4	6
0	0.000000	0.021467	0.024700	0.031800
2	-0.02147	0.000000	0.003233	0.010333
4	-0.0247	-0.00323	0.000000	0.007100
6	-0.0318	-0.01033	-0.0071	0.000000

Alpha=0.05

Comparisons for all pairs using Tukey-Kramer HSD

q*
3.20238

Abs(Dif)-LSD	0	2	4	6
0	-0.02316	-0.00169	0.001539	0.008639
2	-0.00169	-0.02316	-0.01993	-0.01283
4	0.001539	-0.01993	-0.02316	-0.01606
6	0.008639	-0.01283	-0.01606	-0.02316

Positive values show pairs of means that are significantly different.

Oneway Analysis of 80 Eq Stiffness By Week #
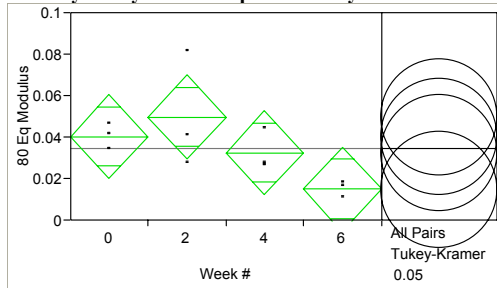
Oneway Anova

Source	DF	Sum of Squares	Mean Square	F Ratio	Prob > F
Week #	3	0.00196132	0.000654	2.8139	0.1076
Error	8	0.00185867	0.000232		
C. Total	11	0.00381999			

Means Comparisons

Dif=Mean[i]-Mean[j]	2	0	4	6
2	0.000000	0.009433	0.017233	0.034833
0	-0.00943	0.000000	0.007800	0.025400
4	-0.01723	-0.0078	0.000000	0.017600
6	-0.03483	-0.0254	-0.0176	0.000000

Alpha=0.05

Comparisons for all pairs using Tukey-Kramer HSD

q*
3.20238

Abs(Dif)-LSD	2	0	4	6
2	-0.03985	-0.03042	-0.02262	-0.00502
0	-0.03042	-0.03985	-0.03205	-0.01445

	q*				
4		-0.02262	-0.03205	-0.03985	-0.02225
6		-0.00502	-0.01445	-0.02225	-0.03985

Positive values show pairs of means that are significantly different.

Oneway Analysis of 100 Eq Modulus By Week
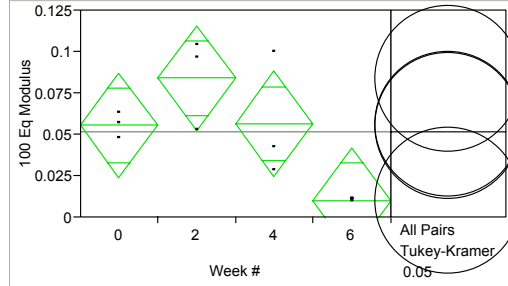
Oneway Anova

Source	DF	Sum of Squares	Mean Square	F Ratio	Prob > F
Week #	3	0.00843958	0.002813	4.9665	0.0311
Error	8	0.00453143	0.000566		
C. Total	11	0.01297101			

Means Comparisons

Dif=Mean[i]-Mean[j]	2	4	0	6
2	0.000000	0.027633	0.028433	0.073933
4	-0.02763	0.000000	0.000800	0.046300
0	-0.02843	-0.0008	0.000000	0.045500
6	-0.07393	-0.0463	-0.0455	0.000000

Alpha=0.05
Comparisons for all pairs using Tukey-Kramer HSD

q*	
3.20238	

Abs(Dif)-LSD	2	4	0	6
2	-0.06223	-0.0346	-0.0338	0.011703
4	-0.0346	-0.06223	-0.06143	-0.01593
0	-0.0338	-0.06143	-0.06223	-0.01673
6	0.011703	-0.01593	-0.01673	-0.06223

Positive values show pairs of means that are significantly different.

Oneway Analysis of 120 Eq Stiffness By Week
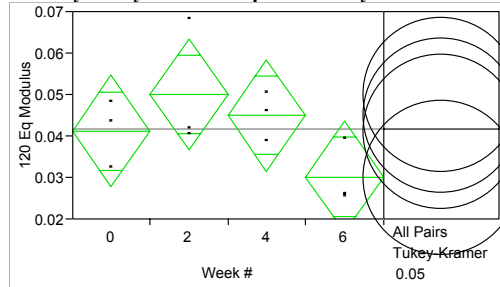
Oneway Anova

Source	DF	Sum of Squares	Mean Square	F Ratio	Prob > F
Week #	3	0.00064230	0.000214	2.1063	0.1778
Error	8	0.00081318	0.000102		
C. Total	11	0.00145548			

Means Comparisons

Dif=Mean[i]-Mean[j]	2	4	0	6
2	0.000000	0.005067	0.008833	0.019900
4	-0.00507	0.000000	0.003767	0.014833
0	-0.00883	-0.00377	0.000000	0.011067
6	-0.0199	-0.01483	-0.01107	0.000000

Alpha=0.05
Comparisons for all pairs using Tukey-Kramer HSD

	q*			
	3.20238			
Abs(Dif)-LSD	2	4	0	6
2	-0.02636	-0.0213	-0.01753	-0.00646
4	-0.0213	-0.02636	-0.0226	-0.01153
0	-0.01753	-0.0226	-0.02636	-0.0153
6	-0.00646	-0.01153	-0.0153	-0.02636

Positive values show pairs of means that are significantly different.

Oneway Analysis of Peak Stress (MPa) By Concentration (mg/mL)
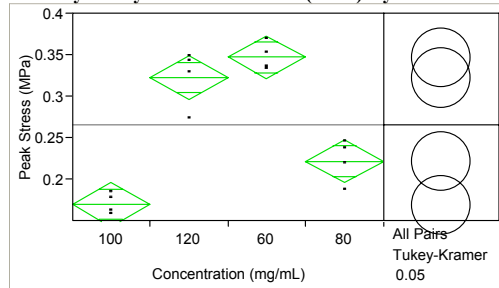
Oneway Anova

Source	DF	Sum of Squares	Mean Square	F Ratio	Prob > F
Concentration (mg/mL)	3	0.08400719	0.028002	48.9071	<.0001
Error	12	0.00687075	0.000573		
C. Total	15	0.09087794			

Means Comparisons

Dif=Mean[i]-Mean[j]	60	120	80	100
60	0.000000	0.024250	0.125250	0.177250
120	-0.02425	0.000000	0.101000	0.153000
80	-0.12525	-0.101	0.000000	0.052000
100	-0.17725	-0.153	-0.052	0.000000

Alpha=0.05

Comparisons for all pairs using Tukey-Kramer HSD

	q*			
	2.96883			
Abs(Dif)-LSD	60	120	80	100
60	-0.05023	-0.02598	0.075018	0.127018
120	-0.02598	-0.05023	0.050768	0.102768
80	0.075018	0.050768	-0.05023	0.001768
100	0.127018	0.102768	0.001768	-0.05023

Positive values show pairs of means that are significantly different.

Oneway Analysis of Strain at Break (%) By Concentration (mg/mL)
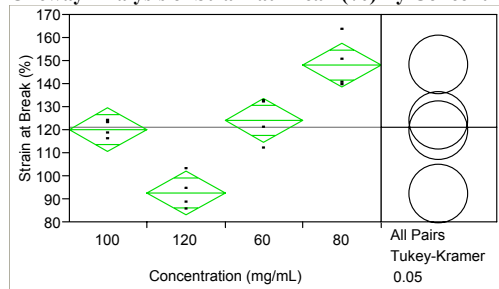
Oneway Anova

Source	DF	Sum of Squares	Mean Square	F Ratio	Prob > F
Concentration (mg/mL)	3	6238.5525	2079.52	28.2267	<.0001
Error	12	884.0650	73.67		
C. Total	15	7122.6175			

Means Comparisons

Dif=Mean[i]-Mean[j]	80	60	100	120
80	0.0000	24.0750	28.1250	55.6500
60	-24.0750	0.0000	4.0500	31.5750

Dif=Mean[i]-Mean[j]	80	60	100	120
100	-28.1250	-4.0500	0.0000	27.5250
120	-55.6500	-31.5750	-27.5250	0.0000

Alpha=0.05
Comparisons for all pairs using Tukey-Kramer HSD

q*
2.96883

Abs(Dif)-LSD	80	60	100	120
80	-18.0186	6.0564	10.1064	37.6314
60	6.0564	-18.0186	-13.9686	13.5564
100	10.1064	-13.9686	-18.0186	9.5064
120	37.6314	13.5564	9.5064	-18.0186

Positive values show pairs of means that are significantly different.

Oneway Analysis of Modulus (MPa) By Concentration (mg/mL)
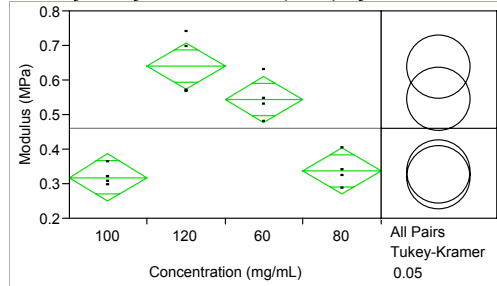
Oneway Anova

Source	DF	Sum of Squares	Mean Square	F Ratio	Prob > F
Concentration (mg/mL)	3	0.29920369	0.099735	26.2271	<.0001
Error	12	0.04563275	0.003803		
C. Total	15	0.34483644			

Means Comparisons

Dif=Mean[i]-Mean[j]	120	60	80	100
120	0.000000	0.096000	0.303500	0.321750
60	-0.096	0.000000	0.207500	0.225750
80	-0.3035	-0.2075	0.000000	0.018250
100	-0.32175	-0.22575	-0.01825	0.000000

Alpha=0.05
Comparisons for all pairs using Tukey-Kramer HSD

q*
2.96883

Abs(Dif)-LSD	120	60	80	100
120	-0.12945	-0.03345	0.174045	0.192295
60	-0.03345	-0.12945	0.078045	0.096295
80	0.174045	0.078045	-0.12945	-0.1112
100	0.192295	0.096295	-0.1112	-0.12945

Positive values show pairs of means that are significantly different.

Oneway Analysis of Week 2 Cell # By Concentration
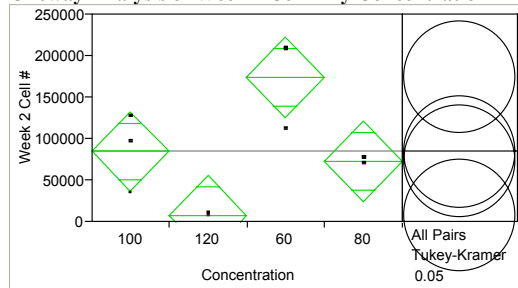
Oneway Anova

Source	DF	Sum of Squares	Mean Square	F Ratio	Prob > F
Concentration	3	4.21282e10	1.4043e10	10.5881	0.0037
Error	8	1.06103e10	1.32628e9		

Source	DF	Sum of Squares	Mean Square	F Ratio	Prob > F
C. Total	11	5.27385e10			

Means Comparisons

Dif=Mean[i]-Mean[j]	60	100	80	120
60	0	89735	101387	166254
100	-89735	0	11651	76519
80	-101387	-11651	0	64868
120	-166254	-76519	-64868	0

Alpha=0.05

Comparisons for all pairs using Tukey-Kramer HSD

q*
3.20238

Abs(Dif)-LSD	60	100	80	120
60	-95223.7	-5488.4	6162.9	71030.8
100	-5488.4	-95223.7	-83572.4	-18704.6
80	6162.9	-83572.4	-95223.7	-30355.8
120	71030.8	-18704.6	-30355.8	-95223.7

Positive values show pairs of means that are significantly different.

Oneway Analysis of Week 4 Cell # By Concentration
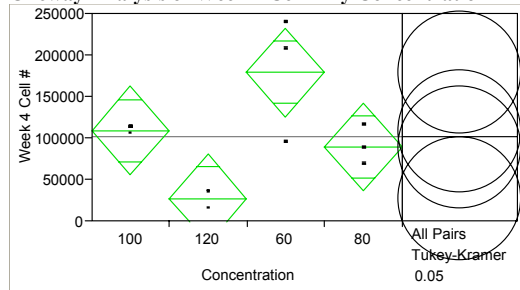
Oneway Anova

Source	DF	Sum of Squares	Mean Square	F Ratio	Prob > F
Concentration	3	3.51814e10	1.1727e10	7.3339	0.0110
Error	8	1.27922e10	1.59903e9		
C. Total	11	4.79736e10			

Means Comparisons

Dif=Mean[i]-Mean[j]	60	100	80	120
60	0	70261	89927	151763
100	-70261	0	19666	81502
80	-89927	-19666	0	61836
120	-151763	-81502	-61836	0

Alpha=0.05

Comparisons for all pairs using Tukey-Kramer HSD

q*
3.20238

Abs(Dif)-LSD	60	100	80	120
60	-104557	-34296	-14630	47206
100	-34296	-104557	-84891	-23056
80	-14630	-84891	-104557	-42722
120	47206	-23056	-42722	-104557

Positive values show pairs of means that are significantly different.

Oneway Analysis of Week 6 Cell # By Concentration
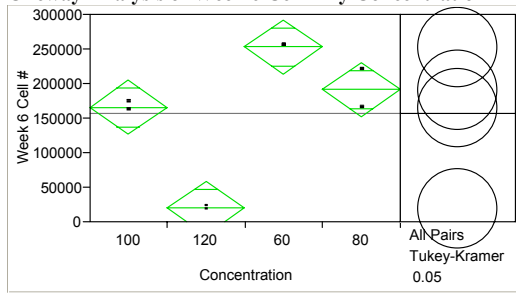
Oneway Anova

Source	DF	Sum of Squares	Mean Square	F Ratio	Prob > F
Concentration	3	5.8741e+10	1.958e+10	49.2456	0.0013
Error	4	1590422455	397605614		
C. Total	7	6.03314e10			

Means Comparisons

Dif=Mean[i]-Mean[j]	60	80	100	120
60	0	61834	87761	233548
80	-61834	0	25927	171714
100	-87761	-25927	0	145788
120	-233548	-171714	-145788	0

Alpha=0.05

Comparisons for all pairs using Tukey-Kramer HSD

q*	
4.07087	

Abs(Dif)-LSD	60	80	100	120
60	-81173	-19339	6587	152375
80	-19339	-81173	-55247	90541
100	6587	-55247	-81173	64614
120	152375	90541	64614	-81173

Positive values show pairs of means that are significantly different.

Oneway Analysis of 60 Cell # By Week #
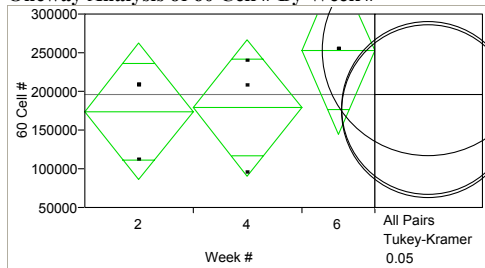
Oneway Anova

Source	DF	Sum of Squares	Mean Square	F Ratio	Prob > F
Week #	2	8855489021	4.42774e9	1.2524	0.3623
Error	5	1.76771e10	3.53543e9		
C. Total	7	2.65326e10			

Means Comparisons

Dif=Mean[i]-Mean[j]	6	4	2
6	0.0	74151.8	79188.2
4	-74151.8	0.0	5036.4
2	-79188.2	-5036.4	0.0

Alpha=0.05

Comparisons for all pairs using Tukey-Kramer HSD

q*	
3.25387	

Abs(Dif)-LSD	6	4	2
6	-193473	-102464	-97428
4	-102464	-157970	-152934
2	-97428	-152934	-157970

Positive values show pairs of means that are significantly different.

Oneway Analysis of 80 Cell # By Week #
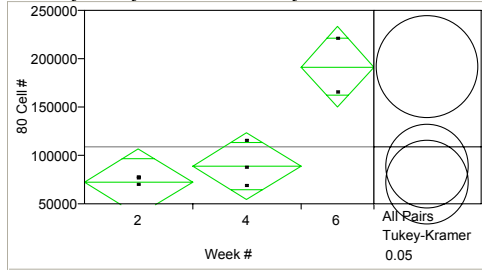
Oneway Anova

Source	DF	Sum of Squares	Mean Square	F Ratio	Prob > F
Week #	2	1.87212e10	9.36061e9	17.7091	0.0054
Error	5	2642875222	528575044		
C. Total	7	2.13641e10			

Means Comparisons

Dif=Mean[i]-Mean[j]	6	4	2
6	0	102245	118741
4	-102245	0	16496
2	-118741	-16496	0

Alpha=0.05
Comparisons for all pairs using Tukey-Kramer HSD

q*
3.25387

Abs(Dif)-LSD	6	4	2
6	-74808.9	33954.4	50450.0
4	33954.4	-61081.2	-44585.6
2	50450.0	-44585.6	-61081.2

Positive values show pairs of means that are significantly different.

Oneway Analysis of 100 Cell # By Week #
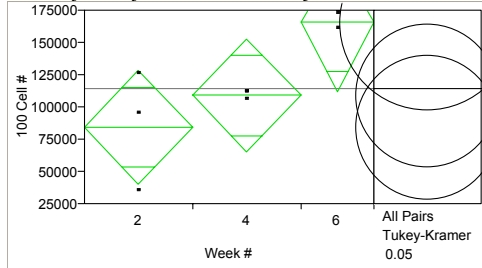
Oneway Anova

Source	DF	Sum of Squares	Mean Square	F Ratio	Prob > F
Week #	2	8023554493	4.01178e9	4.5757	0.0742
Error	5	4383773201	876754640		
C. Total	7	1.24073e10			

Means Comparisons

Dif=Mean[i]-Mean[j]	6	4	2
6	0.0	56652.3	81163.0
4	-56652.3	0.0	24510.6
2	-81163.0	-24510.6	0.0

Alpha=0.05
Comparisons for all pairs using Tukey-Kramer HSD

q*
3.25387

Abs(Dif)-LSD	6	4	2
6	-96347.1	-31300.2	-6789.5
4	-31300.2	-78667.1	-54156.5
2	-6789.5	-54156.5	-78667.1

Positive values show pairs of means that are significantly different.

Oneway Analysis of 120 Cell # By Week #
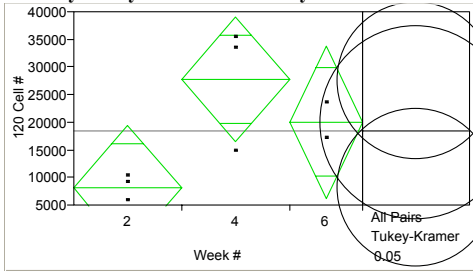
Oneway Anova

Source	DF	Sum of Squares	Mean Square	F Ratio	Prob > F
Week #	2	578815023	289407512	5.0047	0.0640
Error	5	289133546	57826709		
C. Total	7	867948570			

Means Comparisons

Dif=Mean[i]-Mean[j]	4	6	2
4	0.0	7633.2	19527.8
6	-7633.2	0.0	11894.6
2	-19527.8	-11894.6	0.0

Alpha=0.05

Comparisons for all pairs using Tukey-Kramer HSD

q*
3.25387

Abs(Dif)-LSD	4	6	2
4	-20203.1	-14954.5	-675.3
6	-14954.5	-24743.7	-10693.2
2	-675.3	-10693.2	-20203.1

Positive values show pairs of means that are significantly different.

Oneway Analysis of Week 0 GAG By Concentration
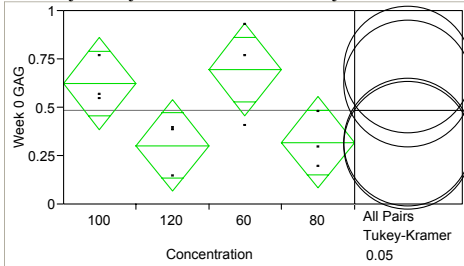
Oneway Anova

Source	DF	Sum of Squaes	Mean Square	F Ratio	Prob > F
Concentration	3	0.37112887	0.123710	3.8958	0.0551
Error	8	0.25403471	0.031754		
C. Total	11	0.62516358			

Means Comparisons

Dif=Mean[i]-Mean[j]	60	100	80	120
60	0.000000	0.073048	0.376239	0.392261
100	-0.07305	0.000000	0.303191	0.319213
80	-0.37624	-0.30319	0.000000	0.016022
120	-0.39226	-0.31921	-0.01602	0.000000

Alpha=0.05

Comparisons for all pairs using Tukey-Kramer HSD

q*
3.20238

Abs(Dif)-LSD	60	100	80	120
60	-0.46594	-0.39289	-0.0897	-0.07368
100	-0.39289	-0.46594	-0.16275	-0.14673
80	-0.0897	-0.16275	-0.46594	-0.44992
120	-0.07368	-0.14673	-0.44992	-0.46594

Positive values show pairs of means that are significantly different.

Oneway Analysis of Week 2 GAG By Concentration
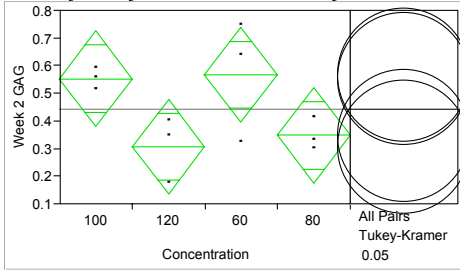
Oneway Anova

Source	DF	Sum of Squares	Mean Square	F Ratio	Prob > F
Concentration	3	0.16558488	0.055195	3.2879	0.0792
Error	8	0.13429777	0.016787		
C. Total	11	0.29988265			

Means Comparisons

Dif=Mean[i]-Mean[j]	60	100	80	120
60	0.000000	0.014583	0.219451	0.260881
100	-0.01458	0.000000	0.204868	0.246297
80	-0.21945	-0.20487	0.000000	0.041430
120	-0.26088	-0.2463	-0.04143	0.000000

Alpha=0.05

Comparisons for all pairs using Tukey-Kramer HSD

q*
3.20238

Abs(Dif)-LSD	60	100	80	120
60	-0.33878	-0.3242	-0.11933	-0.0779
100	-0.3242	-0.33878	-0.13391	-0.09248
80	-0.11933	-0.13391	-0.33878	-0.29735
120	-0.0779	-0.09248	-0.29735	-0.33878

Positive values show pairs of means that are significantly different.

Oneway Analysis of Week 4 GAG By Concentration
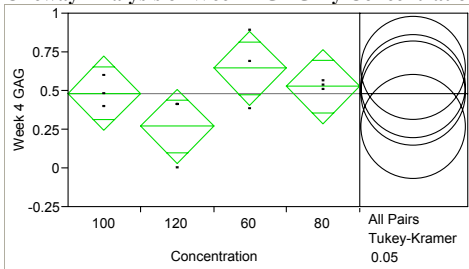
Oneway Anova

Source	DF	Sum of Squares	Mean Square	F Ratio	Prob > F
Concentration	3	0.22316000	0.074387	2.2756	0.1568
Error	8	0.26151516	0.032689		
C. Total	11	0.48467517			

Means Comparisons

Dif=Mean[i]-Mean[j]	60	80	100	120
60	0.000000	0.118975	0.162049	0.377216
80	-0.11898	0.000000	0.043074	0.258240
100	-0.16205	-0.04307	0.000000	0.215167
120	-0.37722	-0.25824	-0.21517	0.000000

Alpha=0.05

Comparisons for all pairs using Tukey-Kramer HSD

q*
3.20238

Abs(Dif)-LSD	60	80	100	120
60	-0.47275	-0.35377	-0.3107	-0.09553
80	-0.35377	-0.47275	-0.42968	-0.21451

	q*				
100		-0.3107	-0.42968	-0.47275	-0.25758
120		-0.09553	-0.21451	-0.25758	-0.47275

Positive values show pairs of means that are significantly different.

Oneway Analysis of Week 6 GAG By Concentration
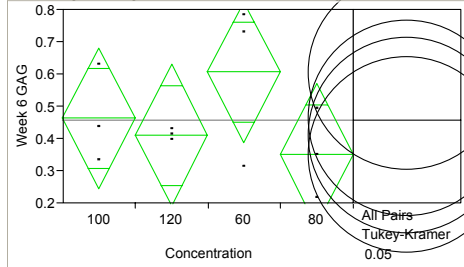
Oneway Anova

Source	DF	Sum of Squares	Mean Square	F Ratio	Prob > F
Concentration	3	0.10779934	0.035933	1.3286	0.3313
Error	8	0.21637248	0.027047		
C. Total	11	0.32417182			

Means Comparisons

Dif=Mean[i]-Mean[j]	60	100	120	80
60	0.000000	0.143309	0.196455	0.255994
100	-0.14331	0.000000	0.053147	0.112686
120	-0.19646	-0.05315	0.000000	0.059539
80	-0.25599	-0.11269	-0.05954	0.000000

Alpha=0.05

Comparisons for all pairs using Tukey-Kramer HSD

	q*			
	3.20238			

Abs(Dif)-LSD	60	100	120	80
60	-0.43001	-0.28671	-0.23356	-0.17402
100	-0.28671	-0.43001	-0.37687	-0.31733
120	-0.23356	-0.37687	-0.43001	-0.37048
80	-0.17402	-0.31733	-0.37048	-0.43001

Positive values show pairs of means that are significantly different.

Oneway Analysis of 60 GAG By Week #
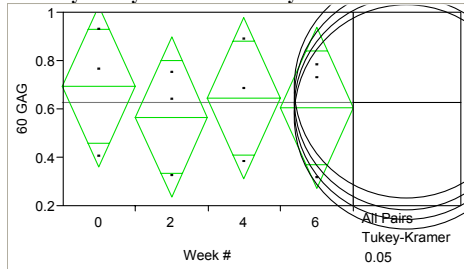
Oneway Anova

Source	DF	Sum of Squares	Mean Square	F Ratio	Prob > F
Week #	3	0.02715937	0.009053	0.1446	0.9303
Error	8	0.50077633	0.062597		
C. Total	11	0.52793570			

Means Comparisons

Dif=Mean[i]-Mean[j]	0	4	6	2
0	0.000000	0.048926	0.089364	0.128138
4	-0.04893	0.000000	0.040438	0.079212
6	-0.08936	-0.04044	0.000000	0.038774
2	-0.12814	-0.07921	-0.03877	0.000000

Alpha=0.05

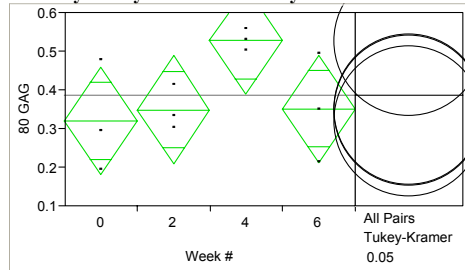Comparisons for all pairs using Tukey-Kramer HSD

	q*

q*				
3.20238				
Abs(Dif)-LSD	0	4	6	2
0	-0.65419	-0.60526	-0.56483	-0.52605
4	-0.60526	-0.65419	-0.61375	-0.57498
6	-0.56483	-0.61375	-0.65419	-0.61542
2	-0.52605	-0.57498	-0.61542	-0.65419

Positive values show pairs of means that are significantly different.

Oneway Analysis of 80 GAG By Week #

Oneway Anova

Source	DF	Sum of Squares	Mean Square	F Ratio	Prob > F
Week #	3	0.08172200	0.027241	2.4740	0.1360
Error	8	0.08808536	0.011011		
C. Total	11	0.16980736			

Means Comparisons

Dif=Mean[i]-Mean[j]	4	6	2	0
4	0.000000	0.177457	0.179688	0.208338
6	-0.17746	0.000000	0.002231	0.030880
2	-0.17969	-0.00223	0.000000	0.028650
0	-0.20834	-0.03088	-0.02865	0.000000

Alpha=0.05
Comparisons for all pairs using Tukey-Kramer HSD

q*				
3.20238				
Abs(Dif)-LSD	4	6	2	0
4	-0.27437	-0.09691	-0.09468	-0.06603
6	-0.09691	-0.27437	-0.27214	-0.24349
2	-0.09468	-0.27214	-0.27437	-0.24572
0	-0.06603	-0.24349	-0.24572	-0.27437

Positive values show pairs of means that are significantly different.

Oneway Analysis of 100 GAG By Week #
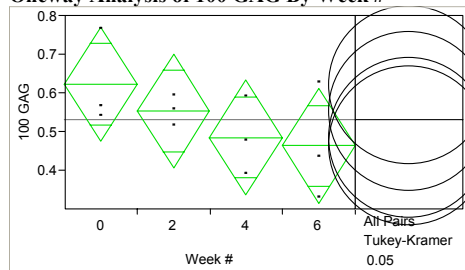
Oneway Anova

Source	DF	Sum of Squares	Mean Square	F Ratio	Prob > F
Week #	3	0.04693408	0.015645	1.2648	0.3499
Error	8	0.09895725	0.012370		
C. Total	11	0.14589133			

Means Comparisons

Dif=Mean[i]-Mean[j]	0	2	4	6
0	0.000000	0.069673	0.137927	0.159625
2	-0.06967	0.000000	0.068253	0.089951
4	-0.13793	-0.06825	0.000000	0.021698

Dif=Mean[i]-Mean[j]	0	2	4	6
6	-0.15962	-0.08995	-0.0217	0.000000

Alpha=0.05
Comparisons for all pairs using Tukey-Kramer HSD

q*
3.20238

Abs(Dif)-LSD	0	2	4	6
0	-0.29081	-0.22113	-0.15288	-0.13118
2	-0.22113	-0.29081	-0.22255	-0.20086
4	-0.15288	-0.22255	-0.29081	-0.26911
6	-0.13118	-0.20086	-0.26911	-0.29081

Positive values show pairs of means that are significantly different.

Oneway Analysis of 120 GAG By Week #
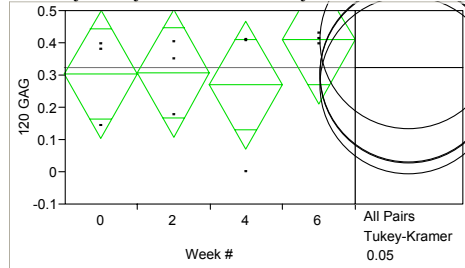
Oneway Anova

Source	DF	Sum of Squares	Mean Square	F Ratio	Prob > F
Week #	3	0.03315500	0.011052	0.4956	0.6954
Error	8	0.17840118	0.022300		
C. Total	11	0.21155618			

Means Comparisons

Dif=Mean[i]-Mean[j]	6	2	0	4
6	0.000000	0.103200	0.106441	0.140322
2	-0.1032	0.000000	0.003242	0.037122
0	-0.10644	-0.00324	0.000000	0.033881
4	-0.14032	-0.03712	-0.03388	0.000000

Alpha=0.05
Comparisons for all pairs using Tukey-Kramer HSD

q*
3.20238

Abs(Dif)-LSD	6	2	0	4
6	-0.39046	-0.28726	-0.28402	-0.25014
2	-0.28726	-0.39046	-0.38722	-0.35334
0	-0.28402	-0.38722	-0.39046	-0.35658
4	-0.25014	-0.35334	-0.35658	-0.39046

Positive values show pairs of means that are significantly different.

Oneway Analysis of Week 6 Type II Collagen By Concentration
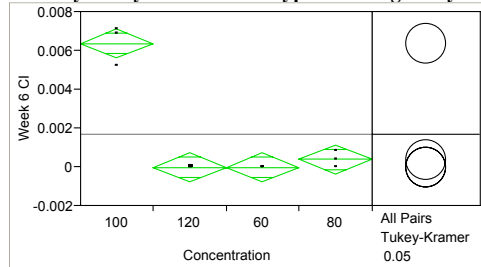
Oneway Anova

Source	DF	Sum of Squares	Mean Square	F Ratio	Prob > F
Concentration	3	0.00008827	0.000029	94.8396	<.0001
Error	8	0.00000248	0.000000		
C. Total	11	0.00009076			

Means Comparisons

Dif=Mean[i]-Mean[j]	100	80	60	120
100	0.000000	0.005987	0.006385	0.006385
80	-0.00599	0.000000	0.000398	0.000398
60	-0.00638	-0.0004	0.000000	0.000000
120	-0.00638	-0.0004	0.000000	0.000000

Alpha=0.05

Comparisons for all pairs using Tukey-Kramer HSD

q*
3.20238

Abs(Dif)-LSD	100	80	60	120
100	-0.00146	0.004531	0.004928	0.004928
80	0.004531	-0.00146	-0.00106	-0.00106
60	0.004928	-0.00106	-0.00146	-0.00146
120	0.004928	-0.00106	-0.00146	-0.00146

Positive values show pairs of means that are significantly different.

Oneway Analysis of 100 Type II Collagen By Week #
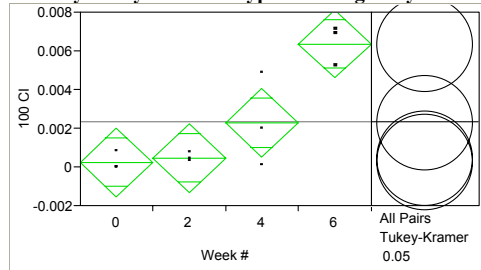
Oneway Anova

Source	DF	Sum of Squares	Mean Square	F Ratio	Prob > F
Week #	3	0.00007229	0.000024	13.5837	0.0017
Error	8	0.00001419	0.000002		
C. Total	11	0.00008648			

Means Comparisons

Dif=Mean[i]-Mean[j]	6	4	2	0
6	0.000000	0.004077	0.005903	0.006114
4	-0.00408	0.000000	0.001826	0.002037
2	-0.0059	-0.00183	0.000000	0.000211
0	-0.00611	-0.00204	-0.00021	0.000000

Alpha=0.05

Comparisons for all pairs using Tukey-Kramer HSD

q*
3.20238

Abs(Dif)-LSD	6	4	2	0
6	-0.00348	0.000594	0.002421	0.002632
4	0.000594	-0.00348	-0.00166	-0.00145
2	0.002421	-0.00166	-0.00348	-0.00327
0	0.002632	-0.00145	-0.00327	-0.00348

Positive values show pairs of means that are significantly different.
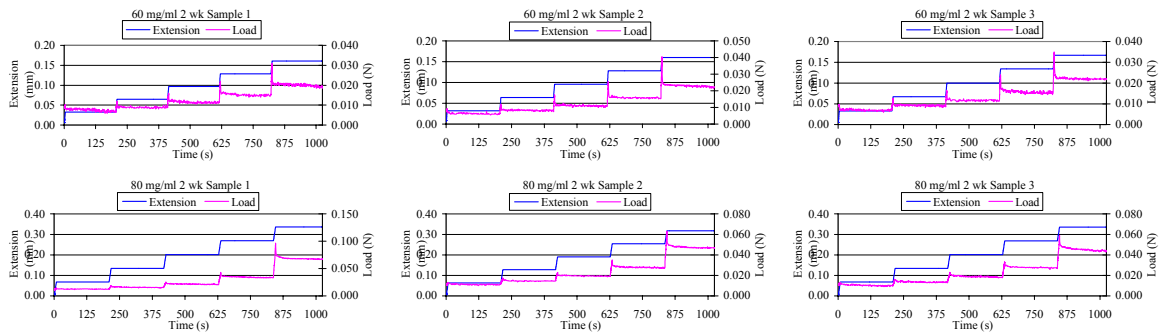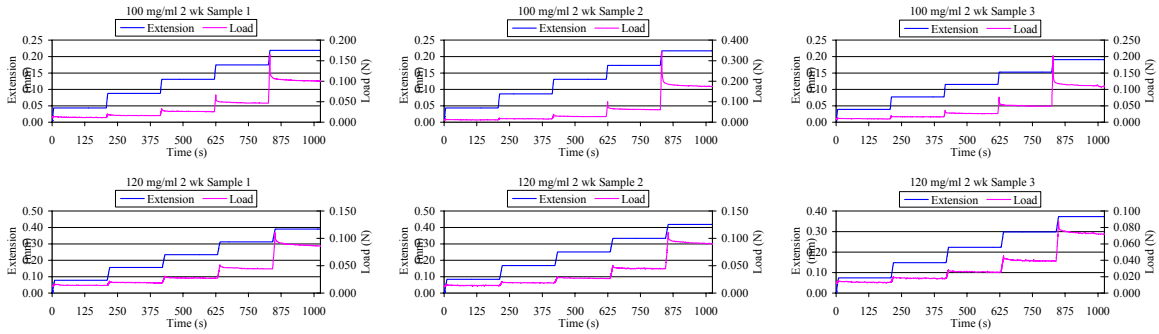
APPENDIX D: Stress Relaxation Data

Extension versus time and load versus time curves used to construct the equilibrium stress versus strain curves in the stress relaxation mechanical testing.
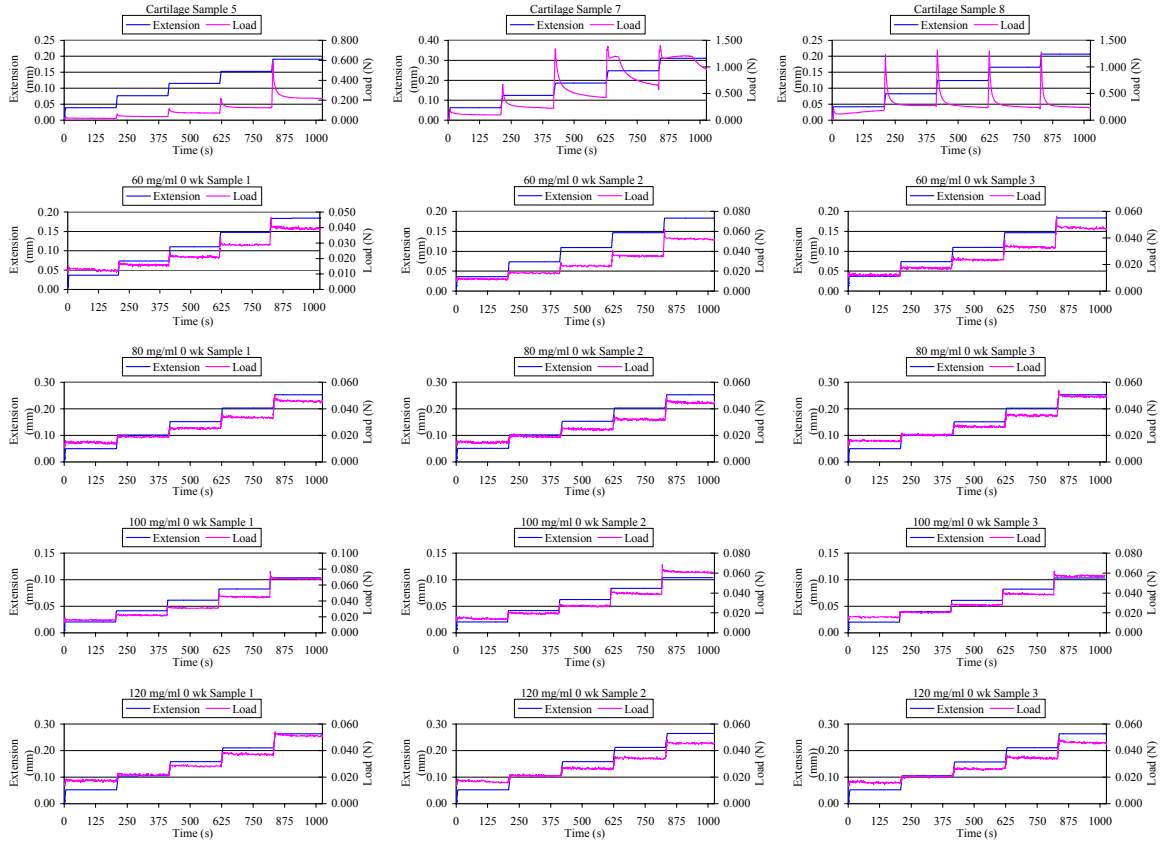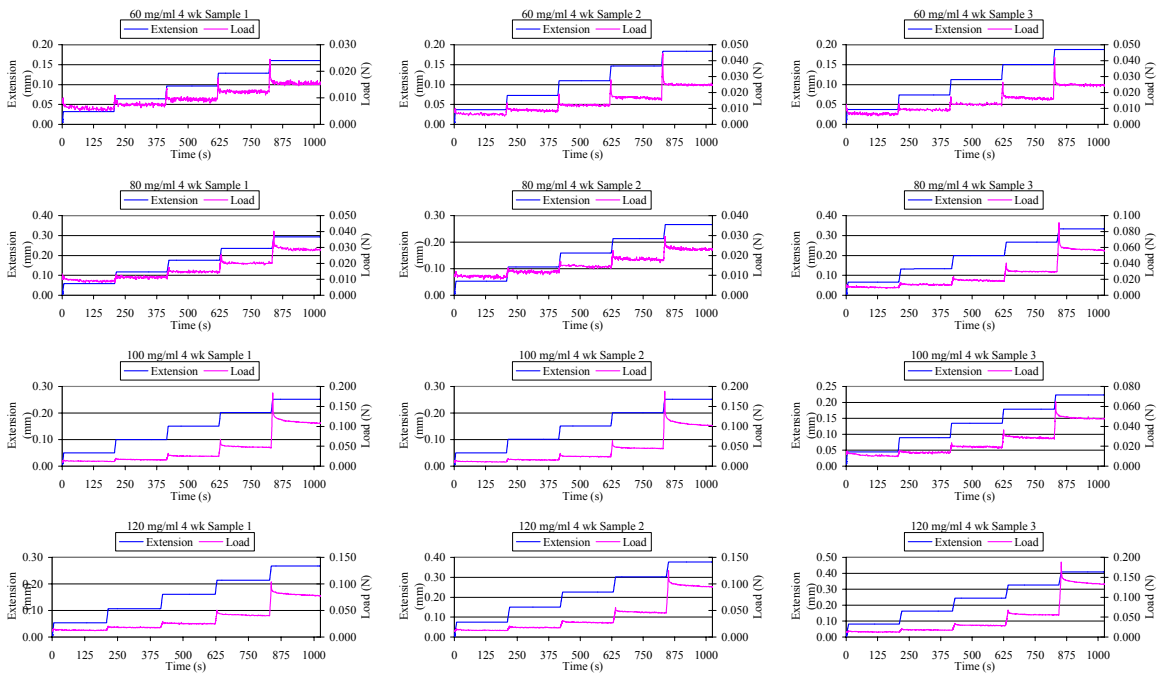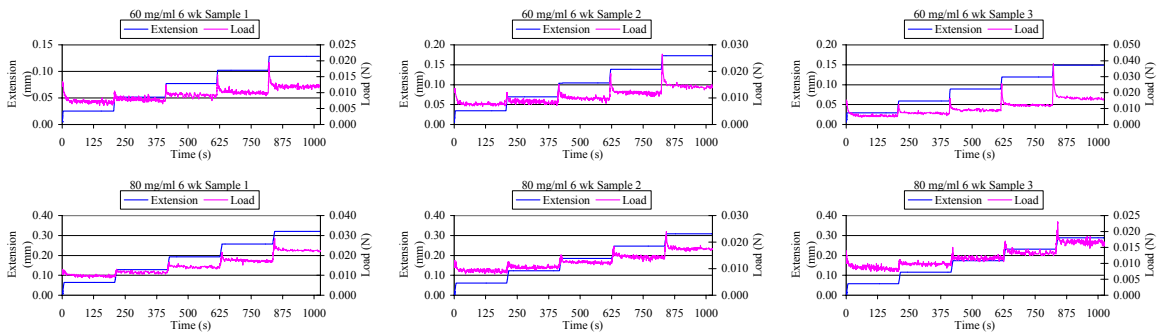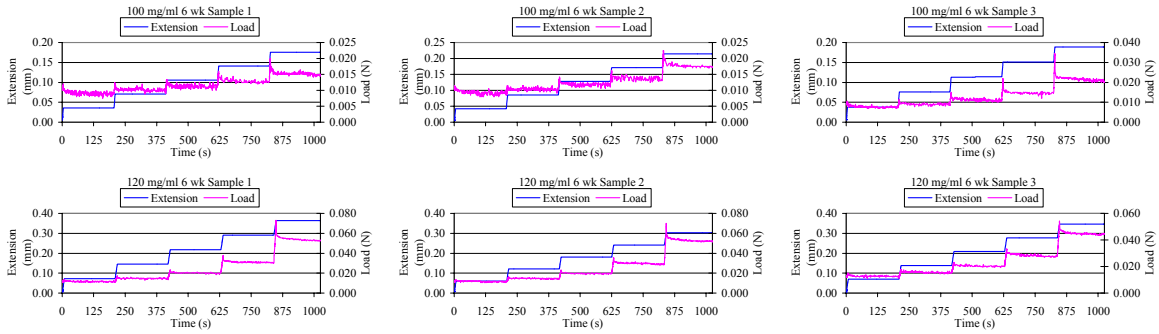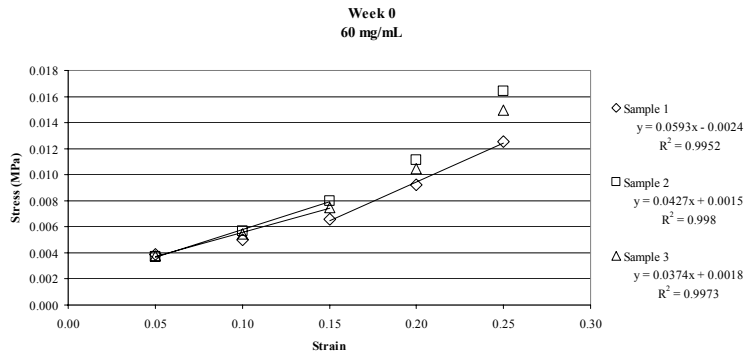
WEEK 0

WEEK 2

WEEK 4

WEEK 6

Equilibrium stress versus strain curves used to determine the equilibrium stiffness in the stress relaxation mechanical testing.

WEEK 0

159

Week 0
80 mg/mL

◇ Sample 1
y = 0.0462x + 0.0013
R^2 = 0.997

□ Sample 2
y = 0.0412x + 0.0018
R^2 = 0.9943

△ Sample 3
y = 0.0341x + 0.0032
R^2 = 0.9992

Week 0
100 mg/mL

◇ Sample 1
y = 0.0478x + 0.0026
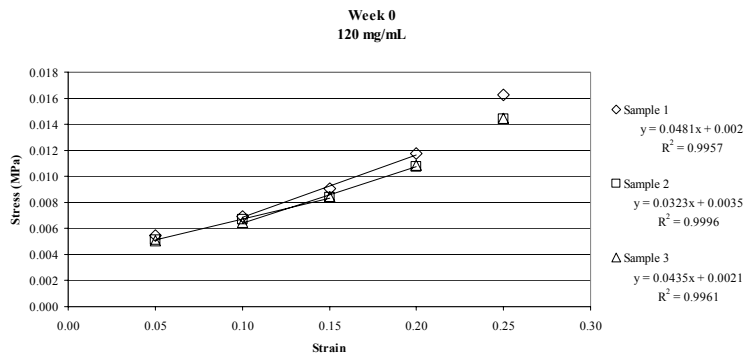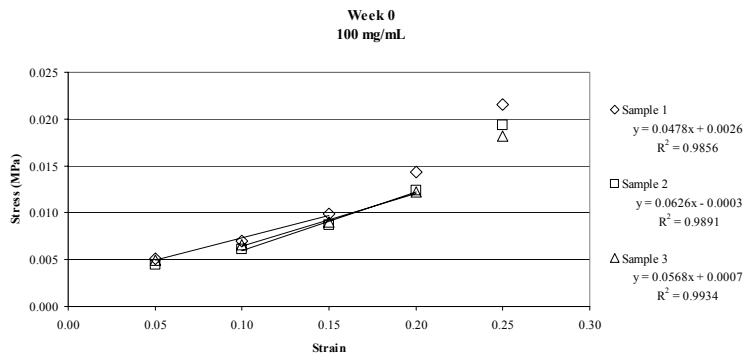R^2 = 0.9856

□ Sample 2
y = 0.0626x - 0.0003
R^2 = 0.9891

△ Sample 3
y = 0.0568x + 0.0007
R^2 = 0.9934

Week 0
120 mg/mL

◇ Sample 1
y = 0.0481x + 0.002
R^2 = 0.9957

□ Sample 2
y = 0.0323x + 0.0035
R^2 = 0.9996

△ Sample 3
y = 0.0435x + 0.0021
R^2 = 0.9961

WEEK 2

Week 2
60 mg/mL

◇ Sample 1
y = 0.0249x - 0.0002
R^2 = 0.9993

□ Sample 2
y = 0.0361x - 0.0021
R^2 = 0.9948

△ Sample 3
y = 0.014x + 0.0015
R^2 = 0.9932

Week 2
80 mg/mL

◇ Sample 1
y = 0.0277x + 0.0024
R^2 = 0.9638

□ Sample 2
y = 0.0407x + 0.0004
R^2 = 0.9758

△ Sample 3
y = 0.0814x - 0.0068
R^2 = 0.9749

Week 2
100 mg/mL

◇ Sample 1
y = 0.0965x - 0.0051
R^2 = 0.9568

□ Sample 2
y = 0.0521x + 0.0006
R^2 = 0.9405

△ Sample 3
y = 0.1039x - 0.0059
R^2 = 0.9531

Week 2
120 mg/mL

◇ Sample 1
y = 0.0417x + 0.0022
R^2 = 0.9691

□ Sample 2
y = 0.0405x + 0.0022
R^2 = 0.9842

△ Sample 3
y = 0.0682x - 0.0015
R^2 = 0.9748

WEEK 4

Week 4
60 mg/mL

◇ Sample 1
y = 0.0189x + 0.0002
R^2 = 0.9973

□ Sample 2
y = 0.0245x + 0.0002
R^2 = 0.9999

△ Sample 3
y = 0.0219x + 0.0007
R^2 = 0.9999

Week 4
80 mg/mL

◇ Sample 1
$y = 0.0439x - 0.002$
$R^2 = 0.9871$

□ Sample 2
$y = 0.0276x + 0.0003$
$R^2 = 0.9802$

△ Sample 3
$y = 0.0266x + 0.0017$
$R^2 = 0.9844$

Week 4
100 mg/mL

◇ Sample 1
$y = 0.0994x - 0.0056$
$R^2 = 0.9468$

□ Sample 2
$y = 0.0419x + 0.0011$
$R^2 = 0.981$

△ Sample 3
$y = 0.0283x + 0.0017$
$R^2 = 0.9909$

Week 4
120 mg/mL

◇ Sample 1
$y = 0.0387x + 0.002$
$R^2 = 0.9863$

□ Sample 2
$y = 0.0461x + 0.0014$
$R^2 = 0.9722$

△ Sample 3
$y = 0.0504x + 0.0012$
$R^2 = 0.9501$

WEEK 6

Week 6
60 mg/mL

◇ Sample 1
$y = 0.0075x + 0.0017$
$R^2 = 0.9461$

□ Sample 2
$y = 0.0144x + 0.0009$
$R^2 = 0.9997$

△ Sample 3
$y = 0.0221x - 0.0005$
$R^2 = 0.9917$

Week 6
80 mg/mL

◇ Sample 1
y = 0.0179x + 0.0018
R^2 = 0.9935

□ Sample 2
y = 0.0164x + 0.0014
R^2 = 0.9917

△ Sample 3
y = 0.011x + 0.002
R^2 = 0.996

Week 6
100 mg/mL

◇ Sample 1
y = 0.0092x + 0.0022
R^2 = 0.9998

□ Sample 2
y = 0.0107x + 0.0021
R^2 = 0.9976

△ Sample 3
y = 0.0108x + 0.0018
R^2 = 0.9982

Week 6
120 mg/mL

◇ Sample 1
y = 0.0255x + 0.0023
R^2 = 0.9897

□ Sample 2
y = 0.026x + 0.0022
R^2 = 0.979

△ Sample 3
y = 0.0392x + 0.0008
R^2 = 0.9842
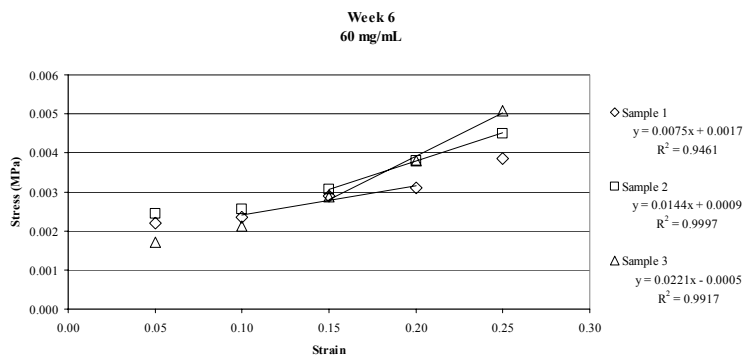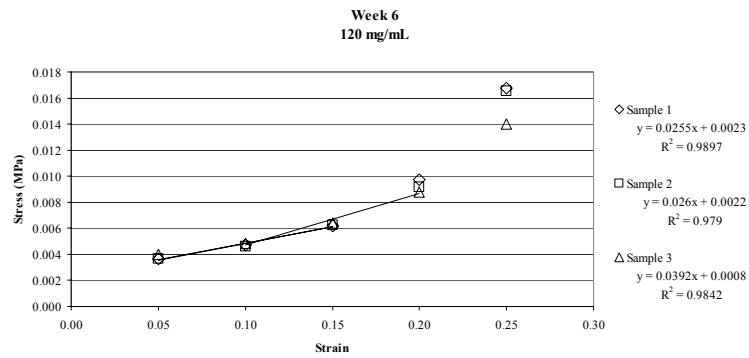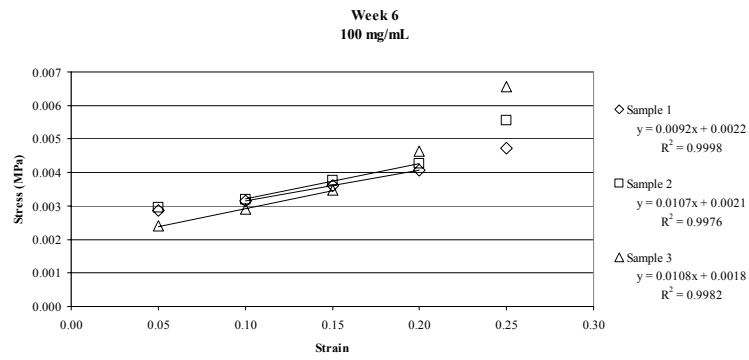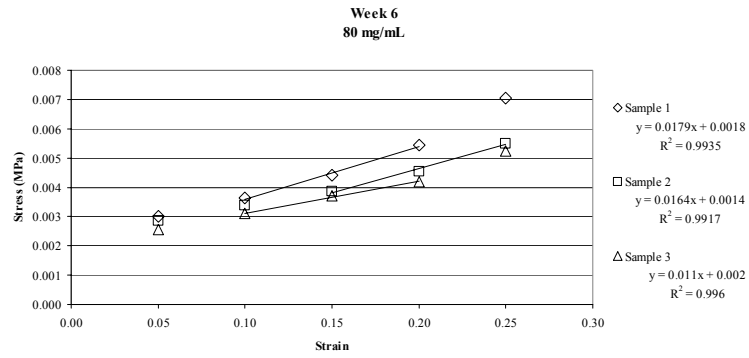
VITA

Catherine Pemble Barnes was born in 1975 in Vero Beach, Florida, and is a United States citizen. She graduated from Laurel High School in Laurel, Maryland, in 1993. She then attended Mercer University in Macon, Georgia, and graduated in 1997 with the Bachelor of Science in Engineering with specialization in Biomedical Engineering. Also in 1997, Catherine Barnes earned her Fundamentals of Engineering exam (EIT) certification. Following completion of her undergraduate work, she attended Arizona State University in Tempe, Arizona, where she earned the Master of Science degree in 1999 and completed her thesis titled "Development of a Glucose Sensor Combining Microdialysis and Colorimetry for Use in Biotechnology". Catherine Barnes worked as a Design Engineer for Insight Product Development and Woodhead Connectivity in Chicago, Illinois, for several years, and then returned to school in 2002 to earn a Doctor of Philosophy in Biomedical Engineering at Virginia Commonwealth University in Richmond, Virginia. While studying there, she has authored numerous research papers (in such journals as *Tissue Engineering*, *Acta Biomaterialia*, *Journal of Biomedical Materials Research Part A*, *International Journal of Electrospun Nanofibers and Applications*, *Advanced Drug Delivery Reviews*, and *Polymer International*) and has given presentations at a variety of conferences (including the Engineering Tissues Annual Hilton Head Workshop, the Annual Meeting of Tissue Engineering Society International, and the

Regenerate Conference). She has worked as a research assistant and as lab manager in the

Tissue Engineering Laboratory at Virginia Commonwealth University, and she has taught

several classes for the following courses: Tissue Engineering, Biomaterials, Mechanics of

Deformables, and Engineering Materials. In 2005 Catherine Barnes received two

scholarships, the Professional Engineers in Industry Scholarship awarded by the National

Society of Professional Engineers and another from the Honor Society of Phi Kappa Phi.

She is a member of the Tissue Engineering Regenerative Medicine International Society,

the Biomedical Engineering Society, the American Society of Mechanical Engineers,

Order of the Engineer, Inc., and is President and co-founder of the Virginia

Commonwealth University chapter of the Alpha Eta Mu Beta Biomedical Engineering

Honor Society.